

สมบัติเชิงแสงของแผ่นอะราโกไนต์เคลือบคาร์บอนได้จากเปลือกหอยแมลงภู่ *Perna viridis*

นายชุตินันท์ เลิศวชิรไพบูลย์

จุฬาลงกรณ์มหาวิทยาลัย  
CHULALONGKORN UNIVERSITY

บทคัดย่อและแฟ้มข้อมูลฉบับเต็มของวิทยานิพนธ์ตั้งแต่ปีการศึกษา 2554 ที่ให้บริการในคลังปัญญาจุฬาฯ (CUIR)  
เป็นแฟ้มข้อมูลของนิสิตเจ้าของวิทยานิพนธ์ ที่ส่งผ่านทางบัณฑิตวิทยาลัย

The abstract and full text of theses from the academic year 2011 in Chulalongkorn University Intellectual Repository (CUIR)  
are the thesis authors' files submitted through the University Graduate School.

วิทยานิพนธ์นี้เป็นส่วนหนึ่งของการศึกษาตามหลักสูตรปริญญาวิทยาศาสตรดุษฎีบัณฑิต

สาขาวิชาเคมี ภาควิชาเคมี

คณะวิทยาศาสตร์ จุฬาลงกรณ์มหาวิทยาลัย

ปีการศึกษา 2557

ลิขสิทธิ์ของจุฬาลงกรณ์มหาวิทยาลัย

OPTICAL PROPERTY OF PLATE-SHAPED ARAGONITE  
CALCIUM CARBONATE FROM GREEN MUSSEL *Perna viridis* SHELL

Mr. Chutiparn Lertvachirapaiboon



A Dissertation Submitted in Partial Fulfillment of the Requirements  
for the Degree of Doctor of Philosophy Program in Chemistry

Department of Chemistry

Faculty of Science

Chulalongkorn University

Academic Year 2014

Copyright of Chulalongkorn University

Thesis Title	OPTICAL PROPERTY OF PLATE-SHAPED ARAGONITE CALCIUM CARBONATE FROM GREEN MUSSEL <i>Perna viridis</i> SHELL
By	Mr. Chutiparn Lertvachirapaiboon
Field of Study	Chemistry
Thesis Advisor	Associate Professor Sanong Ekgasit, Ph.D.
Thesis Co-Advisor	Associate Professor Chuchaat Thammacharoen

---

Accepted by the Faculty of Science, Chulalongkorn University in Partial  
Fulfillment of the Requirements for the Doctoral Degree

..... Dean of the Faculty of Science  
(Professor Supot Hannongbua, Dr.rer.nat.)

THESIS COMMITTEE

..... Chairman  
(Associate Professor Vudhichai Parasuk, Ph.D.)

..... Thesis Advisor  
(Associate Professor Sanong Ekgasit, Ph.D.)

..... Thesis Co-Advisor  
(Associate Professor Chuchaat Thammacharoen)

..... Examiner  
(Numpon Insin, Ph.D.)

..... Examiner  
(Sakulsuk Unarunotai, Ph.D.)

..... External Examiner  
(Associate Professor Chinapong Kritayakornupong, Ph.D.)

ชุตีพันธ์ เลิศวชิรไพบุลย์ : สมบัติเชิงแสงของแผ่นอะราโกไนต์แคลเซียมคาร์บอเนตจากเปลือกหอยแมลงภู่ *Perna viridis* (OPTICAL PROPERTY OF PLATE-SHAPED ARAGONITE CALCIUM CARBONATE FROM GREEN MUSSEL *Perna viridis* SHELL) อ.ที่ปรึกษาวิทยานิพนธ์หลัก: สนอง เอกสิทธิ์, อ.ที่ปรึกษาวิทยานิพนธ์ร่วม: ชูชาติ ธรรมเจริญ, หน้า.

ปรากฏการณ์ประกายมุกของเปลือกหอยแมลงภู่ (*Perna viridis*) เกิดจากอันตรกิริยาระหว่างแสงกับโครงสร้างที่เกิดจากการเรียงตัวกันเป็นชั้นอย่างเป็นระเบียบของแผ่นอะราโกไนต์แคลเซียมคาร์บอเนตสลับกับชั้นของสารอินทรีย์ งานวิจัยนี้ทำการศึกษาความสัมพันธ์ระหว่างโครงสร้างและปรากฏการณ์ประกายมุกของเปลือกหอยแมลงภู่ และใช้ประโยชน์จากปรากฏการณ์ดังกล่าวในงานนวัตกรรมที่หลากหลาย ปรากฏการณ์ประกายมุกสามารถศึกษาได้โดยผู้วิจัยพัฒนาวิธีการแยกชั้นมุกเป็นแผ่นอะราโกไนต์แคลเซียมคาร์บอเนตแบบแผ่นซ้อนโดยไม่ทำลายการจัดเรียงตัวของแผ่นอะราโกไนต์แคลเซียมคาร์บอเนต แผ่นอะราโกไนต์แคลเซียมคาร์บอเนตแบบแผ่นซ้อนยังสามารถถูกแยกเป็นแผ่นอะราโกไนต์แคลเซียมคาร์บอเนตแบบแผ่นเดี่ยวต่อไปได้อีก นอกจากนี้ยังใช้การคำนวณเชิงทฤษฎีเพื่ออธิบายการเกิดปรากฏการณ์ประกายมุกอันเนื่องมาจากโครงสร้างของเปลือกหอยแมลงภู่ และการเกิดสีของแผ่นอะราโกไนต์แคลเซียมคาร์บอเนตแบบแผ่นซ้อน จากปรากฏการณ์เชิงแสงที่เป็นเอกลักษณ์ของแผ่นอะราโกไนต์แคลเซียมคาร์บอเนตแบบแผ่นซ้อนซึ่งสามารถนำมาใช้เป็นสีสำหรับตกแต่งและสีที่มีความเป็นเอกลักษณ์ใช้สำหรับระบุตัวตนหรือป้องกันการปลอมแปลงของผลิตภัณฑ์ แผ่นอะราโกไนต์แคลเซียมคาร์บอเนตแบบแผ่นเดี่ยวสามารถนำมาใช้เป็นวัสดุรองรับสำหรับงานวิจัยที่หลากหลายเช่น วัสดุรองรับสำหรับตัวเร่งปฏิกิริยา วัสดุรองรับสำหรับงานวิจัยเซอร์เฟสเอนแฮนซ์รามานสเปกโทรสโกปี นอกจากนี้ยังสามารถนำไปใช้เป็นสารเติมแต่งชนิดโปรงใสสำหรับพอลิเมอร์เคลือบผิว สีเคลือบประกายมุก และดินปืนสำหรับงานตกแต่ง

ภาควิชา เคมี  
สาขาวิชา เคมี  
ปีการศึกษา 2557

ลายมือชื่อนิสิต .....

ลายมือชื่อ อ.ที่ปรึกษาหลัก .....

ลายมือชื่อ อ.ที่ปรึกษาร่วม .....

# # 5273896623 : MAJOR CHEMISTRY

KEYWORDS: ASIAN GREEN MUSSEL SHELL / PEARLESCENT FLAKES / PEARLESCENT EFFECT / ARAGONITE PLATES

CHUTIPARN LERTVACHIRAPAIBOON: OPTICAL PROPERTY OF PLATE-SHAPED ARAGONITE CALCIUM CARBONATE FROM GREEN MUSSEL *Perna viridis* SHELL. ADVISOR: ASSOC. PROF. SANONG EKGASIT, Ph.D., CO-ADVISOR: ASSOC. PROF. CHUCHAAT THAMMACHAROEN, pp.

An interaction between the incident light and the structural architecture, i.e. stratified bilayers of aragonite calcium carbonate and organic matrix, of Asian green mussel (*Perna viridis*) induces visually observable pearlescent colors. In this work, we investigate the influence of the structure on the color expression and exploit it in several innovative applications. The developed treatment technique for disintegrating nacre to pearlescent flakes enables us to gain the insight understanding of structure-color relationship as only the organic binder was disintegrated without destroying the structural assembly of nacre of shells. Moreover, the pearlescent flakes were further disintegrated to transparent aragonite plates with unique structure. The modified transfer matrix method was employed to verify the structural colors of virgin nacre (aragonite/organic matrix) and pearlescent flakes (aragonite/air gap). Due to a unique optical characteristic of pearlescent flakes, we can be used it as a color-shifting pigment for decorative applications as well as a pigment for products identification or forgery prevention purpose. The individual aragonite plates disintegrated from pearlescent flakes can be used as a solid support in several applications (e.g. catalysis, surface enhance Raman spectroscopy), transparent filler for coating polymer, pearlescent pigment, and art clay for decorative applications.

Department: Chemistry

Field of Study: Chemistry

Academic Year: 2014

Student's Signature .....

Advisor's Signature .....

Co-Advisor's Signature .....

## ACKNOWLEDGEMENTS

I would like to express my sincere gratitude to my thesis advisor, Associate Professor Dr. Sanong Ekgasit and my thesis co-advisor Associate Professor Chuchaat Thammacharoen for wholeheartedly providing the useful guidance, understanding, training and teaching the theoretical background and technical skills during my research.

I would like to thank Associate Professor Dr. Vudhichai Parasuk, Dr. Numpon Insin, Dr. Sakulsuk Unarunotai, and Associate Professor Dr. Chinapong Kritayakornupong for useful suggestions as the thesis committee.

Warmest thanks to my friends and colleagues, my colleagues and organization: Sensor Research Unit, Department of Chemistry, Faculty of Science, Chulalongkorn University, and all good friends for the suggestions and spiritual supports throughout this research.

Partial financial support from National Research Council of Thailand (NRCT), Center of Innovative Nanotechnology, Chulalongkorn University (CIN-CU), National Center of Excellence for Petroleum, Petrochemicals, and Advanced Materials (CE-PPAM).

Whatever shortcomings in the dissertation remaining, they are the sole responsibility of the author.

Above all, I am profoundly grateful to my parents and endearing family for all their loves, understanding, support, and encouragement during the whole period of my study.

## CONTENTS

	Page
THAI ABSTRACT.....	iv
ENGLISH ABSTRACT .....	v
ACKNOWLEDGEMENTS .....	vi
CONTENTS.....	vii
CHAPTER I.....	1
INTRODUCTION.....	1
1.1 RESEARCH BACKGROUND AND RATIONALE.....	1
1.2 OBJECTIVES.....	2
1.3 SCOPE OF THE DISSERTATION .....	2
1.4 BENEFIT OF THE DISSERTATION.....	2
CHAPTER II.....	3
THEORETICAL BACKGROUND .....	3
2.1 Nacre.....	3
2.2 Pearlescent effect .....	5
2.3 Nacre like structure and plate-shaped calcium carbonate: Biomimetic design of biomaterials inspired by nacre .....	6
2.4 Transfer matrix method.....	7
CHAPTER III.....	10
EXPERIMENTAL SECTION .....	10
3.1 Air-gap-enhanced pearlescent effect in periodic stratified bilayers of AGM shell.....	10
3.2 Selective colors reflection from stratified aragonite calcium carbonate plates of AGM shell.....	10
3.3 Individual aragonite plates from nacre of shells.....	11
3.4 Characterization techniques .....	12
CHAPTER IV .....	15
RESULTS AND DISCUSSION .....	15
4.1 Air-gap-enhanced pearlescent effect in periodic stratified bilayers of AGM shell.....	15

	Page
4.2 Selective colors reflection from stratified aragonite calcium carbonate plates of shell .....	27
4.3 Individual aragonite plates from nacre of shells.....	35
CHAPTER V.....	44
CONCLUSIONS .....	44
.....	46
REFERENCES.....	46
APPENDIX A .....	49
APPENDIX B .....	55
APPENDIX C .....	63
VITA.....	98





# CHAPTER I

## INTRODUCTION

### 1.1 RESEARCH BACKGROUND AND RATIONALE

*Perna viridis* or Asian green mussel (AGM) shell is the two valves shell with sharp and smooth surface covered with a periostacum layer (i.e. the green organic layer covering the outer surface of the shell). The inner layer of shell shows color and luster like pearl. This layer is called nacreous layer or nacre. Nacre of AGM shell is hierarchical structure of aragonite calcium carbonate layers (200-500 nm thick) bound by thin organic binding layers (20-30 nm thick) [1-13]

Every year, over 100,000 tons of the shells become an agricultural waste [14]. Most of the shells are disposed as landfill [15]. There were several reports on using the wasted mussel shells as a raw material for high value applications [16-20]. For example, the mussel shells were utilized as an ingredient for high strength cement and mortar [16-18]. The calcined mussel shells exhibited promising applications in environmental remediation as an excellent absorber for heavy metals, especially arsenic and mercury ions [19]. Calcium oxide with high surface area after calcination at 1,050 °C was employed as an efficient solid alkaline catalyst for biodiesel production having a high yield of 94.1% [20]. Although, the several applications have been reported, the benefit of expressed colors derived from its own structural assembly of the AGM shells in order to realize novel applications of the optical effect.

In this work, we developed a method to study pearlescent effect expressed from AGM shells, pearlescent flakes disintegrated from AGM shells and individual aragonite plates using simple chemical techniques. The pearlescent flakes and individual aragonite plates were exploited for some innovative applications such as a color-shifting pigment, pearlescent pigment, surface coating pigment for decorative applications, solid support materials, and transparent filler for coating polymer.

## **1.2 OBJECTIVES**

Study optical phenomena of pearlescent flakes and individual plate-shaped aragonite plates prepared from Asian green mussel shells.

## **1.3 SCOPE OF THE DISSERTATION**

- 1.3.1 Develop process to prepare pearlescent flakes and individual aragonite plates.
- 1.3.2 Study optical phenomena of pearlescent flakes and individual aragonite plates.
- 1.3.3 Study morphology, surface roughness, composition and molecular information obtained produces.
- 1.3.4 Exploit the pearlescent flakes and individual aragonite plates in several applications such as colors-shifting pigment, coating pigment, transparent filler for coating polymer.

## **1.4 BENEFIT OF THE DISSERTATION**

- 1.4.1 Gain insight understanding of structure-color relationship of AGM shell nacre as well as nacre of other shells, pearls, natural and artificial structure composed of stratified layer.
- 1.4.2 Value creation for agricultural waste in Thailand.

## CHAPTER II

### THEORETICAL BACKGROUND

#### 2.1 Nacre

The nacre of mollusk shells exhibit alternating layer of aragonite calcium carbonate and organic matrix composed of protein, chitin, peptide, lipid, and polysaccharide [1-13]. The chitin coated with protein and polysaccharide acts as a template and induces a deposition of amorphous calcium carbonate (ACC). In case of nacre, ACC is grown and transformed into aragonite microplates [5,6]. The brick-and-mortar like structure of nacre could be explained by mineral bridge model where the aragonite crystals grow through the pore of organic layers [2,4,7].

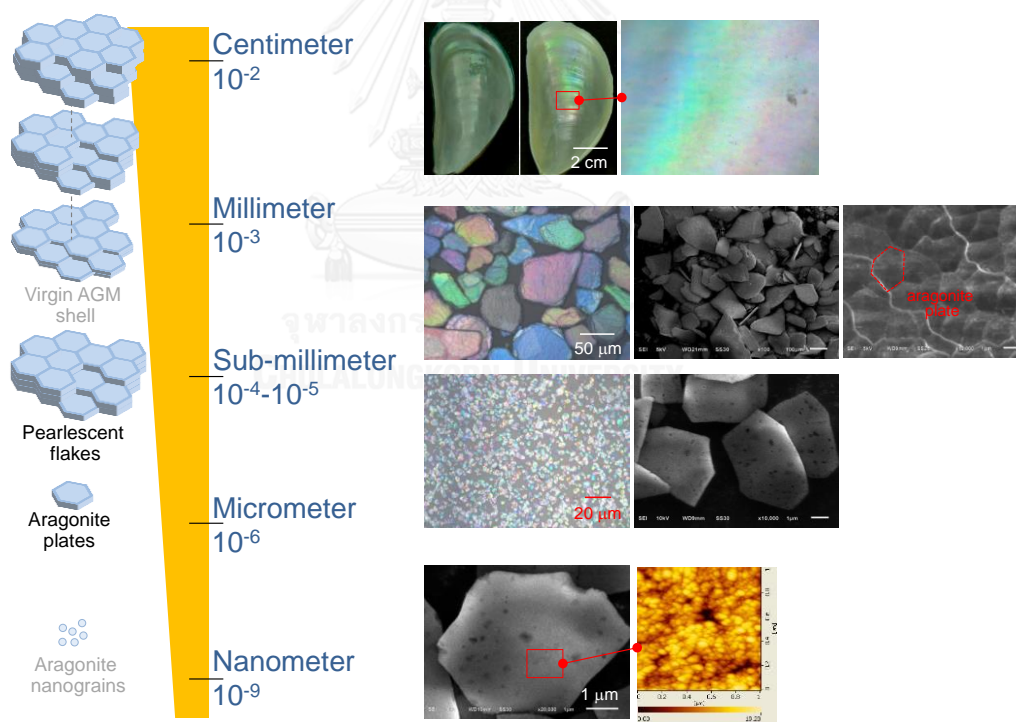


Figure 2-1. Hierarchical organization in nacre of Asian green mussel shell.

Nevertheless, the aragonite plates have been under debate in terms of structural development. The number of research articles interested in this topic has increased [2,5,7,8,12,13,22-24]. Briefly, there have three different famous models explaining the formation of aragonite plates.

1. A single crystal model. This model is based on crystallographic explanation. The biopolymers act as a template to induce the formation of plates from calcium and carbonate ions to ACC. ACC can grow to single crystal of aragonite plate [2, 22-24].
2. The tablet is an ACC-coated single crystal model. The plates have single crystal core covered by ACC shell. The ACC will be transformed into aragonite under electron irradiation [5].
3. Pseudo-single-crystal model. This model was observed based on atomic force microscopy and high-resolution transmission electron microscope. The aragonite plate comprises co-oriented nanocrystals (mesocrystal) to form aragonite plate [7,8,12,13].

Nacre structure is one of the natural-material models receiving considerable research attentions in the past two decades due to their excellent mechanical properties and unique optical effect [25-28]. Jackson *et al.* reported that a Young's modulus *Pinctada imbricata* nacre of 70 GPa and tensile strength of approximately 170 MPa [25]. Moreover, the toughness of nacre was also very interesting as the hydration effect could increase the toughness of nacre from 350-450 J m<sup>-2</sup> to 1,240 J m<sup>-2</sup>, 1,000 times tougher than calcium carbonate monolith [25]. In case of optical effect of nacre, due to the stratified bilayers of aragonite and organic binding layers, nacre expressed the rainbow reflection called pearlescent colors. This fascinating effect could be explained by diffraction, interference or their combination [3, 27-28]. Many applications of nacre related to decoration and were used as an ingredient in cosmetic industry [29,30]. Recently, the pearlescent colors from AGM shell and pearlescent enhancement by replacing of organic binding layers with air gaps were reported by our group [3].

## 2.2 Pearlescent effect

Pearlescent effect is a unique optical phenomenon originated by an interference of visible light with biomaterial having periodic structure such as pearls, mother-of-pearls, mollusk shells, beetle wings, and butterfly wings. The pearlescent colors were attributed to reflective index of matters, angle of incidence, and thickness of stratified layers within periodic structure [31-33]. The word ‘pearlescent colors’ is normally used with the color expression of mollusk-shells nacre such as mussel, pearl oyster, abalone shells [3,27,28]. Liu, *et al.* demonstrated that the pearlescent colors of *Pinctada Margaritifera* shell were due to the diffraction induced by the grating-like structure of the shell [27]. Tan, *et al.* described that the exceptionally vivid pink and blue-green pearlescent colors in the abalone (*Haliotis Glabra*) shell was due to the interaction of light with the uniform stack of calcium carbonate layers [28].

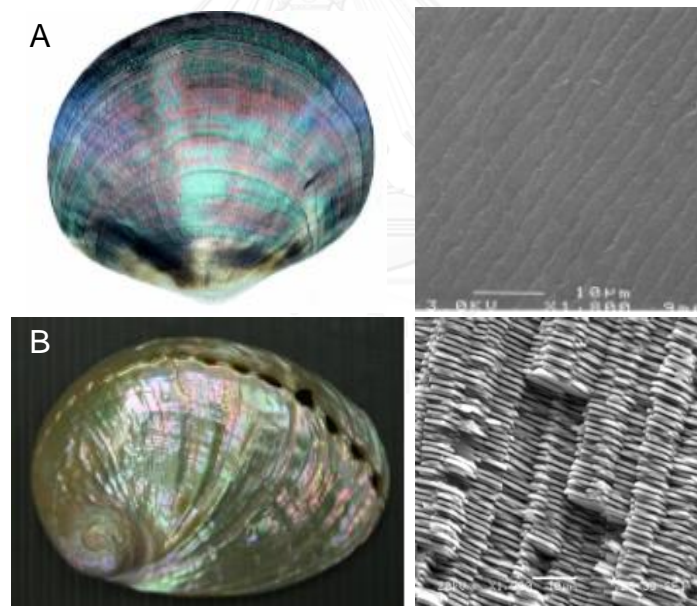


Figure 2-2. Photographic images of (A) *Pinctada Margaritifera*, (B) *Haliotis Glabra* and their SEM images. The pearlescent colors expressed from the mollusk shells originated from interaction of white light with periodic structure [27,28].

### 2.3 Nacre like structure and plate-shaped calcium carbonate: Biomimetic design of biomaterials inspired by nacre

Nacre is a high-performance composite materials for researchers to produce tough, strong and stiff structural materials. The nacre inspired composite materials of poly(vinyl alcohol) (PVA)/nanoclay composite provided high strength and stiffness as this material could dissipate the external force. The PVA/nanoclay was prepared by immersion of dispersed montmorillonite into PVA solution under subsequently stirred overnight. The excess PVA was removed by centrifugation and the composite material was then purified by washing with water. Finally, composite films were obtained after vacuum filtration PVA/nanoclay composite solution through a hydrophilic membrane and drying at 80 °C for 48 h [34].

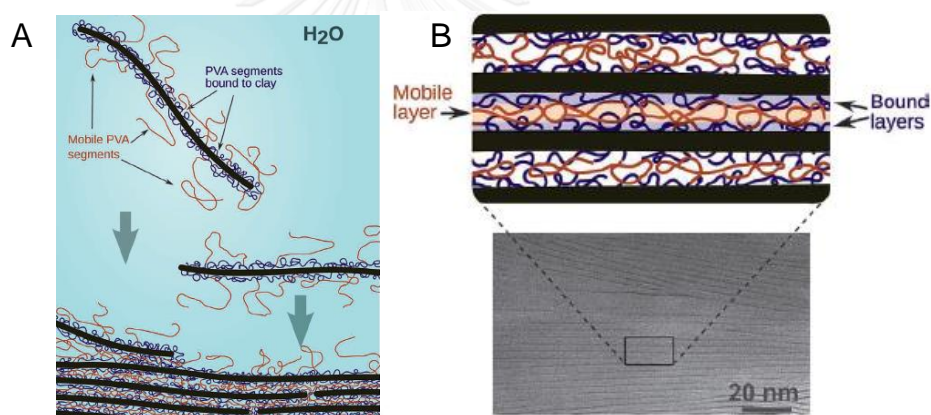


Figure 2-3. Hierarchical structure of PVA/nanoclay composite bioinspired by nacre.

(A) A schematic representation of the film formation process for construction of PVA/nanoclay nacre. (B) TEM image of a PVA/nanoclay nacre film and schematic representation of layer structure [34].

In case of plate-shaped  $\text{CaCO}_3$ , there have been many researches inspired by the fascinating mechanical and optical properties of this biomaterials. The  $\text{CaCO}_3$  microplates could be synthesized in the presence of protein [9-11], ammonia [35], cellulose derivative [36], controlling the supersaturation condition of ACC [37], and microemulsion route [38]. The uniform hexagonal plate-shaped  $\text{CaCO}_3$  with average

diameter of 5-10  $\mu\text{m}$  synthesized in the presence of *N*-trimethylammonium derivative of hydroxyethyl cellulose by aggregation-mediated crystallization was reported [36].

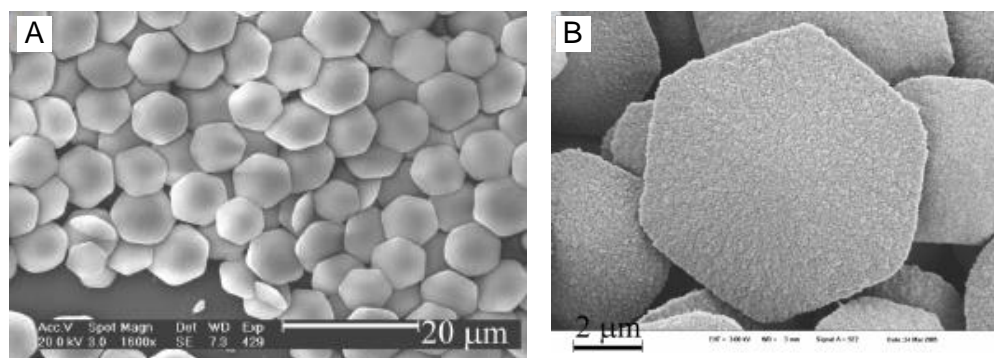


Figure 2-4. (A and B) SEM images of the obtained uniform  $\text{CaCO}_3$  microplates grown in the presence of hydroxyethyl cellulose. (B) A high-resolution SEM image shows each hexagonal plate consists of  $\text{CaCO}_3$  nanoparticles [36].

## 2.4 Transfer matrix method

The unique optical effect of nacre, pearlescent flakes and individual aragonite plates prepared from nacre of sea shells were achieved because we have strong theoretical background on the interaction of light with stratified materials. The modified transfer matrix method was employed to calculate the reflectance. Based on stratified bilayers of our system, the shell consists of  $N$  isotropic bilayers. The aragonite calcium carbonate is represented by layer A while organic matrix and air are represented by layer B. The  $j$ th bilayer consists of layer A and layer B with a thicknesses of  $d_A$  and  $d_B$  and a reflective indices of  $n_A$  and  $n_B$ . The stratified bilayer is bounded by air (i.e., air function as both incident medium and substrate in the simulation algorithm).

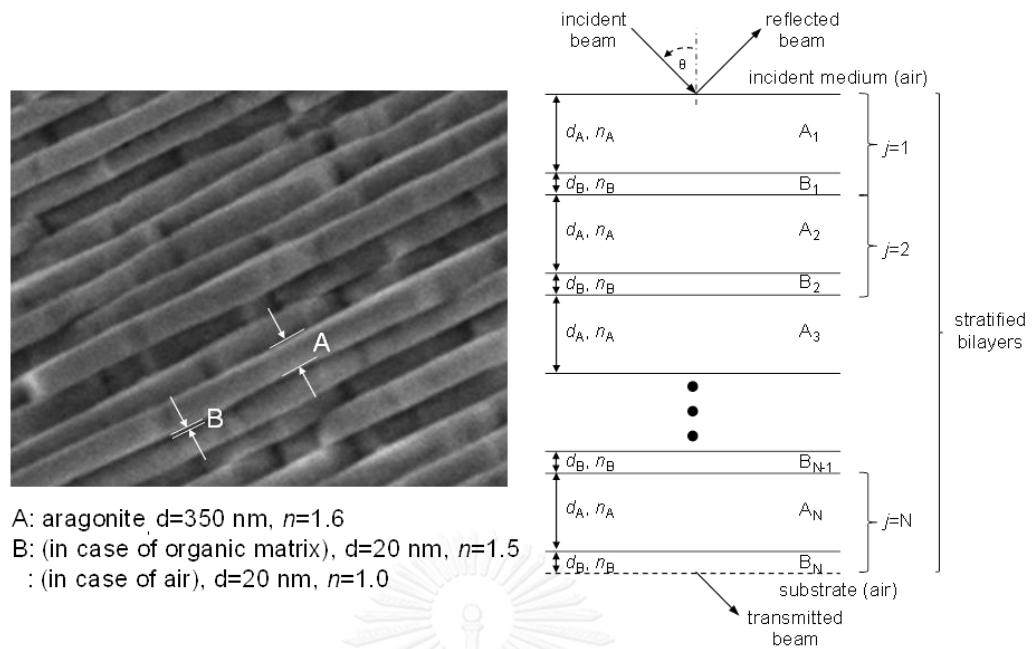


Figure 2-5. A cross-sectioned SEM image of nacre and the corresponding schematic representation of stratified bilayers. The thicknesses and reflective indexes of the stratified layers were adopted from our experimental results and literatures [2,3,27,28]. The aragonite layers, organic binder, and air gaps were assumed non-absorbing in the visible region (i.e., absorption coefficient  $k=0$ ) [3].

When an incident radiation of wavelength  $\lambda$  impinges on the stratified bilayers with an angle of incidence  $\theta$ , the Fresnel reflection and transmission coefficients are given by: [3,39,40]

$$r_{\parallel,\perp} = \frac{(M_{11} + M_{12}q_{\text{air}})q_{\text{air}} - (M_{21} + M_{22}q_{\text{air}})}{(M_{11} + M_{12}q_{\text{air}})q_{\text{air}} + (M_{21} + M_{22}q_{\text{air}})}, \quad (\text{Eq. 1})$$

$$t_{\parallel,\perp} = \frac{2q_{\text{air}}}{(M_{11} + M_{12}q_{\text{air}})q_{\text{air}} + (M_{21} + M_{22}q_{\text{air}})}. \quad (\text{Eq. 2})$$

Where  $\parallel$  indicates parallel-polarized radiation and  $\perp$  indicates perpendicular-polarized radiation.  $M_{mn}$  is an element of the characteristic matrix  $M(2 \times 2)$  of the



stratified bilayers. The matrix  $M$  is expressed in terms of the experimental conditions and material parameters by:

$$M = \prod_{j=1}^N \begin{bmatrix} \cos(k_{Aj}d_{Aj}) & \frac{-i}{q_{Aj}} \sin(k_{Aj}d_{Aj}) \\ -iq_{Aj} \sin(k_{Aj}d_{Aj}) & \cos(k_{Aj}d_{Aj}) \end{bmatrix} \begin{bmatrix} \cos(k_{Bj}d_{Bj}) & \frac{-i}{q_{Bj}} \sin(k_{Bj}d_{Bj}) \\ -iq_{Bj} \sin(k_{Bj}d_{Bj}) & \cos(k_{Bj}d_{Bj}) \end{bmatrix}, \quad (\text{Eq.3})$$

where  $i = (-1)^{1/2}$ ,  $q_j = k_j / n_j^2$  for parallel-polarized radiation, and  $q_j = k_j$  for perpendicular-polarized radiation.  $k_j$  ( $k_j = [(2\pi/\lambda)^2 n_j^2 - k_{\text{air}}^2]^{1/2}$ ) is the wavevector in each layer while  $k_{\text{air}}$  ( $k_{\text{air}} = (2\pi/\lambda)[n_{\text{air}}^2 \sin^2 \theta]^{1/2}$ ) is the wavevector in the incident medium (air). The reflectance and transmittance are given in terms of the Fresnel reflection and transmission coefficients as:

$$R_{\parallel} = |r_{\parallel}|^2 \quad \text{and} \quad T_{\parallel} = \frac{\text{Re}[k_{\text{air}} / \varepsilon_{\text{air}}]}{k_{\text{air}} / n_{\text{air}}^2} |t_{\parallel}|^2; \quad \text{for parallel polarized radiation,} \quad (\text{Eq.4})$$

$$R_{\perp} = |r_{\perp}|^2 \quad \text{and} \quad T_{\perp} = \frac{\text{Re}[k_{\text{air}}]}{k_{\text{air}}} |t_{\perp}|^2; \quad \text{for perpendicular polarized radiation,} \quad (\text{Eq.5})$$

$$R = (R_{\perp} + R_{\parallel})/2 \quad \text{and} \quad T = (T_{\perp} + T_{\parallel})/2; \quad \text{for non-polarized radiation.} \quad (\text{Eq.6})$$

## **CHAPTER III**

### **EXPERIMENTAL SECTION**

#### **3.1 Air-gap-enhanced pearlescent effect in periodic stratified bilayers of AGM shell**

Sodium hydroxide (NaOH) pellets were purchased from Merck (Thailand). Tap water was employed as the solvent throughout the experiment. The AGM were thoroughly cleaned to remove residual tissues and other contaminants. The shells were then boiled in sodium hydroxide solution (0.5 M) under a high pressure (2.5 bar) for 2 h. The detached periostacum, i.e., the green organic layer covering the outer surface of the shells, was removed by washing with water. The dried shells were later baked at 200 °C for 2 h. The thermally treated shells were then immersed in water for 24 h to remove the degraded organic matrix. The dissolution of organic residues could be noticed as the water turned brownish yellow. The shells were thoroughly cleaned with water and air dried before keeping in a desiccator for further investigation. The treated shells were slightly whitened with an enhanced pearlescent effect as indicated by a greater reflection with a more vivid color compared to the virgin shells. Scanning electron microscopy (SEM) and atomic force microscopy (AFM) were used to verify the structural integrity of the shell. A decrease of organic content after the treatment was confirmed by thermal gravimetric analysis (TGA). A development of the air gaps inside the treated shell were confirmed by an incorporation of dyes.

#### **3.2 Selective colors reflection from stratified aragonite calcium carbonate plates of AGM shell**

The pearlescent flakes from AGM shells were thoroughly cleaned to remove residual tissues and other contaminants before drying under an ambient air. The dried shells were baked at 300 °C for 2 h. The shells were then immersed in 30 % wt. hydrogen peroxide (H<sub>2</sub>O<sub>2</sub>, Merck, Thailand) for 24 h to dissolve the brownish-degraded organic binder. The H<sub>2</sub>O<sub>2</sub>-whiten shells showed observable rainbow colors. The shells were brittle and easily broken-down into small flakes. The flakes were

cleaned with tap water several times to remove dust particles. The flakes showed vivid rainbow colors observable by naked eyes when they were dispersed in water. The flakes were air dried before keeping in a desiccator for further investigation. SEM and AFM were employed to investigate the structural architecture of the flakes. The expressed colors of pearlescent flakes were recorded by a CCD attached on an optical microscope (OM). The reflection spectra of pearlescent flakes were collected by a fiber optic spectrometer

### **3.3 Individual aragonite plates from nacre of shells**

Powders of individual aragonite plates were disintegrated from nacles of AGM shells including of abalone (*Haliotis asinina*), pearl oyster (*Pinctada maxima*) shells. The shells were cleaned to remove residual tissues and other contaminants before drying under an ambient air. The dried shells were baked at 300 °C for 2 h to thermally decompose the organic matrices. The thermally treated shells were immersed in 30 wt % H<sub>2</sub>O<sub>2</sub> (Merck, Thailand) for 2 h to remove the degraded organic matrices. During H<sub>2</sub>O<sub>2</sub> treatment, ultrasonic radiation (VCX750, SONICS & MATERIALS Inc.) was employed to accelerate the disintegration. The shells were broken down to small fragments of individual CaCO<sub>3</sub> microplates with glittering reflection observable by naked eyes. The large fragments were filtrated out using a 200 mesh stainless steel. The CaCO<sub>3</sub> microplates were cleaned with tap water to remove the residual chemicals and degraded organic binder before drying at 100 °C. The white powder of CaCO<sub>3</sub> microplates was kept in a desiccator for further investigation. Optical microscope images of CaCO<sub>3</sub> microplates were recorded by a CCD camera (Carl Zeiss, AxioCam HRc) attached on an OM. SEM was employed for structural characterization of microplates. The average bisector length of microplates was calculated from 300 plates selected from unique SEM images. Surface topology and average surface roughness ( $R_a$ ) of the plates were examined by AFM. The organic contents and organic residuals in the microplates were quantified by TGA.

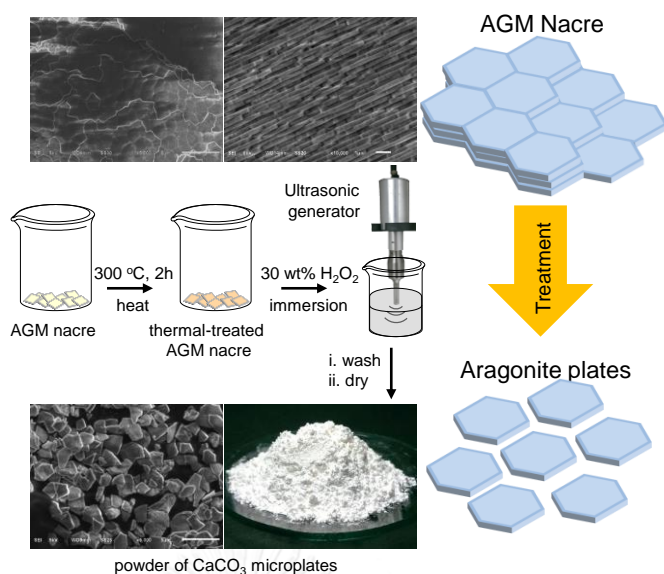


**Figure 3-1.** An experimental procedure for the preparation of  $\text{CaCO}_3$  microplates from AGM shells.

### 3.4 Characterization techniques

#### *Optical image acquisition*

To record the pearlescent effect of virgin and treated shells, photographic images were taken with a Nikon D90 digital camera. The pearlescent colors of the fragmented shells were recorded by a CCD camera (Carl Zeiss, AxioCam HRc) attached on an optical microscope (OM, Carl Zeiss Axio Scope.A1). The reflection spectra of both the virgin and the treated shells were collected by a fiber optic spectrometer (OceanOptics USB4000 portable UV-visible spectrometer) coupled to the OM.

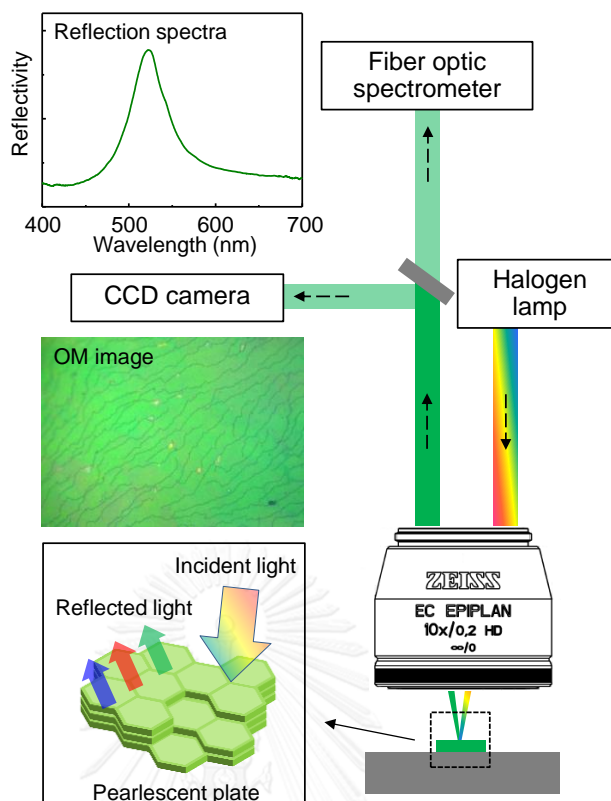


**Figure 3-2.** Experimental setup of simultaneously acquires a visible spectrum and the corresponding OM image of a pearlescent flake.

#### *Organic content determination*

The organic contents of virgin and treated shells were quantitatively determined by thermal gravimetric analysis (PerkinElmer, Pyris 1). The sample (~10 mg) was loaded into a ceramic crucible and heated up to 850 °C at a heating rate of 10 °C/min under a nitrogen environment.

#### *Structural characterization*

Scanning electron microscope (SEM, JEOL, JSM-6510A) was employed for the structural investigation of the stratified architecture of virgin AGM shells and the calcium carbonate prepared from treated shells using a low acceleration voltage of 5 kV. To collect cross-sectioned SEM images of a large fragment of virgin and treated shells, a specimen were wrapped with an aluminum foil before mounting onto a

modified stub normal to the electron beam. The small flakes and also calcium carbonate powder were dispersed in water and dropped on carbon tape attracted to stub. The samples were dried under vacuum condition at room temperature.

Surface topology, thickness of aragonite layers, and their roughness ( $R_a$ ) were determined by an atomic force microscope (AFM, SPA 400, SII NanoTechnology Inc.). The AFM images were recorded by a non-contact mode with a scanning rate of 1 Hz using silicon cantilever with a tip rounding size of 20 nm, force constant of 17 N/m, and a resonance frequency of 139 KHz.

#### *The air gaps determination*

The developed air gaps between aragonite layers after the removal of organic binder were verified by a dye diffusion experiment. Solutions of rhodamine 6G (R6G, 1 mM, 5  $\mu$ L), methylene blue (MB, 1 mM, 5  $\mu$ L), and water were diffused into the generated air gaps via capillary effect by placing a drop of the solution on the treated shell. The dye residual on the shell surface was removed by washing several times until the water become colorless. An incorporation of the dye into the air gaps was examined by the OM under bright field and dark field illuminations.

#### *Raman spectroscopy*

Raman spectroscopy (DXR Raman Microscope, Thermo Scientific) was employed to acquire molecular information of the microplates using 780 nm laser (5 mW laser power) with 2s exposure time and 32 number of exposures.

## CHAPTER IV

# RESULTS AND DISCUSSION

### 4.1 Air-gap-enhanced pearlescent effect in periodic stratified bilayers of AGM shell

The pearlescent colors originated by an interaction between visible light with materials having periodic stratified layers are a well-established phenomenon. An AGM shell is a stratified bilayers assembly of alternated 200-500 nm thick aragonite calcium carbonate layers bound by 20-30 nm thick organic binding layer. However, after a consecutive alkaline/thermal treatment that removed the organic layer, the shell expresses a more vivid pearlescent effect, Figures 4-1A and 4-1B. Although the treated shells were more brittle than the virgin shells due to the removal of organic binder, the treated shells still retained its original structure without any dimensional change. The reflection spectrum of the virgin shell shows a narrow peak at 657 nm and a broad shoulder at 450-600 nm which agrees with the red and yellow colors observed in the OM image (Figure 4-1C). The reflection spectrum of the treated shell, on the other hand, shows two broad peaks centered at 512 and 598 nm, Figure 4-1D. Since the reflection bands cover 475-650 nm spectral range, the treated shell expresses vivid green, yellow, and red pearlescent colors under a normal observation as seen in Figure 4-1B and OM image in Figure 4-1D. The spectral change corroborated the more vivid and brighter pearlescent colors observed in treated shell compared to that of the virgin shell. The Raman spectra of the virgin and treated AGM shells with characteristic external lattice vibrations at 147, 183, and 194  $\text{cm}^{-1}$ , a strong scattering at 209  $\text{cm}^{-1}$ , and a doublet at 703 and 706  $\text{cm}^{-1}$  of carbonate moiety confirm the aragonite crystal (Figure 4-2A and Table 4-1) [1, 2]. The corresponding FT-IR spectra in Figure 4-2B also confirm the aragonite crystal by the doublet at 705 and 708  $\text{cm}^{-1}$  associated with the in-plane bending of carbonate vibrations [3-6]. Since the molecular information did not show any spectroscopic signature of calcite or vaterite forms, the calcium carbonate building block of the AGM shell is presumably pure aragonite crystal.

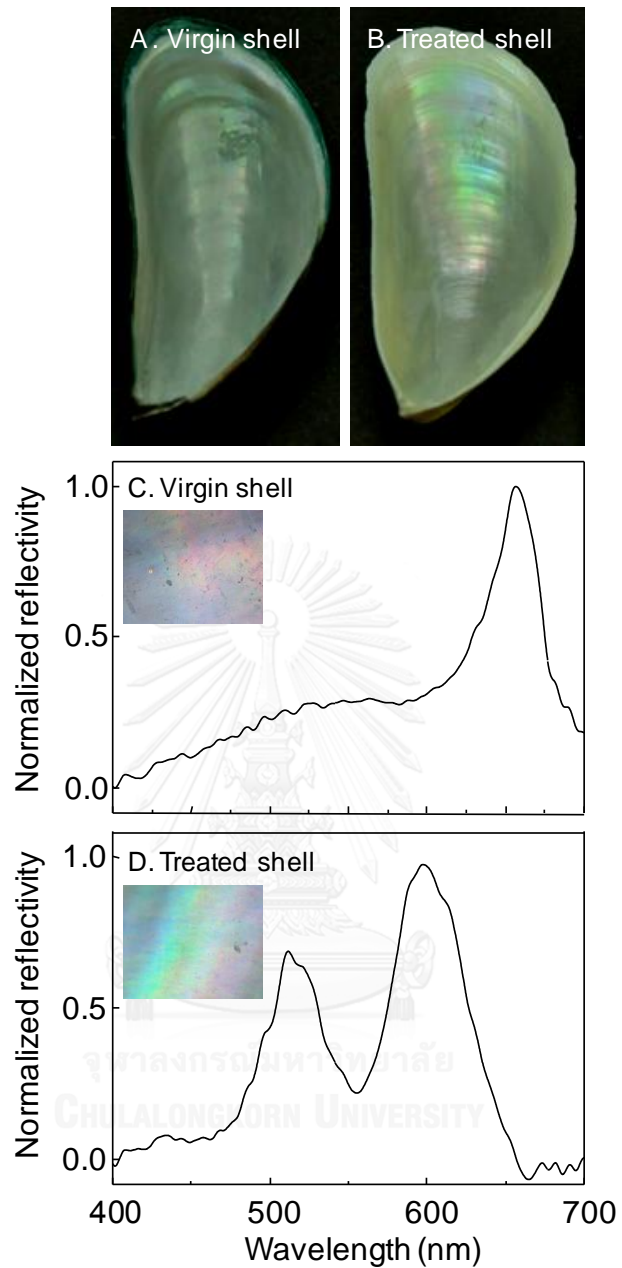


**Figure 4-1** Photographic images of (A) virgin and (B) treated AGM shells. Normalized reflection spectra of (C) virgin and (D) treated shells. The inserts are 500X magnification OM images of the shells under the bright field illumination.



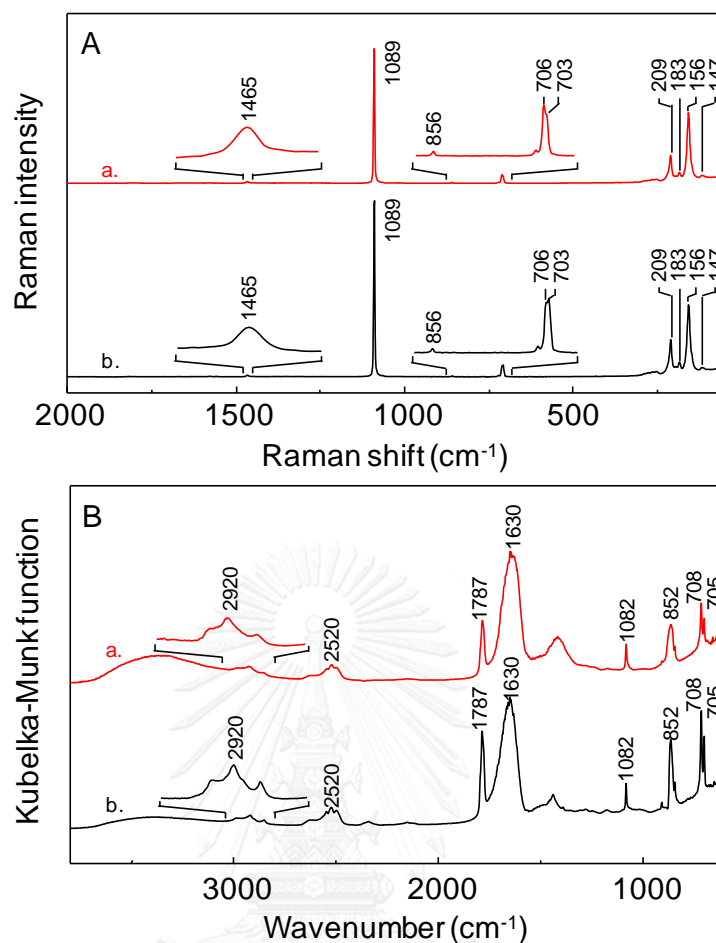


**Figure 4-2** (A) Raman and (B) Diffuse reflectance FT-IR spectra of virgin and treated shells.

According to the TGA profiles in Figure 4-3, there are two major thermal decompositions. The first weight loss at 200-300 °C was due to organic matrix decomposition. The TG curve indicates that the organic content in the virgin shell was 6.9 % while that of the treated shell was 2.1 %. A 4.8 % reduction in organic content was due to the degradation and dissolution of organic matrix from the AGM shell by the treatment process. The remaining organic matrix in the treated shell was expected to be the un-removable organic matrix within the aragonite tiles [5-7]. The existence of organic matrix in both the virgin and treated shells were confirmed by the amide I absorption at 1630  $\text{cm}^{-1}$  [4,5], Figure 4-2B. The second decomposition with ~42 % weight loss at 600-800 °C was due to the liberation of carbon dioxide as calcium carbonate was thermally decomposed to calcium oxide. According to the results from

thermal and spectroscopic analyses, the treatment process removed organic matrix from the nacreous layer without altering the aragonite crystal as the Raman and FT-IR spectra of the treated shell are the same as those of the virgin shell, Figure 4-2.

**Table 4-1** Raman and FT-IR spectrum peak assignment of virgin and treated shells

[1-6].

Green mussel shell	Raman band (cm <sup>-1</sup> )	FTIR band (cm <sup>-1</sup> )
<b><i>Aragonite calcium carbonate vibration</i></b>		
in plane bending, $\nu_4$	703, 706 (m)	705, 708 (m)
out of plane bending, $\nu_2$	856 (w)	858 (w)
symmetric stretching, $\nu_1$	1089 (s)	1082 (m)
asymmetric stretching, $\nu_3$	1465 (w)	
combination band, $\nu_1+\nu_4$		1787 (s)
external lattice vibration	147 (m), aragonite 156 (s) 183 (w), aragonite 194 (w), aragonite 209 (s), aragonite	
O-H stretching from $\text{HCO}_3^-$		2520 (s)
<b><i>Protein vibration</i></b>		
amide I		1630 (s)
C-H stretching		2920 (m)

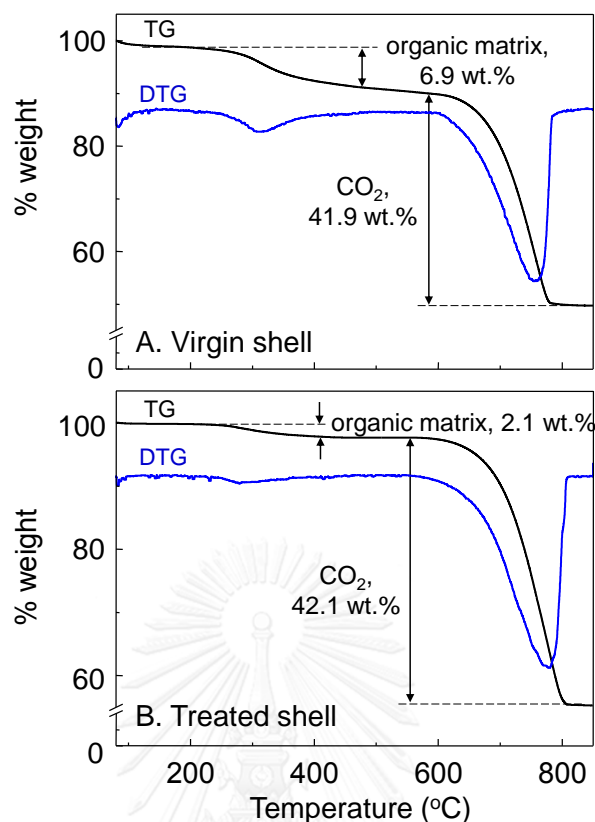


**Figure 4-3** Thermal gravimetric (TG) thermogram and the corresponding differential thermal gravimetric (DTG) thermogram of (A) virgin and (B) treated AGM shells.

SEM images of cross-sectioned shell in Figures 4-4A and 4-4B show characteristic stratified structure of the AGM shell where a distinct structural assembly of aragonite layers into a stratified structure is clearly observed. A single layer consists of aragonite tiles connected together. Based on the cross-sectioned and top-view SEM images, an individual pseudo-hexagonal aragonite tile has 3-5 micrometer bisector length and ~350-nm thick. The organic binding layers between aragonite layers are not noticeable in the SEM image (Figure 4-4A). This may be due to its extremely thin thickness of 20-30 nm [8-13]. A noticeable electrostatic charge up of the bombarding electron beam could be noticed in Figure 4-4A. After treatment, the organic layers were removed. A significant improvement in clarity of the SEM image with less electrostatic charge up in Figure 4-4B implied a disappearance of organic binder.

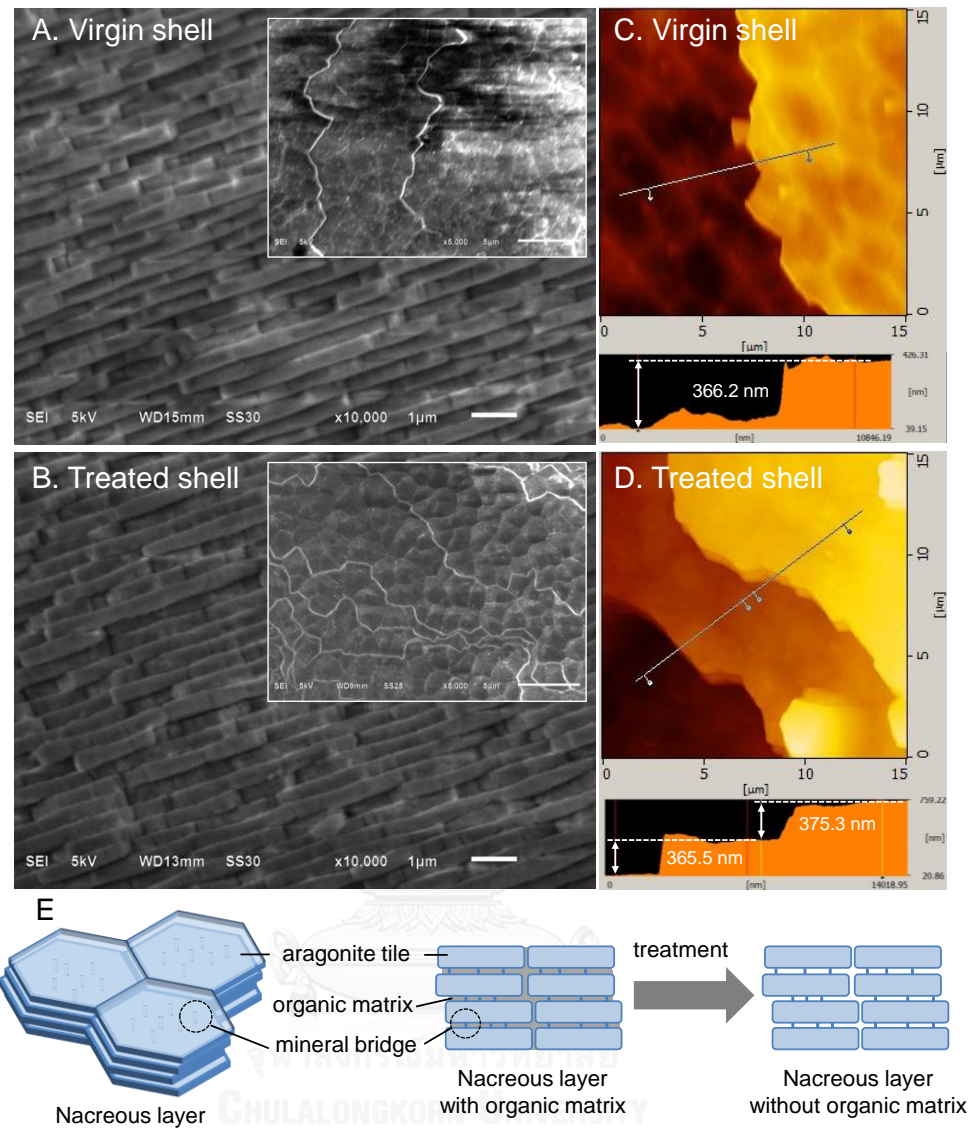


**Figure 4-4** Cross-sectioned SEM images of (A) virgin and (B) treated AGM shells (scale bar = 1 μm). The inserts are the corresponding top-view images (scale bar = 5 μm). The SEM images were acquired without a coating of conductive metals. The thickness of the aragonite layer is estimated from AFM images of (C) virgin and (D) treated AGM shells. (E) Schematic drawing of organic matrix removal in nacreous layer without alternation of aragonite building block.

To verify thickness and surface roughness of aragonite layers, surface topologies of stacked aragonite layers were probed by the AFM technique. AFM images in Figures 4-4C and 4-4D indicate an average thickness of the aragonite layer in virgin and treated shells are 366 and 370 nm, respectively. The average roughness ( $R_a$ ) of the treated and non-treated aragonite layers was 1.3 nm. The insignificant difference in thicknesses and similarity in surface roughness of the virgin and the treated shells suggested that the treatment process did not alter the original structure of the shell. The structural stability is may be due to the mineral bridges connecting between aragonite layers [11-13]. Figure 4-4E shows schematic drawing of nacreous assembly and related changes upon the alkaline/thermal treatment.

The existence of the air gaps were confirmed by the dye-diffusion experiments where the vacancies were filled with dyes and transparent liquid while the corresponding optical changes due to the incorporated liquids were monitored by an optical microscope (Figure 4-5). When the air gaps were filled with water (Figure 4-5C), the OM images of the water-filled shell were the same as those of the unmodified shell (Figure 4-5B). However, when the treated shells were filled with red rhodamine 6G (R6G, Figure 4-5D) and methylene blue (MB, Figure 4-5E), the characteristic colors of the dyes was enhanced under the dark field illumination. The expressions of the colors were due to the multiple reflection within the stratified bilayers under the oblique angle of incidences as the radiation was coupled into the structures via the dark field illumination. These results implied the existence of air gaps after the organic matrix removal. The OM images of the dye-filled shells under the bright field illumination were similar to those of the un-modified shell. A slight variation of the color expression in bright field illumination in Figures 4-5B-4-5E was due to the minor interference of the reflection beyond the first layer. A pale color of the incorporated dyes observed under the bright field illuminations in Figures 4-5D and 4-5E is due to the interference of reflectance beyond the surface. Since the water soluble dyes can be efficiently trapped within the generated air gaps (i.e., the dyes remain within the treated shells after a multiple washing), the treated shells with nanometer size air gaps can be employed as solid encapsulation media.

In the case of the virgin shell, the dye cannot diffuse into the organic layers, even when the shell was ground into small pieces (data does not show). The structural stability of the shell is very excellent as an insignificant change was observed after an hour of boiling in hot water. However, some dye can be adsorbed onto the surface of the untreated shell. As a result, color expression of the virgin shell under the bright field illumination was similar to that of the dark field illumination since the observed color was due to the adsorbed dye on the surface.

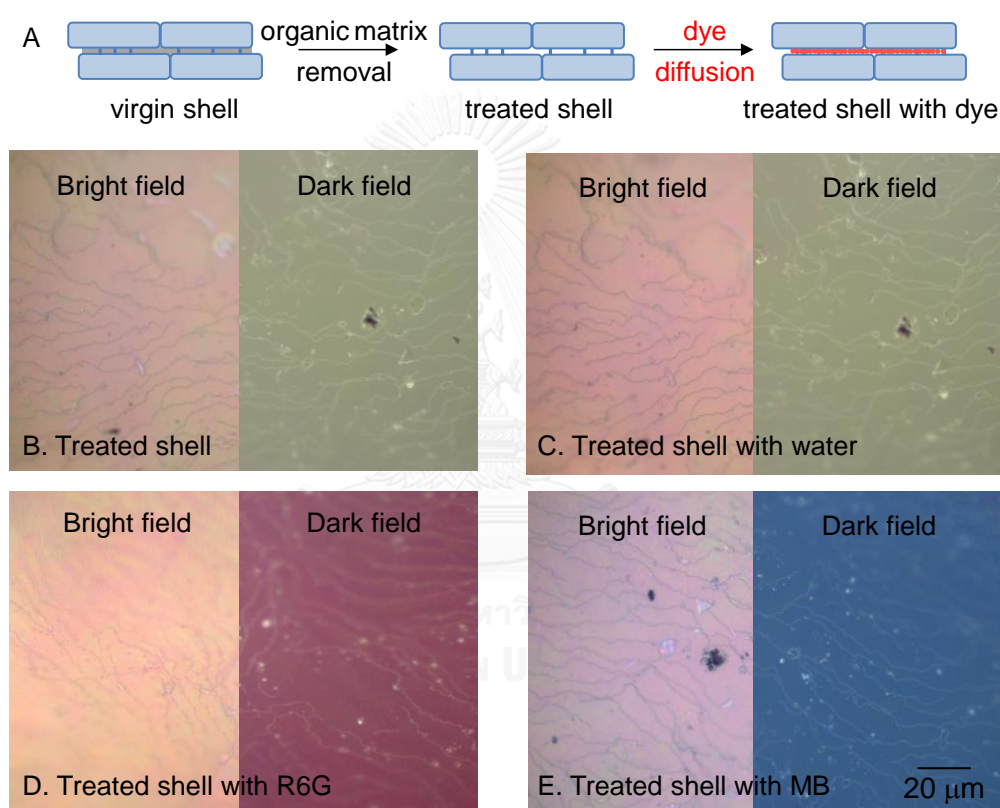


**Figure 4-5** (A) Schematic drawing of dye diffuses into the treated AGM shell structure. (B) OM images (500X magnification) of treated shell under bright field and dark field illuminations. The corresponding OM images with water-, R6G-, and MB-filled air gaps are shown in C, D, and E, respectively.

The generated air gaps after the removal of organic layers significantly affect the optical expression of the treated shell as observed in Figure 4-1. The air gaps increased the difference in reflective indices at the interface of the aragonite layer ( $n=1.6$ ) as the organic binder layer ( $n=1.5$ ) was replaced by air ( $n=1.0$ ). To theoretically verify the effect of air gaps on the observed pearlescent colors, the modified transfer matrix method was employed for the calculation of the reflectance. A schematic representation of the interaction between incident light and nacreous layer is shown in Figure 4-6. The virgin shell is the stratified bilayers consisting of aragonite calcium carbonate layers (thickness=200-500 nm,  $n=1.6$ ) and organic binding layers (thickness=20-30 nm,  $n=1.5$ ) [3, 11-13]. According to the result in Figure 4-4, the treated shell consists of the same aragonite layers separated by air gaps ( $n=1.0$ ) of the same thickness as that of the organic layers.

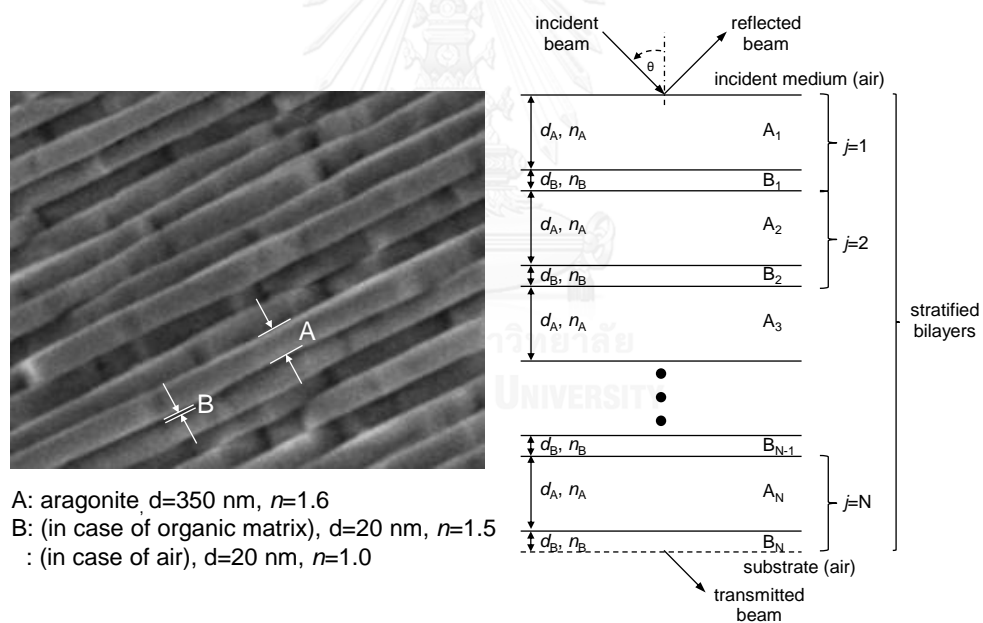
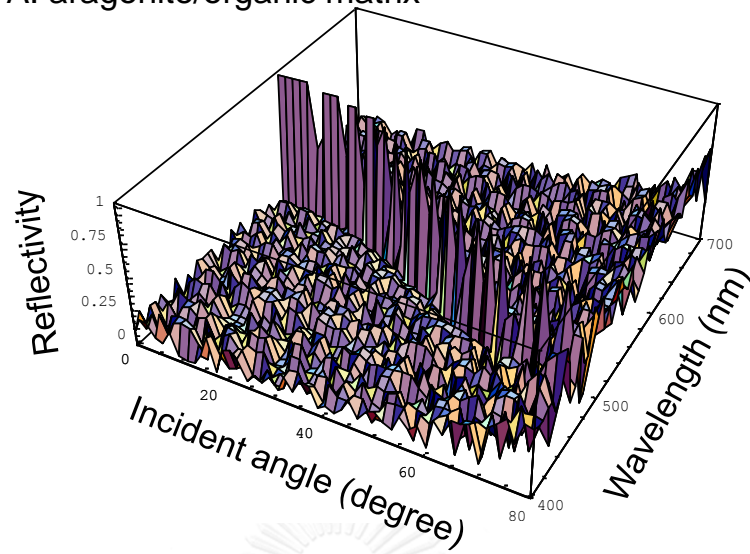


**Figure 4-6** A cross-sectioned SEM image of AGM shell and the corresponding schematic representation of stratified bilayers. The thicknesses and reflective indexes of the stratified layers were adopted from our experimental results and literatures [3, 11-13]. The aragonite layers, organic binder, and air gaps were assumed non-absorbing in the visible region (i.e., absorption coefficient  $k=0$ ).

A. aragonite/organic matrix



B. aragonite/air

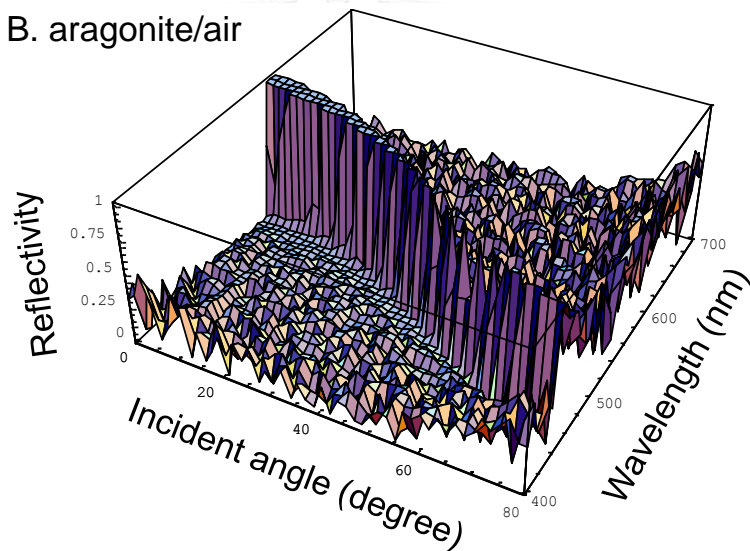


**Figure 4-7** 3D plots of angle dependent reflection spectra of stratified bilayers representation of (A) virgin and (B) treated shells. The following parameters were employed:  $n_A=1.6$ ,  $n_B=1.5$  (organic matrix) or 1.0 (air),  $d_A=350$  nm,  $d_B=20$  nm,  $N=1,000$  bilayers,  $\theta = 0^\circ-80^\circ$  and  $\lambda = 400-700$  nm.



Figure 4-7 shows 3D plots of angle dependent reflection spectra of a virgin shell consisting of alternative aragonite layers (350 nm thick) and organic binder layers (20 nm thick) and the corresponding treated shell consisting of alternative aragonite layers (350 nm thick) and air gaps (20 nm thick) with  $N=1000$ . When a white light ( $\lambda = 400\text{-}700$  nm) is impinged on the virgin shell with a normal angle of incidence ( $\theta=0^\circ$ ), the reflection spectrum showed a predominant total reflection band centered at 589 nm (FWHM=6.4 nm). The band indicated a selective reflection of yellow color of the incident white light. Since all components of the stratified layers are transparent with zero extinction coefficient ( $n_{CaCO_3}=1.6$ ,  $k_{CaCO_3}=0$ ,  $n_{protein}=1.5$ ,  $k_{protein}=0$ ), the selective reflection is originated by the interference within the stratified bilayers. The reflection band blue shifts (i.e., with 589-460 nm reflection maxima) as the angle of incidence was increased from  $0^\circ$  to  $80^\circ$ . The blue shift of the angle dependent reflection is the origin of pearlescent phenomenon (i.e., the color at a particular spot changes with the angle of incidence) observed in nacreous materials such as green mussel shells, pearls, mother-of-pearl, and abalone shells [3, 14-16].

In case of the treated shell, the organic binder was replaced by the air gaps of the exact same thickness. The pearlescent phenomenon as that observed in the virgin shell was also observed but with a more vivid color and greater intensity. A greater blue shift (with reflection maxima of 590-440 nm) and a wider FWHM of the reflectivity shown in Figure 4-7B support the more vivid visual observation in Figure 4-1B. With a normal incidence ( $\theta=0^\circ$ ), a 4-time more intense reflectance is expected from the treated shell compared to that of the virgin shell as indicated by an increase of the FWHM from 6.4 nm to 25.1 nm.

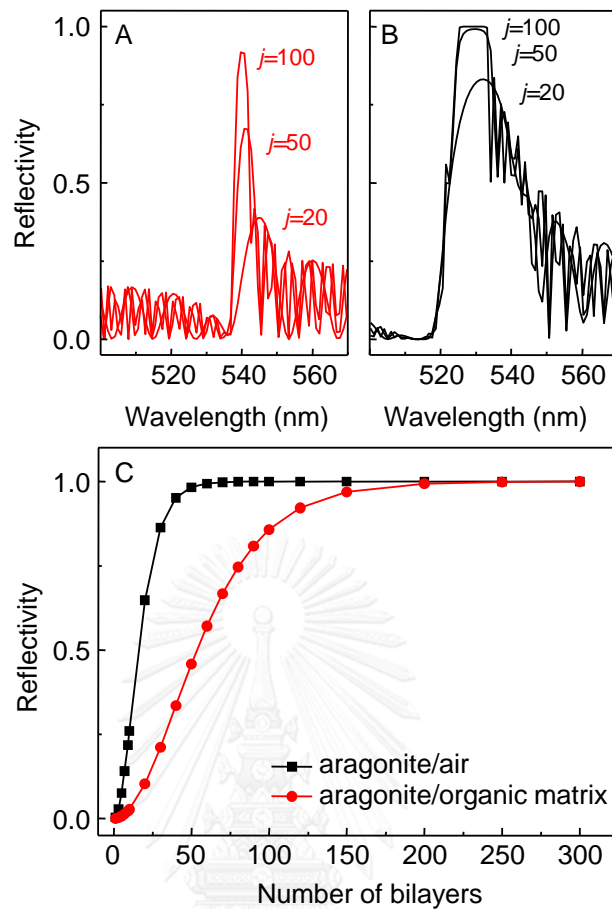


**Figure 4-8.** Calculated reflectivity of (A) aragonite/organic matrix, (B) aragonite/air stratified layers of various thicknesses, and (C) the reflectivity as a function of number of bilayer: (square) aragonite/air, (circle) aragonite/organic matrix. The reflectivity was measured at the reflection maxima. The simulation parameters are:  $n_A=1.6$ ,  $n_B=1.5$  (organic matrix) or 1.0 (air),  $d_A=350$  nm,  $d_B=20$  nm, and  $\theta=40^\circ$ .

The influences of the number of bilayers on the pearlescent effect were also investigated. As indicated by the reflectivity plots in Figure 4-8, at an incident angle of  $40^\circ$ , the reflectance of the treated shell reaches total reflection ( $R=1$ ) with the number of bilayers of 50. The reflectance of the virgin shell, on the other hand, reaches the total reflection with a number of bilayers of 200. Moreover, the FWHM of the total reflection band in the reflection spectrum of the treated shell was 3-time broader than that of the virgin shell ( $\theta=40^\circ$ ). The simulated results confirmed a

brighter and more vivid color of the pearlescent effect observed in the treated shell (i.e., a wider range of blue shift and broader FWHM) compared to those of the virgin shell.

#### 4.2 Selective colors reflection from stratified aragonite calcium carbonate plates of shell

The flakes from AGM shells were used as a model material for our study on color expression of the nacre structure. The pearlescent effect of a virgin AGM shell originated by an interaction between light with nacre is shown in Figure 4-9A. . To acquire the structural information of the shell, we recorded SEM images across the thickness of the AGM shell. The cross-sectioned SEM images in Figure 4-9C show a gradual increment of the thickness of aragonite plates as they aged (i.e., the thickness increases toward the outside layers).

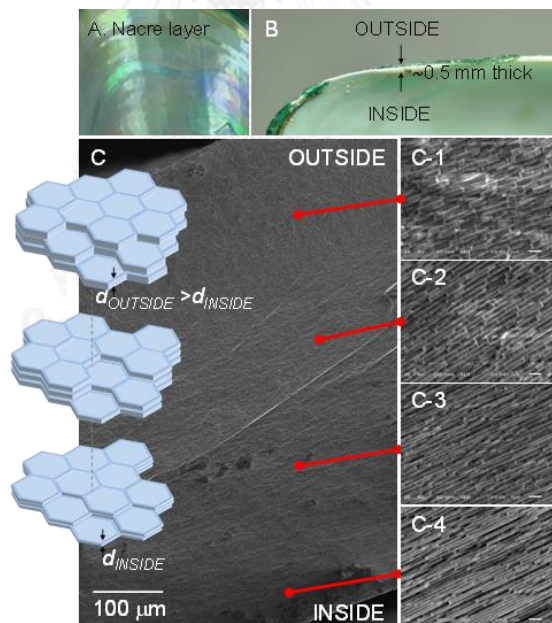


**Figure 4-9.** (A) Pearlescent colors of AGM shell. (B) Thickness of AGM shell. (C) A cross-sectioned SEM images of AGM shell. The detailed SEM images across the thickness (C1-C4) show a gradual thickness increment of the aragonite plates from the inner layers towards the outside layers. The scale bars indicate 1 μm.

After the removal of organic matrix, the treated shells showed stronger reflection with more vivid colors compared to the virgin shells. The shells became brittle and easily broken into small fragments (i.e., the pearlescent flakes). Due to scattering effect, the pearlescent flakes appeared white to the naked eyes (Figure 4-10A) but expressing vivid colors at normal angle of OM (Figure 4-10B) The SEM images suggest that the pearlescent flake is in fact an alternated stack of aragonite layers and air gaps [17]. The removal of organic binder with a consecutive development of air gaps was confirmed by TGA analyses (Figure 4-11). The 200-to-500-nm-thick aragonite layer is a single ply assembly of 3-5  $\mu\text{m}$  bisector length pseudo-hexagonal aragonite plates, Figures 4-9.

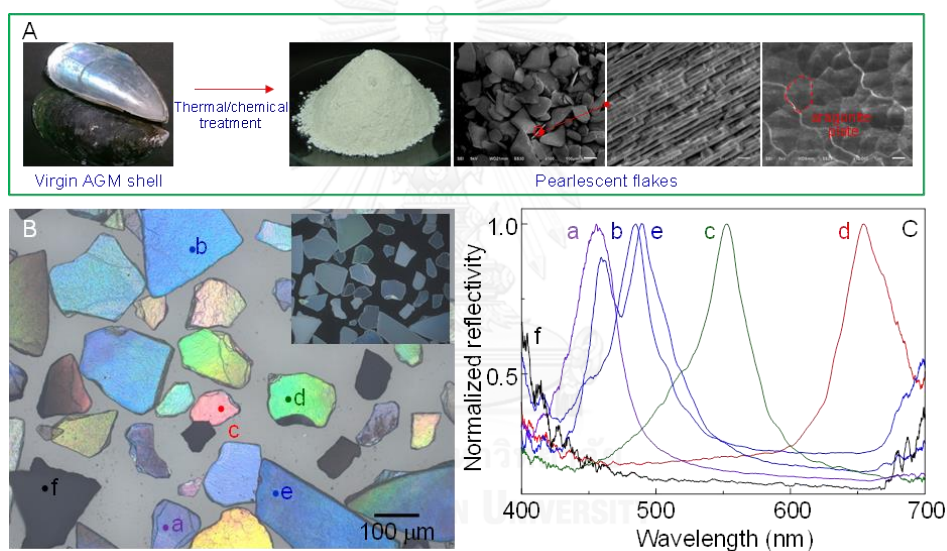


**Figure 4-10.** (A) SEM images of pearlescent flakes. The flakes are stratified bilayers of aragonite layers and air gaps. The flakes appear white to the naked eyes. (B) OM image of pearlescent flakes under a bright-field illumination (10X objective). The inset shows the corresponding dark-field illumination image. (C) Reflection spectra of selected pearlescent flakes acquired by coupling the reflected light into a fiber optic spectrometer via a 50X objective.

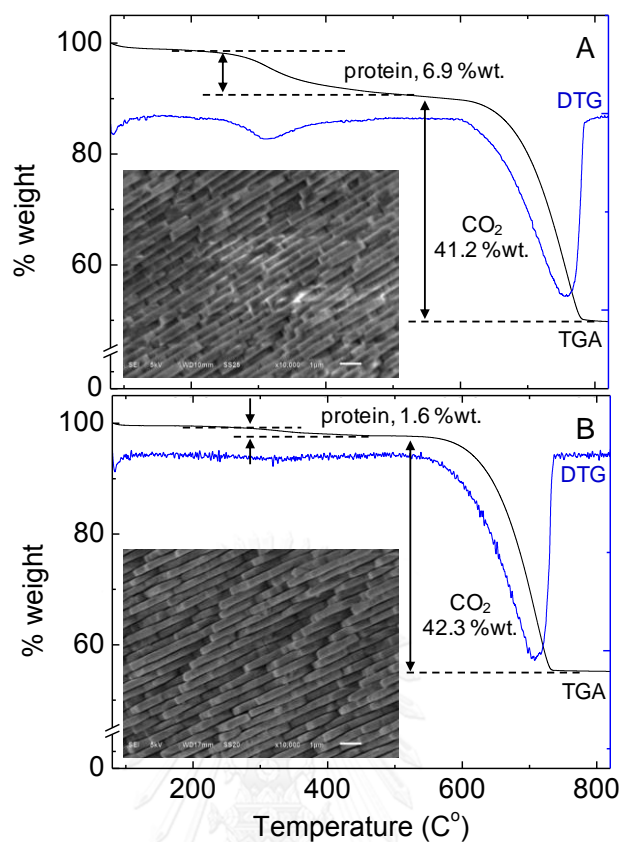


**Figure 4-11.** TG and DTG curves of (A) AGM shell and (B) pearlescent flakes and their corresponding cross-sectioned SEM images. The thermal analyses results indicated a removal of organic binding layers between aragonite layers. The remaining organic binder (1.6 % wt.) is expected to be those within the aragonite plates [7]. The SEM images confirm the removal of the organic binder layers. Air gaps could be noticed in Fig. S3B. The significant reduction of the electron charge up in SEM image in Fig. S3B compare to that in Fig. S3A corroborate the removal of the organic binding layer [11].

Figure 4-10B shows OM image of pearlescent flakes while Figure 4-10C shows the corresponding reflection spectra of selected pearlescent flakes. Although, the flakes were white powder when observed by the naked eyes, the vivid colors appeared under an OM. The strong and narrow reflection spectra corresponded to the expressed colors under OM. The purple-blue, blue, green and red pearlescent flakes show spectra with reflection maxima at 457, 485, 553, and 654 nm, respectively.

In Figure 3B, the aragonite flake ‘f’ appears dark while its corresponding reflection spectrum in Figure 3C was rough across the visible region as the flake does not reflect any incident radiation. The corresponding SEM images (Figure 4-12) suggest that the flake was fragmented from the outer part of the shell where the aragonite plates are irregularly thick with highly rough surface.

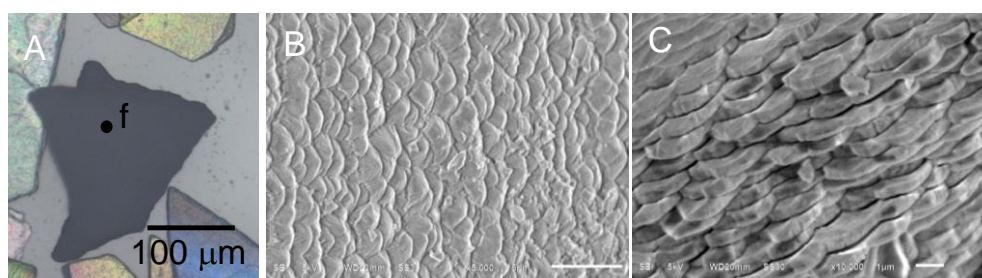


**Figure 4-12.** (A) The flake ‘f’ (from OM image of Figure 4-10B) does not express any color due to its structure architecture. (B and C) SEM and cross-sectioned SEM image of flake ‘f’.

The pearlescent flakes with blue, green, and red were selected for further detailed investigation (Figure 4-13). As indicated by the OM images and the corresponding SEM and AFM images (Figures 4-13A-4-13I), the aragonite plates of the flakes expressing blue, green, and red colors with reflection maxima at 441, 523, and 577 nm have thickness of  $256 \pm 10$ ,  $310 \pm 12$ , and  $353 \pm 10$  nm, respectively. The histogram in Figure 4-13J suggests that the pearlescent flakes expressing single vivid color composed of aragonite layers having narrow thickness distribution. When the thicknesses were employed for spectral simulations, the calculated spectra agreed very well with the experimentally measured spectra (Figure 4-13K). The results in Figure 4-13 confirm that the thickness of transparent aragonite layers govern the expressed colors of the pearlescent flakes.

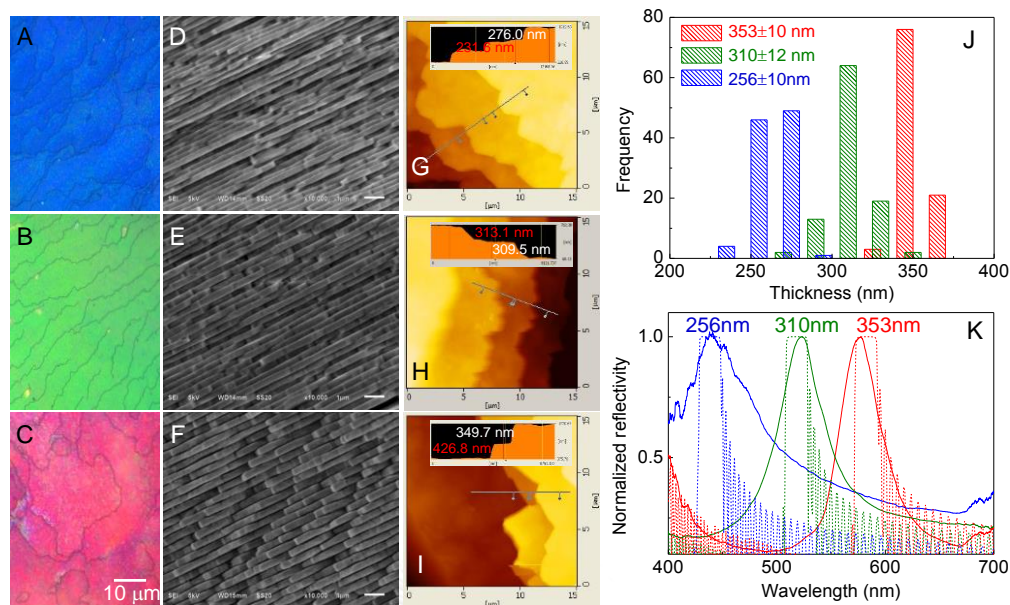


**Figure 4-13.** OM, cross-sectioned SEM and AFM images of pearlescent flakes expressing colors: (A, D, G) blue, (B, E, H) green, and (C, F, I) red. Histogram (J) show thickness distribution of aragonite layers within the colored pearlescent flakes. (K) Comparisons of experimental (solid line) and calculated (dash line) reflection spectra of pearlescent flakes. The experimentally measured thicknesses were employed for the calculations.

To calculate the reflection spectra of pearlescent flakes expressing blue, green, and red colors, the thickness of the aragonite layers were assigned according to the experimental results shown in Figure 4 with a refractive index of 1.6 ( $n_A=1.6$ ). The air gaps ( $n_B=1.0$ ) with 20 nm thick assumed [17]. At an incident angle perpendicular to the stratified layers, the calculated reflection spectrum with aragonite thicknesses of 256, 310, and 353 nm showed reflection peaks centered at 439, 519 and 583 nm, respectively, Figure 4-13K. The calculated spectra agreed very well with the experimentally measured spectra (Figure 4-13K). Since the flake was constructed from transparent aragonite layers and air gaps, the interaction between incident light and structural architecture of the flake (i.e., aragonite thickness, air gap thickness, and number of layer) induced color selective reflection spectrum. The noticeable broader

reflection peaks in the experimentally measured spectra in Figure 4-13K were expected to originate from a non-uniform thickness and surface roughness aragonite plates.

The uniform blue and green colors of aragonite flake with rough surfaces (Figures 4-14A and 4-14B) suggest that the number aragonite layers did not alter the color expression. We employed spectral simulation to verify this experimentally observed phenomenon. The thicknesses of aragonite plates were assigned to 256 nm for the blue pearlescent flakes and 310 nm for the green pearlescent flakes. As the number of bilayers was increased from 1 to 120 bilayers, the reflected intensity was increased with a concomitant blue-shift of peak position. The color-selective reflection of the transparent aragonite layers was noticeable at 5-bilayer with ~50% reflectivity of the incident light (Figures 4-14C and 4-14D). Interestingly, the total reflection was achieved when the number of the aragonite layer was greater than 30 layers (Figure 4-14E). As a result, a thick pearlescent flake composes of aragonite plates of narrow thickness distribution expresses its unique color. As shown in Figure 4-14, aragonite flake with 256 nm thick plates selectively reflect blue color ( $\lambda_{\max}=439$  nm) while that with 310 nm plates selectively reflect green color ( $\lambda_{\max}=519$  nm) across their rough surfaces.



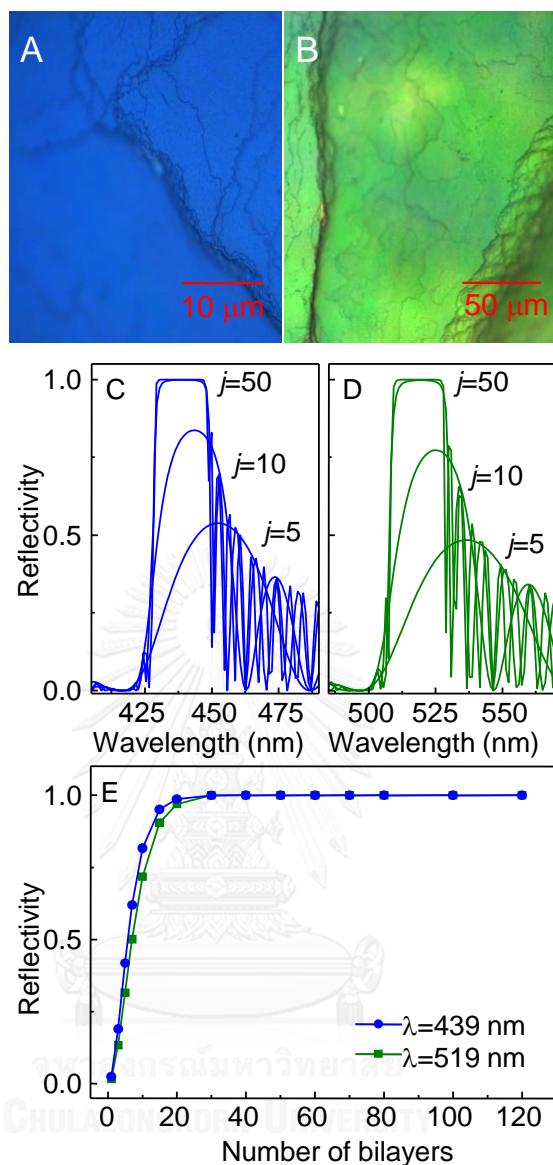


**Figure 4-14.** OM images of pearlescent flake selectively reflect (A) blue and (B) green colors. The flakes show thickness variation across the surfaces but expressing uniform colors. Calculated reflection spectra of stratified bilayers of (C) the blue pearlescent flakes ( $d_A=256$  nm) and (D) the green pearlescent flake ( $d_A=310$  nm). The thickness of the air gap was assumed 20 nm. (E) The reflectivity-number of bilayer plot for blue and green flakes. The total reflection (color saturation) was achieved after a 30-bilayer.

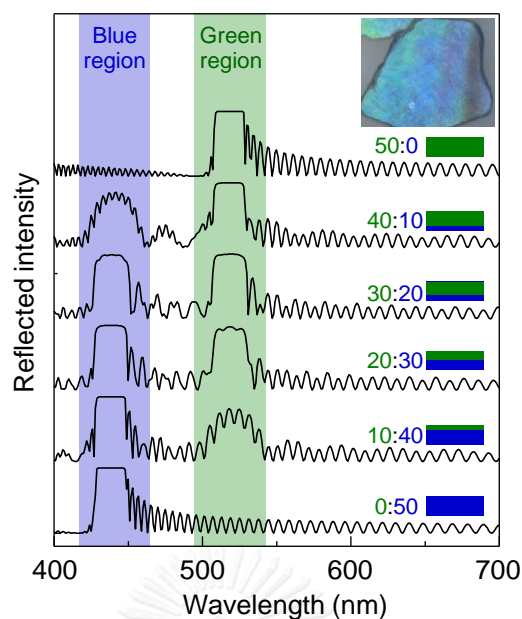


**Figure 4-15.** Calculated reflection spectrum of a 50-bilayer flake with different ratio of 256-nm aragonite layer (expressing blue color) and 310-nm aragonite layer (expressing green color). The inset OM image shows an experimentally observed pearlescent flake expressing both blue and green colors.

According to the spectra in Figure 4-13K, a flake with a certain thickness of aragonite layer selectively reflect a particular color. The pearlescent flake shows red-shifted reflecting color as the thickness of aragonite layer increases. In the experimental observation, flakes with multicolor were frequently observed (Figures 4-9 and 4-15). To gain an insight understanding of the phenomenon, we performed spectral simulation on pearlescent flake containing aragonite layers with two different thicknesses (i.e., 256 nm and 310 nm). We calculate spectra of a flake containing 50-bilayer with various combinations on the number of layers from each aragonite. Although the thin 256-nm layer was covered by a thick 310-nm layer, the blue reflection could be observed since the green reflection spectrum is transparent in the blue reflection. The blue reflection became more intense as the number of the 310-nm layer decreased. The results from Figure 4-15 suggest that the multicolor expression of a pearlescent flake is due to the thickness variation of the aragonite layers within the flake.

### 4.3 Individual aragonite plates from nacre of shells

The brick-and-mortar like structure of nacre of AGM shells including abalone and pearl oyster shells could be disintegrated to individual  $\text{CaCO}_3$  microplates while preserving original plate-shape structure. Figure 4-16 shows disintegration of AGM nacre to  $\text{CaCO}_3$  microplates. After treatment,  $\text{CaCO}_3$  microplates showed vivid glittering reflection in water under laboratory lighting condition (photographic image in Figure 4-16). SEM images of nacre and  $\text{CaCO}_3$  microplates after treatment are shown in Figure 4-17. The glittering reflection indicated micron size  $\text{CaCO}_3$  plates with flat surfaces. Since the selected sea shells comprised nacre with stratified layer of aragonite plates and organic matrices, we hypothesized that the disintegrated  $\text{CaCO}_3$  microplates were aragonite polymorph [11, 17-22].

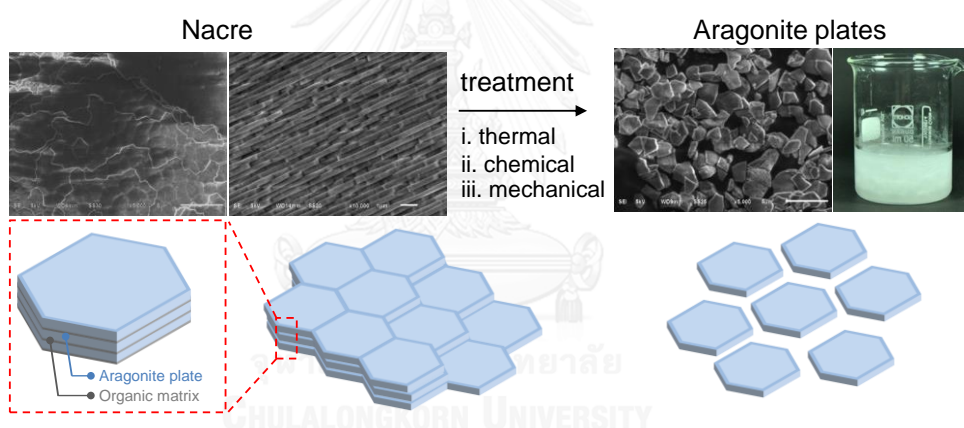


**Figure 4-16.** A schematic illustration shows a fragmentation of nacre into individual aragonite plates. The plates dispersed very well in water while expressing vivid glittering reflection.

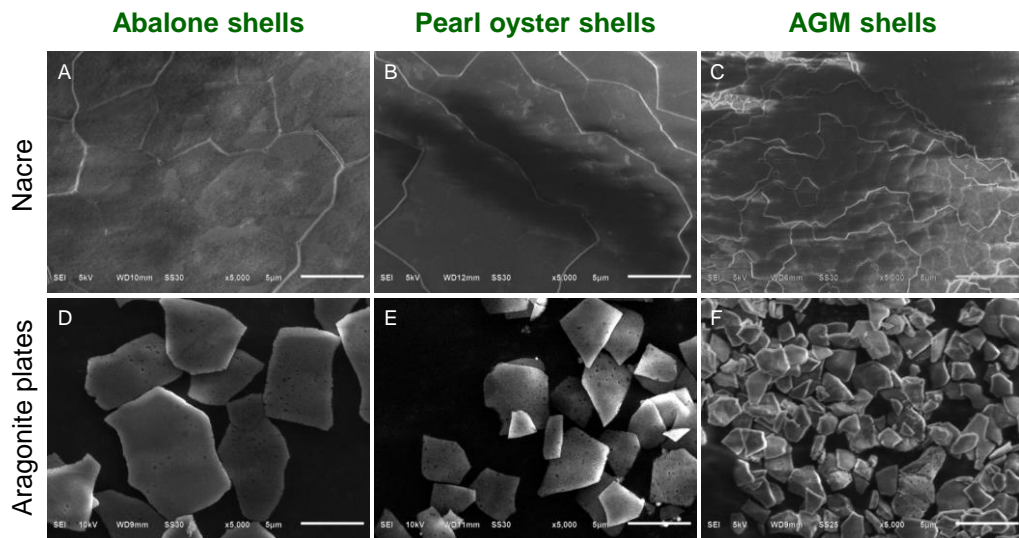


**Figure 4-17.** SEM images of nacre and aragonite plates from (A, D) abalone, (B, E) oyster, and (C, F) AGM shells, respectively.

The OM images under bright-field and dark-field illuminations of  $\text{CaCO}_3$  microplates from nacre of abalone, pearl oyster, and AGM shells are shown in Figures 4-18A-4-18C. The plates under the bright-field illumination show colorful reflection while those of individual plates under dark-field illumination show transparent appearance. The size and size distribution of  $\text{CaCO}_3$  microplates were investigated by SEM. The significant difference in average bisector-length of  $\text{CaCO}_3$  microplates from abalone, pearl oyster, and, AGM shells, respectively, were  $7.3 \pm 1.2$ ,  $5.2 \pm 1.0$ , and  $3.1 \pm 0.5$   $\mu\text{m}$  (as indicated by the histograms) while the average thickness of  $\text{CaCO}_3$  microplates from abalone, pearl oyster, and AGM shells were  $454 \pm 73$ ,  $360 \pm 33$ , and  $344 \pm 85$  nm, respectively, as determined from cross-sectioned SEM images (data does not show). The microplates showed flat surface with minor defect indicated as small holes. The small holes on the surface of microplates might be due to the disengagement of nanoparticles [20-22] during treatment process. The holes were observable in both SEM and AFM images. The slightly difference of average roughness ( $R_a$ ) of aragonite plates acquired from different sea shells over  $1 \times 1$   $\mu\text{m}^2$  were also observed by AFM technique.

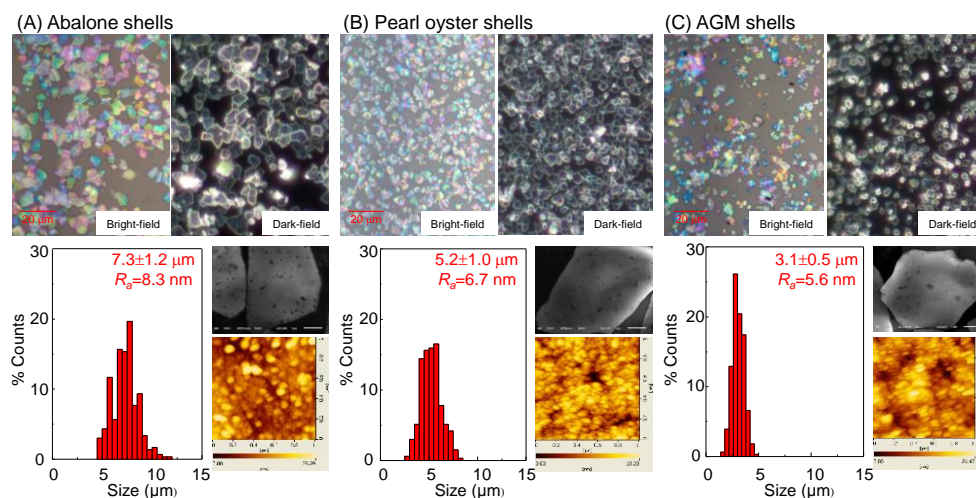


**Figure 4-18.** OM images under bright-field and dark-field illuminations, histogram of size distribution, SEM micrograph, and AFM images of aragonite plates from (A) abalone, (B) pearl oyster, and (C) AGM shells.

The thermogravimetric (TG) and the corresponding differential thermogravimetric (DTG) curves of  $\text{CaCO}_3$  microplates in Figure 4-19 show two major weight losses. The first weight loss at 200-300 °C was due to the organic matrices decomposition. An insignificant difference of organic contents remaining in the  $\text{CaCO}_3$  microplates from abalone, pearl oyster, and AGM shells were observed. The second decomposition with  $\sim 42$  % weight loss at 600-800 °C was due to the liberation of carbon dioxide as  $\text{CaCO}_3$  was thermally decomposed. The residual organic contents in  $\text{CaCO}_3$  microplates were expected to be the organic matrices within the  $\text{CaCO}_3$  microplates.

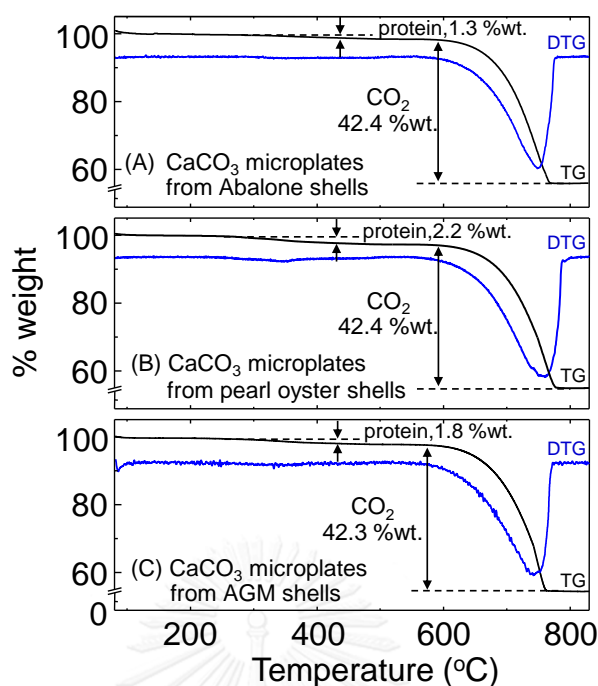


**Figure 4-19.** TG curves and the corresponding DTG curves of  $\text{CaCO}_3$  microplates from (A) abalone, (B) pearl oyster, and (C) AGM shells.

Figure 4-20 shows Raman spectrum of nacre from abalone, pearl oyster, and AGM aragonite plates. The characteristic vibrations including out-of-plane bending ( $\nu_2$ ) at  $856\text{ cm}^{-1}$ , symmetric stretching ( $\nu_1$ ) at  $1089\text{ cm}^{-1}$ , and asymmetric stretching ( $\nu_3$ ) at  $1465\text{ cm}^{-1}$  indicated carbonate compound. The unique external lattice vibration at  $147, 156, 183, 209\text{ cm}^{-1}$ , and a doublet at  $703$  and  $706\text{ cm}^{-1}$  indicated carbonate specie of aragonite polymorph [1,17,23-25]. The results from SEM, AFM, TGA, and Raman spectroscopy suggested that the treatment process could efficiently remove organic matrices from the nacre without destroying aragonite plates.

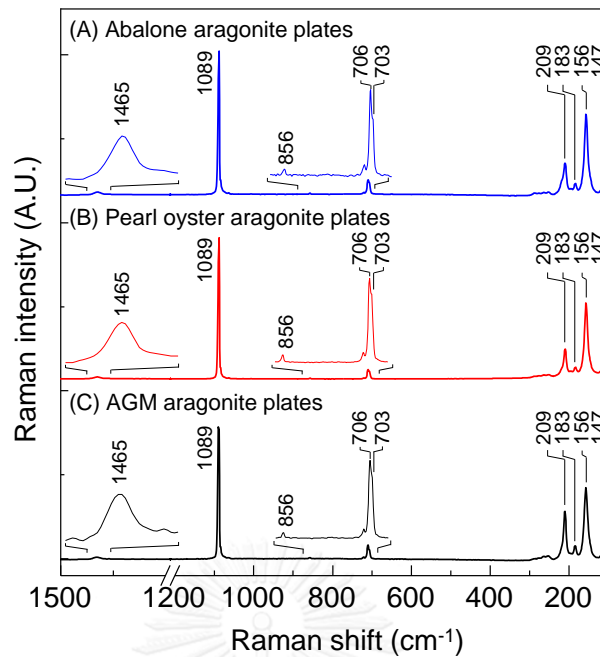


**Figure 4-20.** Raman spectra of aragonite prepared from (A) abalone, (B) pearl oyster, and (C) AGM aragonite plates.

The OM images in Figure 4-18 and enlarged OM images in Figure 4-21A show aragonite plates in various colors as the plates selectively reflected certain range of white light. This phenomenon could be distinctively observed from aragonite plates of abalone shells (OM images in Figure 4-21A) due to a larger size of the microplate. As the OM images under dark-field illumination (Figure 4-18) showed transparent appearance, the observable colors were due to the interference of light with the transparent aragonite plate bounded by air (air/aragonite plate/air). The interference colors were attributed to reflective index of matters, angle of incidence, and thickness of stratified layers. In this experiment, the influence of aragonite thickness, air gap (space between aragonite plate and substrate) thickness, and angle of incidence on the colors expression were verified using the transfer matrix method. In the simulation algorithm, an incident radiation of wavelength  $\lambda$  at the range of 400-700 nm impinged on the aragonite plate under air/aragonite plate/air/glass configuration as illustrated in Figure 4-21A. An air layer over aragonite plate was assigned as an indecent medium while the substrate was glass slide ( $n=1.5$ ). All layers were assumed

transparent. (i.e., the aragonite calcium carbonate does not absorb visible light). The contour plot of reflectance as a function of aragonite thickness are shown in Figure 4-21B. In the calculation, the incident white light was irradiated at a normal angle and the air-gap thickness 50 nm was assumed. The aragonite plate in the thickness range of 350-550 nm which was the natural range of aragonite plates within nacre was assumed. The contour plot showed red-shift when the thickness of the aragonite plate was increased, Figure 4-21B. According to the assigned thickness range of aragonite plates (i.e., 350-550 nm), the reflected color cover the entire visible region. These results indicate that the thickness of aragonite plate played the major role on the color expression. Figure 4-21C shows contour plot of reflectance as a function of air-gap thickness. The incident radiation impinged on the aragonite plate with a thickness of 450 nm at the normal angle. When the thickness of air gap was increased, the reflectivity increased with a slight red-shift of reflection spectra. These results indicated that the air gap between an aragonite plate and a substrate dictated the reflectivity of the reflected color. A contour plot of reflectance as a function of angle of incidence is shown in Figure 4-21D. The blue-shift with slight increment of reflectivity was observed when an angle of incidence was increased. According to the simulation results, the observed reflection color from aragonite plate in Figure 4-18 and enlarged OM images in Figure 4-21A (i.e., blue, green, yellow, red) were originated from selective reflection of aragonite plates with the existing air gap under the plates. Moreover, the variation colors from an aragonite plate were due to the non-uniform surface roughness of the plate. As the calculation results from the color expression as a function of aragonite plate thickness (Figures 4-21B) showed a reflection maxima shift for  $\sim 1.2$  nm when the thickness of an aragonite plate was change for 1 nm, the average surface roughness of an abalone aragonite plate with the surface roughness of 8.3 nm ( $R_a$  from AFM image of Figure 4-18A) induced reflection maxima shift for  $\sim 10$  nm.



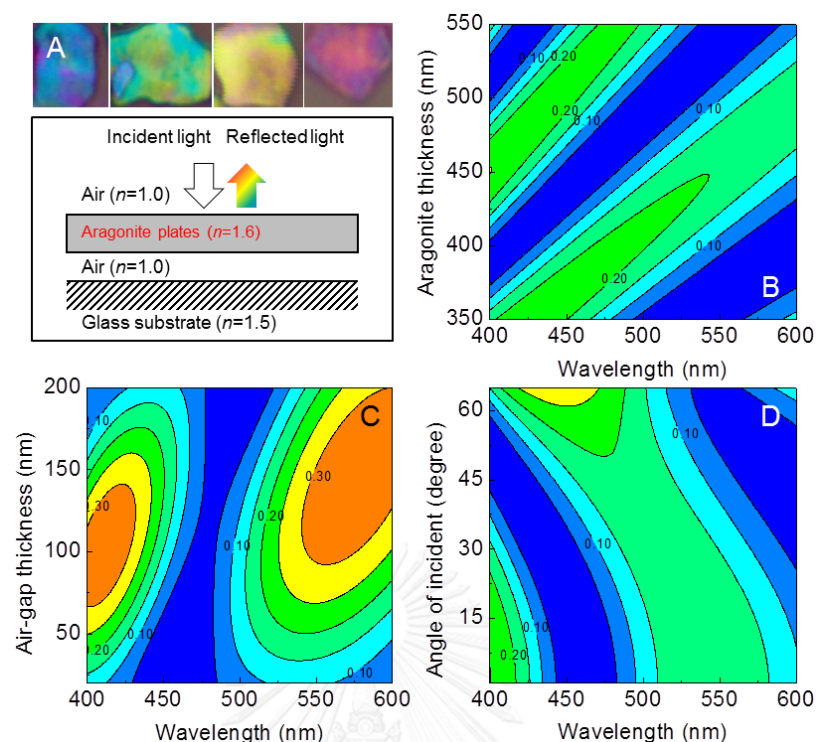


**Figure 4-21.** (A) OM images of abalone aragonite plates on glass substrate and a schematic representation of the reflection of light on the aragonite plate. The color-selective selection is governed by the aragonite thickness, air-gap thickness, and the angle of incidence. Contour plots of reflectance from an aragonite plate on a glass substrate as a function of (B) aragonite thickness, (C) air-gap thickness, and (D) an angle of incidence.

To further verify the effect air gap on the reflectivity of aragonite plate, the air-gap layer was replaced by ethylene glycol (EG,  $n=1.45$ ). The OM images in Figures 4-22 shows more vivid color of aragonite plates with air gap (Figure 4-22B) compared with aragonite plate with EG (Figure 4-22A). The calculation results confirmed that the reflectivity of aragonite plate with air gap (open circles) was stronger than that of aragonite plate with EG-filled gap (filled squares), Figure 4-22C. The calculation results corroborated visual observation as the reflectivity of aragonite plate was governed by the air gap between aragonite plate and a substrate.

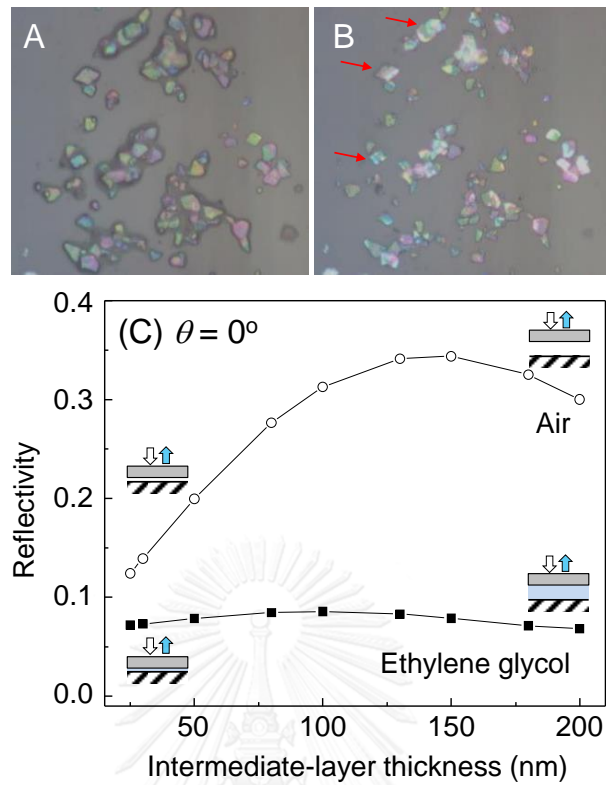


**Figure 4-22.** (A) OM images of abalone aragonite plates on a glass substrate with EG-filled gap between an aragonite plate and glass substrate. (B) OM images of abalone aragonite plates on a glass substrate after the evaporation of EG. (C) Reflectivity plots ( $\lambda = 550$  nm) as a function of the thickness of the medium between the aragonite plate and the glass substrate: air (open circles) and ethylene glycol (filled squares).

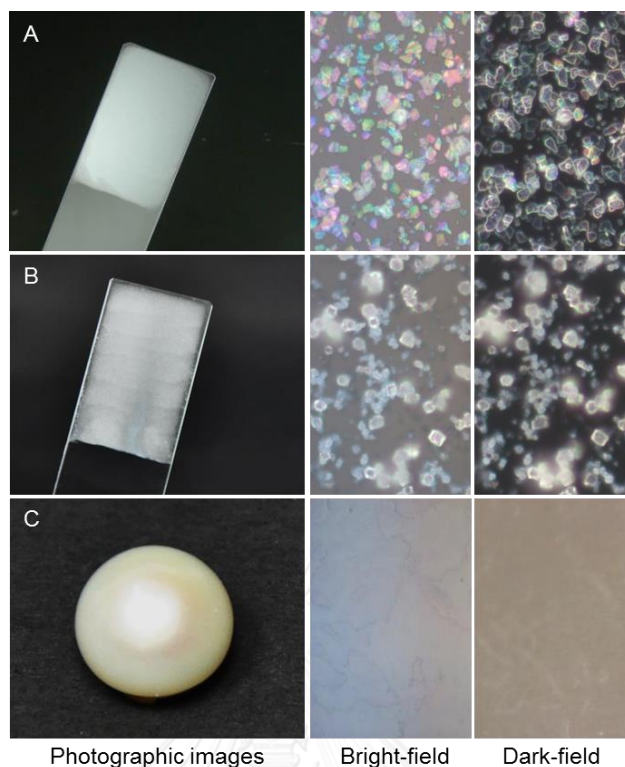


**Figure 4-23.** Photographic images and the corresponding bright-field and dark-field illuminated images of (A) aragonite plates, (B) precipitated calcite  $\text{CaCO}_3$ , and (C) pearl.

As the micro size with flat surface of aragonite plates provided strong reflection, the aragonite plates could be used as a surface coating pigment. The appearance of aragonite-plate-coated surface showed color and luster like pearl (Figure 23A) while that of precipitated calcite  $\text{CaCO}_3$  showed white color reflection surface (Figure 23B). However, the reflection intensity and the colors variety from the aragonite plates were smaller than those of synthetic pearlescent pigment (Timiron starlight red; metal-oxide-coated mica) (data does not show) as surface roughness of mica shows highly flat surface compared with that of aragonite plate. Moreover, this natural coating pigment was produced from the eco-friendly process which the raw materials from seafood industry were abandoned.

## CHAPTER V

# CONCLUSIONS

This work has provided the insight understanding of pearlescent effect expressed from AGM shell and exploited the benefit of its structure and optical properties in several applications that have not been reported before. As the research topics in this work were mainly derived into 3 parts, this work could be concluded that:

1. The pearlescent effect of Asian green mussel shells can be enhanced by the replacement of organic binding layers with air gaps. A consecutive alkaline/thermal treatment could efficiently remove the organic binding layers without altering the structure of the aragonite layers assemble. The theoretical simulation corroborated the enhanced pearlescent effect by the air gaps as greater reflectance and a broader spectral coverage were achieved after organic matrix removal
2. The pearlescent flakes prepared from AGM shells express vivid color when viewing under an optical microscope. The unique structural architecture of this material containing transparent aragonite layers and air gaps enabled a color selective reflection under a bright-field illumination. The results from spectral simulation confirm the governing function of the structural architecture (i.e., aragonite thickness and number of aragonite layer) over the expressed colors. The flakes with thin aragonite layers selectively reflected short wavelength (i.e., blue color) while those with thicker layers reflected longer wavelengths (i.e., red-shifted colors). The AGM shells reflect multiple colors as they contain aragonite layers with various thicknesses.
3. We successfully developed simple technique to disintegrate nacre of sea shells (i.e. abalone, pearl oyster and AGM shells) into aragonite plates while retaining the structure and the polymorphism. The aragonite plates express unique pearlescent colors as it selectively reflect certain range of white light. The different reflected colors of aragonite plates were depended on their thickness while the reflected intensity was depended on the air gap between

aragonite plate and a substrate. The unique optical expression from the aragonite-plate-coated surface showed color and luster like those of natural pearl. The aragonite plates could be employed as a surface coating pigment.



## REFERENCES

1. Saruwatari, K.; Matsui, T.; Mukai, H.; Nagasawa, H.; Kogure, T. Nucleation and growth of aragonite crystals at the growth front of nacre in pearl oyster, *Pinctada fucata*. *Biomaterials* **2009**, 30, 3028-3034.
2. Lin, A.; Meyers, M.A. Growth and structure in abalone shell. *Mat. Sci. Eng. A-Struct* **2005**, 390, 27–41.
3. Lertvachirapaiboon, C.; Jirapisitkul, T.; Pienpinijtham, P.; Wongravee, K.; Thammacharoen, C.; Ekgasit, S. Air-gap-enhanced pearlescent effect in periodic stratified bilayers of *Perna viridis* shell. *J. Mater. Sci.* **2014**, 49, 6282-6289.
4. Lopez, M.I.; Martinez, P.E.M.; Meyers, M.A. Organic interlamellar layers, mesolayers and mineral nanobridge: contribution to strength in abalone (*Haliotis rufescence*) nacre. *Acta Biomater.* **2014**, 10, 2056–2064.
5. Nassif, N.; Pinna, N.; Gehrke, N.; Antonietti, M.; Jäger, C.; Cölfen, H. Amorphous layer around aragonite platelets in nacre. *Proc. Natl. Acad. Sci. U. S. A.* **2005**, 102, 12653-12655.
6. Cartwright, J.H.E.; Checa, A.G. The dynamic of nacre self-assembly. *J. R. Soc. Interface* **2007**, 4, 491-504.
7. Rousseau, M.; Lopez, E.; Stemplé, P.; Brendlé, M.; Franke, L.; Guette, A.; Naslain, R.; Bourrat, X.; Multiscale structure of sheet nacre. *Biomaterials* **2005**, 26, 6254–6262.
8. Huang, Z.; Li, X. Order-Disorder Transition of Aragonite Nanoparticles in Nacre. *Phys. Rev. Lett.* **2012**, 109, 025501-1-025501-5.
9. Younis, S.; Kauffmann, Y.; Bloch, L.; Zolotoyabko, E. Inhomogeneity of Nacre Lamellae on the Nanometer Length Scale. *Cryst. Growth Des.* **2012**, 12, 4574-4579.
10. Tjandra, E.S.; Boulos, R.A.; Duncan, P.C.; Raston, C.L. Unfastening pearl nacre nanostructures under shear. *CrystEngComm.* **2013**, 15, 6896-6900.
11. Boulos, R.A.; Harnagea, C.; Duan, X.; Lamb, R.N.; Rosei, F.; Raston, C.L. Unzipping oyster shell. *RSC Adv.* **2013**, 3, 3284-3290.
12. Li, X.; Chang, W.; Chao, Y.J.; Wang, R.; Chang, M. Nanoscale Structural and Mechanical Characterization of a Natural Nanocomposite material: The Shell of Red Abalone. *Nano. Lett.* **2004**, 4, 613-617.
13. Takahashi, K.; Yamamoto, H.; Onoda, A.; Doi, M.; Inaba, T.; Chiba, M.; Kobayashi, A.; Taguchi, T.; Okamura, T.; Ueyama, N. Highly oriented aragonite nanocrystal–biopolymer composites in an aragonite brick of the nacreous layer of *Pinctada fucata*. *Chem. Commun.* **2004**, 8, 996-997.
14. Food and Agriculture Organization of the United Nation (FAO), 2011, Accessed on May 15, 2014 from: <http://www.fao.org/fishery/species/2691/en>.

15. Chaiya, W.; Gheewala, S.H., Life cycle assessment of MSW-to-energy schemes in Thailand. *J. Clean. Prod.* **2007**, *15*, 1463-1468.
16. Ballester, P.; Mármol, J.; Sánchez, L. Use of limestone obtained from waste of the mussel cannery industry for the production of mortars. *Cement Concrete Res.* **2007**, *37*, 559-564.
17. Mosher, S.; Cope, WG.; Weber, F.X.; Shea, D.; Kwak, T.J. Effects of Lead on Na<sup>+</sup>, K<sup>+</sup>-ATPase and hemolymph ion concentrations in the freshwater mussel *Elliptio Complanata*. *Environ. Toxicol.* **2010**, *27*, 268-276.
18. Lertwattanaruk, P.; Makul, N.; Siripattaraprat, C.; Utilization of ground waste seashells in cement mortars for masonry and plastering. *J. Environ. Manage.* **2012**, *111*, 133-141.
19. Seco-Reigosa, N.; Peña-Rodríguez, S.; Nóvoa-Muñoz, J.C.; Arias-Estévez, M.; Fernández-Sanjurjo, M.J.; Álvarez-Rodríguez, E.; Núñez-Delgado, A. Arsenic, chromium and mercury removal using mussel shell ash or a sludge/ashes waste mixture. *Environ. Sci. Pollut. Res.* **2013**, *20*, 2670-2678.
20. Nair, P.; Singh, B.; Upadhyay, S.N.; Sharma, Y.C. Synthesis of biodiesel from low FFA waste frying oil using calcium oxide derived from *Meretrix meretrix* as a heterogeneous catalyst. *J. Clean. Prod.* **2012**, *29*, 82-90.
21. Rezaei, R.; Mohadesi, M.; Moradi, G.R. Optimization of biodiesel production using waste mussel shell catalyst. *Fuel* **2013**, *109*, 534-541.
22. Addadi, L.; Joester, D.; Nudelman, F.; Weiner, S. Mollusk shell formation: a source of new concepts for understanding biomineralization process. *Chem. Eur. J.* **2006**, *12*, 980-987.
23. Mukai, H.; Saruwatari, K.; Nagasawa, H.; Kogure, T. Aragonite twinning in gastropod nacre. *J. Crst. Growth.* **2010**, *312*, 3014-3019.
24. Checa, A.G.; Cartwright, J.H.E., Willinger, M.G. Mineral bridges in nacre. *J. Struct. Biol.* **2010**, *176*, 330-339.
25. Jackson, A.P.; Vincent, J.F.V.; Turner, R.M. The mechanical design of nacre. *Proc. R. Soc. B* **1988**, *234*, 415-440.
26. Meyers, M.A.; Chen, P.Y.; Lin, A.Y.M.; Seki, Y. Biological materials: structure and mechanical properties. *Prog. Mater. Sci.* **2008**, *53*, 1-206.
27. Liu, Y.; Shigley, J.E.; Hurwit, K.N. Iridescence color of a shell of the mollusk *Pinctada Nargaritifera* caused by diffraction. *Optics Express* **1999**, *4*, 177-182.
28. Tan, T.L.; Wong, D.; Lee, P. Iridescence of a shell of mollusk *Haliotis Glabra*. *Optics Express* **2004**, *12*, 4847-4854.
29. Lopez, E; Chemouni A.E. US10/089,982, **2005**.
30. DeLaRosa, D.M. US2008/0199533 A1, **2008**.
31. Kinoshit, S.; Yoshioka, S. Structural Colors in Nature: The Role of Regularity and Irregularity in the Structure. *ChemPhysChem* **2005**, *6*, 1442-1459.

32. Meadows, M.G.; Butler, M.W.; Morehouse, N.I.; Taylor, L.A.; Toomey, M.B.; McGraw, K.J.; Rutowski, R.L. Iridescence: views from many angles. *J. R. Soc. Interface* **2009**, *6*, S107-S113.
33. Chung, K.; Yu, S.; Heo, C.; Shim, J.W.; Yang, S.; Han, M.G.; Lee, H.; Jin, Y.; Lee, S.Y.; Park, N.; Shin, J.H.; Flexible, Angle-Independent, Structural Color Reflectors Inspired by *Morpho* Butterfly Wings. *Adv. Mater.* **2012**, *24*, 2375–2379.
34. Verho, T.; Karesoja, M.; Das, P.; Martikainen, L.; Lund, R.; Alegría, A.; Walther, A.; Ikkala, O. Hydration and Dynamic State of Nanoconfined Polymer Layer Govern Toughness in Nacre-mimetic Nanocomposite. *Adv. Mater.* **2013**, *25*, 5005-5059.
35. Belcher, A.M.; Wu, X.H.; Christensen, R.J.; Hansma, P.K.; Stucky, G.D.; Morese, D.E. Control of crystal phase switching and orientation by soluble mollusk-shell proteins. *Nature* **1996**, *381*, 56-58.
36. Yan, Z.; Jing, G.; Gong, G.; Li, C.; Zhou, Y.; Xie, L.; Zhang, R. N40, a Novel Nonacidic Matrix Protein from Pearl Oyster Nacre, Facilitates Nucleation of Aragonite in Vitro. *Biomacromolecules* **2007**, *8*, 3597-3601.
37. Metzler, R.A.; Evans, J.S.; Killian, C.E.; Zhou, D.; Churchill, T.H.; Appathurai, N.P.; Coppersmith, S.N.; Gilbert, P.U.P.A. nacre Protein Fragment Templates lamellar Aragonite Growth. *J. Am. Chem. Soc.* **2010**, *132*, 6329-6334.
38. Gehrke, N.; Cölfen, H.; Pinna, N.; Antonietti, M.; Nassif, N. Superstructures of Calcium Carbonate Crystals by Oriented Attachment. *Crystal. Growth. Des.* **2005**, *5*, 1317-1319.
39. Hasen, W.N. Electric fields produced by the propagation of plane coherent electromagnetic radiation in a stratified medium. *J. Opt. Soc. Am.* **1968**, *58*, 380-390.
40. Ekgasit, S.; Thammacharoen, C.; Knoll, W. Surface Plasmon Resonance Spectroscopy Based on Evanescent Field Treatment. *Anal. Chem.* **2004**, *76*, 561-568.



**APPENDIX A**

The logo of Chulalongkorn University, featuring a central emblem with a sunburst and a tiered base, set within a circular frame.

จุฬาลงกรณ์มหาวิทยาลัย  
CHULALONGKORN UNIVERSITY

## ACHIEVEMENT

We successfully developed the method to produce pearlescent flakes and also individual aragonite plates and succeed in explanation of optical effects. Our works were accepted in peer-reviewed journals and obtain many awards from nation and international scientific and engineering societies. The following information shows awards to represent our research achievements.

1. Gold Medals Awards, Title: High quality calcium carboante from green mussel shells, 40<sup>th</sup> Internation Exhibition of Inventions of Gaeneva, 18-22 April 2012, World intellectual property organization (WIPO).



2. Spectial Prize, Title: Pearlescent flake from green mussel shells having unique optical properties and its application in security printing, 5<sup>th</sup> Fajr Internation Inventions and Innovation Exhibitio in Tehran, Islamic Republic of Iran, 4-7 Fedruary 2013, Korea Invention Promotion Association (KIPA)



3. Sci&Tech Initiative and Sustainability Awards 2014 (Grand Prize), Title: Natural calcium carbonate and its innovative applications, The Thai Institute of Chemical Engineering and Applied Chemistry.



4. FIRST PRIZE Oral Presentation Award, Title: Color expression associate of pearlescent plates from green mussel shell, The 30th Annual Conference of the Microscopy Society of Thailand (MST30), 23-25 January 2013, The Microscope Society of Thailand.



5. FIRST PRIZE Oral Presentation Award, Title: Security markers based on dye-loaded stacked aragonite microcrystals, The 31st Annual Conference of the Microscopy Society of Thailand (MST31), 27-28 January 2014, The Microscope Society of Thailand.



Besides our research achievement on academic area, we have strong partners to develop innovative works on art and education. The following information shows prototype materials and awards to represent achievements of our corroboration works.

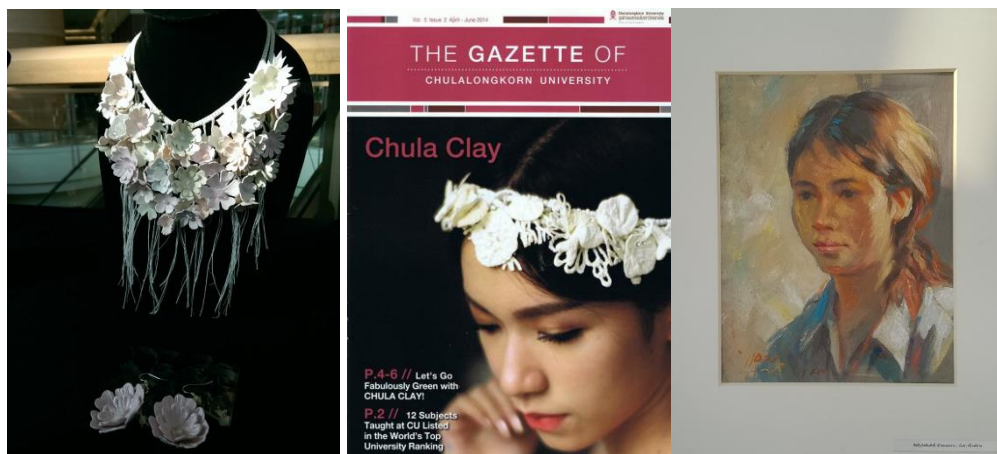


**Figure 1.** Prototype jewelry made from Chula Clay (left), cover page of ‘THE GAZETTE OF CHULALONGKORN UNIVERSITY’ show prototype jewelry made from our developed calcium carbonate (center) and pearlescent colors painting (right).

6. Gold Medals Awards, Title: CHULAClay4SustainableDesign-Development of prototye of jewelry ecologique, 42<sup>th</sup> Internation Exhibition of Inventions of Gaeneva, 2-6 April 2014, World intellectual property organization (WIPO). *The owners of this Award are Dr. Intira Phrompan and Dr. Soamshirne Boonyananta from Facultry of Education, Chulalongkorn University.*
7. Gold Medals Awards, Title: CHULA Argile Perlée-Twinkling Clay frabricated from mussel shells, 42<sup>th</sup> Internation Exhibition of Inventions of Gaeneva, 2-6 April 2014, World intellectual property organization (WIPO). *The owners of this Award are Dr. Intira Phrompan and Dr. Soamshirne Boonyananta from Facultry of Education, Chulalongkorn University.*
8. Gold Medals Awards, Title: CHULA Argile Perlée-Twinkling Clay frabricated from mussel shells, 42<sup>th</sup> Internation Exhibition of Inventions of Gaeneva, 2-6 April 2014, World intellectual property organization (WIPO). *The owners of this Award are Associate Professor Dr. Poonarat Pichayapaiboon and Mr. Puchong Rojsangrat from Facultry of Education, Chulalongkorn University.*

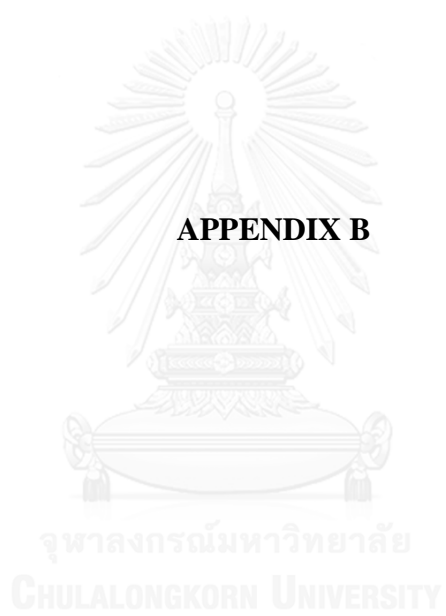
Recently, A team of Faculty of Education got ‘The Best Practice Award’ from Asia-Pacific Centre of Education for International Understanding (APCEIU) under the auspices of UNESCO. Director Mr. CHUNG Utak and Dr. KIM Kwang-Hyun presented EIU Best Practice 2014 Award to Faculty of education research team who successfully well-done in the project of “Enhancing Student Environmental Sustainability Awareness with Innovative Art Materials: Multidisciplinary of art and Science Activities”.



**Figure 2.** A photographic image of a team of faculty of education, Chulalongkorn University got “the best practice award from Asia-Pacific Centre of Education for International Understanding (APCEIU) under the auspices of UNESCO on 7 September 2014.

### References

1. <http://rrm.nrct.go.th/promoting-award-inventors/geneva-inventions/139-geneva2014.html>
2. <http://rrm.nrct.go.th/promoting-award-inventors/geneva-inventions/58-geneva.html>
3. <http://www.chula.ac.th/th/archive/cover/periodicals/cugazette>
4. <http://www.chula.ac.th/en/archive/3402>



## Supporting information

### Air-gap-enhanced pearlescent effect in periodic stratified bilayers of *Perna viridis* shell

Chutiparn Lertvachirapaiboon, Thiluksakorn Jirapisitkul, Prompong Pienpinijtham,

Kanet Wongravee, Chuchaat Thammacharoen, and Sanong Ekgasit\*

Sensor Research Unit, Department of Chemistry, Faculty of Science, Chulalongkorn

University, 254 Phayathai Road, Patumwan, Bangkok 10330, THAILAND.

E-mail: \*[sanong.e@chula.ac.th](mailto:sanong.e@chula.ac.th)

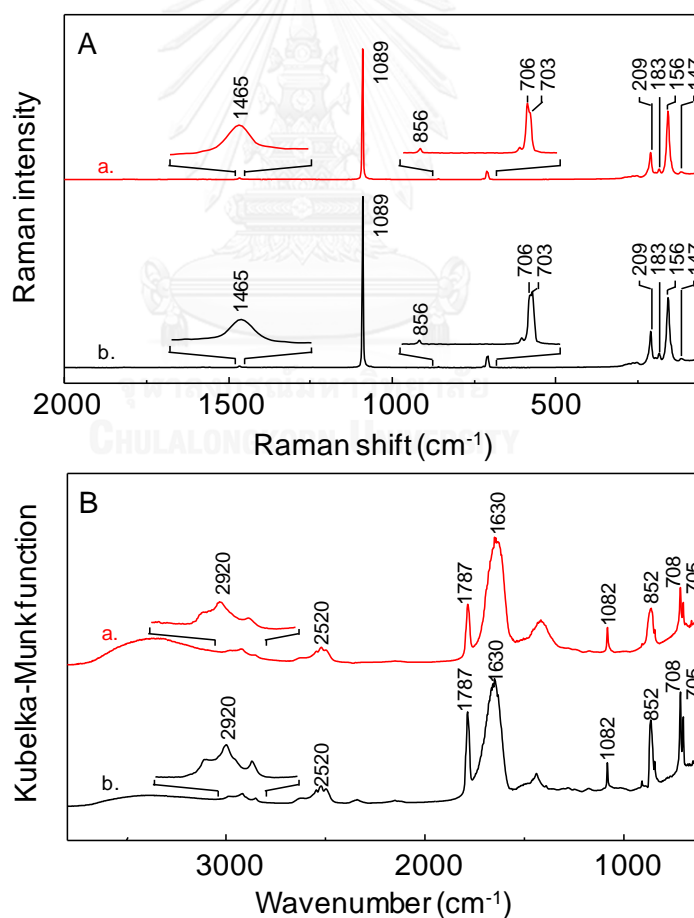


**Fig. S1** (A) Raman and (B) Diffuse reflectance FT-IR spectra of virgin and treated shells.



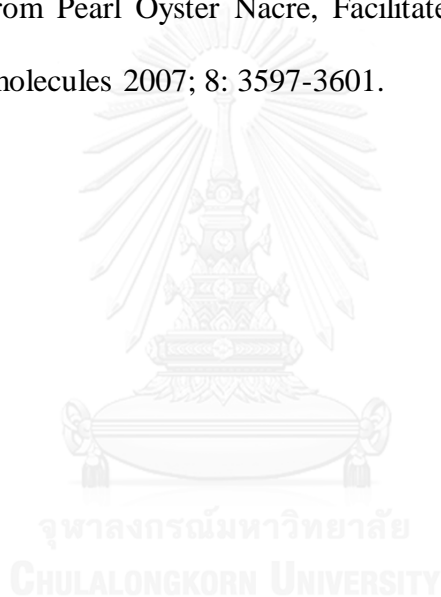
**Table S1** Raman and FT-IR spectrum peaks assignment of virgin and treated shells [1-6].

Green mussel shell	Raman band (cm <sup>-1</sup> )	FTIR band (cm <sup>-1</sup> )
<b><i>Aragonite calcium carbonate vibration</i></b>		
in plane bending, $\nu_4$	703, 706 (m)	705, 708 (m)
out of plane bending, $\nu_2$	856 (w)	858 (w)
symmetric stretching, $\nu_1$	1089 (s)	1082 (m)
asymmetric stretching, $\nu_3$	1465 (w)	
combination band, $\nu_1+\nu_4$		1787 (s)
external lattice vibration	147 (m), aragonite 156 (s) 183 (w), aragonite 194 (w), aragonite 209 (s), aragonite	
O-H stretching from HCO <sub>3</sub> <sup>-</sup>		2520 (s)
<b><i>Protein vibration</i></b>		
amide I		1630 (s)
C-H stretching		2920 (m)

## References

- (1) Tan TL, Wong D, Lee P. Iridescence of a shell of mollusk *Haliotis Glabra*. Opt Express 2004; 12: 4847-4854.
- (2) Parker JE, Thompson SP, Lennie AR, Potter J, Tang CC. A study of the aragonite-calcium transformation using Raman spectroscopy, synchrotron powder diffraction and scanning electron microscopy. CrysEngComm 2010; 12: 1590-1599.
- (3) Perdikouri C, Kasiotas A, Geisler T, Schmidt BC, Putnis A. Experimental study of the aragonite to calcite transition in aqueous solution. Geochim Cosmochim Acta 2011; 75: 6211-6224.

- (4) Balmain J, Hannoyer B, Lopez E. Fourier Transform Infrared Spectroscopy (FTIR) and X-ray Diffraction Analyses of Mineral and Organic Matrix During Heating of Mother of Pearl (Nacre) From the Shell of the Mollusc *Pinctada maxima*. J Biomed Mater Res 1999; 48: 749-754.
- (5) Verma D, Katti K, Katti D. Photoacoustic FTIR spectroscopic study of undisturbed nacre from red abalone. Spectrochim Acta A 2006; 64: 1051-1057.
- (6) Yan Z, Jing G, Gong N, Li C, Zhou Y, Xie L, Zhou R. N40, a novel Nonacidic Matrix Protein from Pearl Oyster Nacre, Facilitates Nucleation of Aragonite in Vitro. Biomacromolecules 2007; 8: 3597-3601.



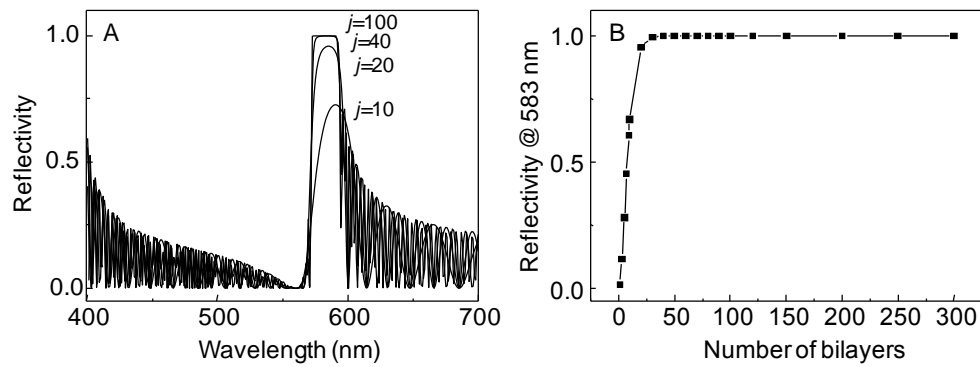


**Fig. S2** (A) Calculated reflectivity reflection spectra of the treated shell with an increasing number of bilayer  $j$  and (B) the reflectivity at 583 nm. The simulation parameters are:  $n_A=1.6$ ,  $n_B=1.0$  (air),  $d_A=350$  nm,  $d_B=20$  nm, and  $\theta = 0^\circ$ . The selective reflection of red color ( $\lambda = 583$  nm) is obtained under configuration. The total reflection is reached with the number of bilayer  $j = 25$ .

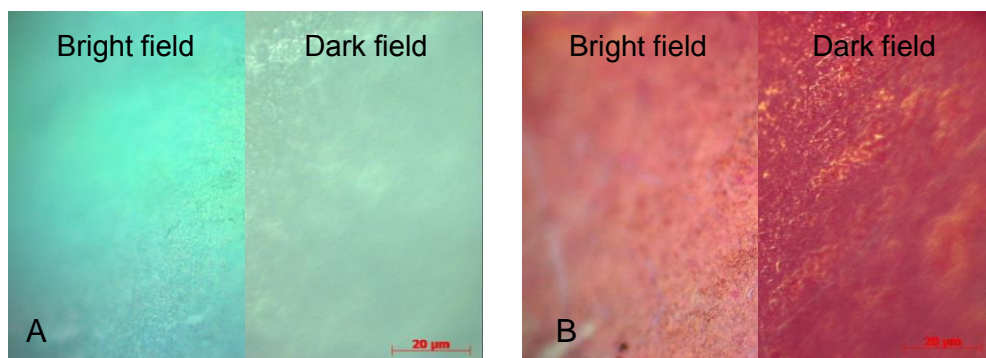


**Fig. S3** The OM images of (A) virgin shell and (B) virgin shell immersed with R6G dye. The images were recorded under the bright field and dark field illuminations.



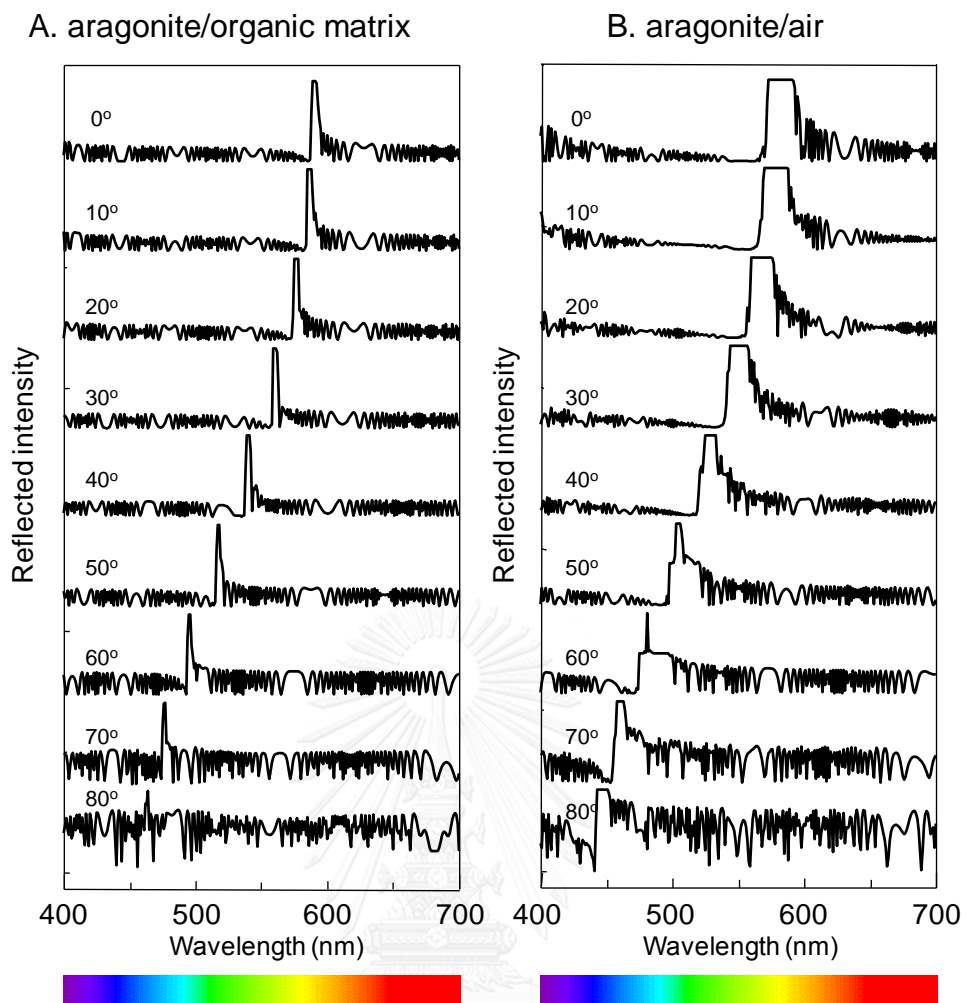


**Fig. S4** Calculated reflection spectrum of (A) aragonite/organic matrix and (B) aragonite/air stratified bilayers (1,000 bilayers) at several incident angles.

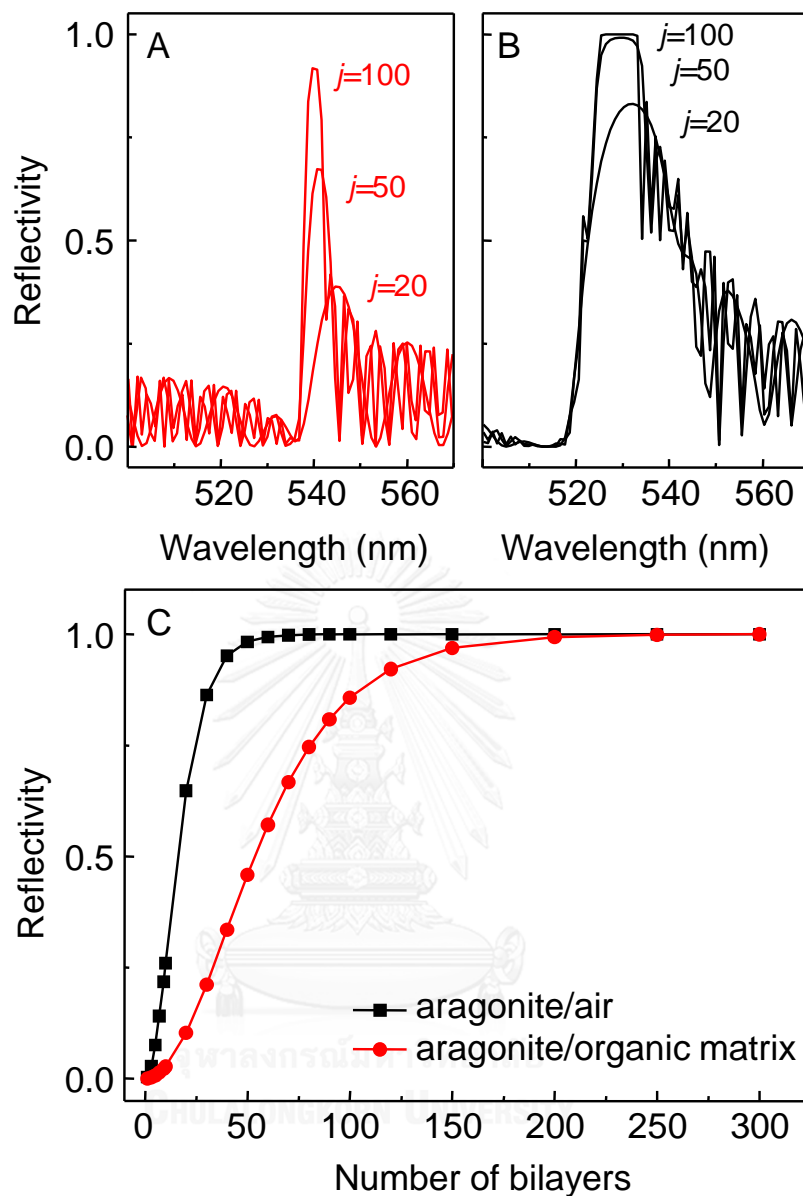
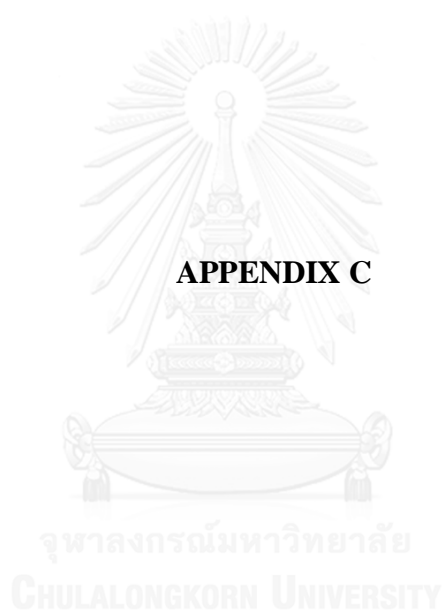


**Fig. S5** Calculated reflectivity of (A) aragonite/organic matrix, (B) aragonite/air stratified layers of various thicknesses, and (C) the reflectivity as a function of number of bilayer: (square) aragonite/air, (circle) aragonite/organic matrix. The reflectivity was measured at the reflection maxima. The simulation parameters are:  $n_A=1.6$ ,  $n_B=1.5$  (organic matrix) or 1.0 (air),  $d_A=350$  nm,  $d_B=20$  nm, and  $\theta = 40^\circ$ .



## Selective colors reflection from stratified aragonite calcium carbonate plates of mollusk shells

Chutiparn Lertvachirapaiboon, Tewarak Parnklang, Prompong Pienpinijtham, Kanet Wongravee, Chuchaat Thammacharoen, and Sanong Ekgasit\*

Sensor Research Unit, Department of Chemistry, Faculty of Science, Chulalongkorn University, Bangkok 10330, THAILAND.

E-mail: \*[sanong.e@chula.ac.th](mailto:sanong.e@chula.ac.th)

### ABSTRACT

An interaction between the incident light and the structural architecture within the shell of Asian green mussel (*Perna viridis*) induces visually observable pearlescent colors. In this paper, we investigate the influence of the structural architecture on the expressed colors and explore its potential application as a color-shifting pigment. After a removal of the organic binder, small flakes from crushed shells appear white as normal calcium carbonate powder. However, they show rainbow reflection when viewing at an oblique angle. Under an optical microscope, they express multiple vivid colors under a bright-field illumination while become transparent under a dark-field illumination. The expressed colors of the flake building up from transparent aragonite layers are directly associated with its structural architecture. The flakes with aragonite thickness of 256, 310, and 353 nm, respectively, appear vividly blue, green, and red under an optical microscope. The spectral simulation corroborates the experimentally observed optical effects as the flakes with thicker aragonite layers selectively reflected color with longer wavelengths. A thick flake totally reflects a selected color



in the incident radiation while a thin flake partially reflected the same color. The flakes with different aragonite layer thicknesses expressed multi-color as the upper transparent aragonite layers allow reflected colors from the lower layers to be observed.

**KEYWORDS** aragonite calcium carbonate, pearlescent flake, color-selective reflection, structural color, color-shifting pigment

## 1. INTRODUCTION

The structural colors in nature mainly originate from interference of light with periodic structure of some living organism such as butterflies, beetles, birds, shells, fishes, plants [1-11]. The structural colors function as attractants to conspecifics, warning signs, and camouflage. The expressed colors were attributed to refractive index of materials, angle of incidence, and thickness of stratified layers within periodic structure [8-10]. A well-known example of structural colors in the nature was butterflies of the genus *Morpho* which selectively reflect brilliant blue color due to a multiple reflection of white light within an alternating multilayers of chitin and air [3,10]. The elytra of many beetles can express the fascinating colors. Yoshioka et al. found that the jewel beetle (*C. fulgidissima*) exhibited a green color at the normal angle and the blue color under an oblique angle due to an optical interference within stacked layers of chitin [2]. The mollusk shell also express colors originated by an interference of light with periodic stratified layers of aragonite and organic matrix. The unique structure of mollusk shells that provide the pearlescent colors is a stratified assembly of alternated 200-500 nm-thick aragonite calcium carbonate layers

bound by 20-30 nm-thick organic binding layers [11-16]. Tan et al. corroborate that the uniform stacking of nacre induces the interference effects. The high groove density on the surface strongly contributes to the vivid pink and blue-green pearlescent colors in abalone (*Haliotis Glabra*) shell [1]. Recently, the pearlescent colors from Asian green mussel (*Perna viridis*) shell and pearlescent enhancement by replacing of organic binding layers with air gaps were reported by our group [11].

Most case of the structural colors related to color-shift from one color to another due to a change in viewing angle. The structural colors from the nacre layer of sea shells provide extraordinary reflections as several colors are visible at the same time. Our developed treatment technique enabled us to characterize the origin of rainbow colors reflected from stratified layer of aragonite calcium carbonate as only the organic binder was disintegrated without destroying the structural assembly of nacre of shells. After organic binder was eliminated, the shells were disintegrated to small fragments called 'pearlescent flakes'. In this current investigation, the relationship between structure of pearlescent flakes and the color expressions were characterized to gain insight understanding of rainbow-colors reflection of nacre. Moreover, a theoretical calculation based on the transfer matrix method provided was used to confirm this structure-color relationship.

## **2. MATERIAL AND METHODS**

The pearlescent flakes from Asian green mussel (AGM), abalone, and oyster shells were prepared by our previously developed methodology with a minor modification [11]. Briefly, the shells were thoroughly cleaned to remove residual tissues and other contaminants before drying under an ambient air. The dried shells

were baked at 300 °C for 2 h. The shells were then immersed in 30 % wt. hydrogen peroxide (H<sub>2</sub>O<sub>2</sub>, Merck, Thailand) for 24 h to dissolve the brownish-degraded organic binder. The H<sub>2</sub>O<sub>2</sub>-whiten shells showed observable rainbow colors. The shells were brittle and easily broken-down into small flakes. The flakes were cleaned with tap water several times to remove dust particles. The flakes showed vivid rainbow colors observable by naked eyes when they were dispersed in water. The flakes were air dried before keeping in a desiccator for further investigation.

Scanning electron microscope (SEM, JSM-6510A, JEOL) and atomic force microscope (AFM, SPA 400, SII NanoTechnology Inc.) were employed to investigate the structural architecture of the flakes. To acquire SEM images, a flake was wrapped with aluminum foil before mounting on a modified stub with the cross-section surface normal to the electron beam. SEM images were acquired under low acceleration voltage of 5 kV. The average thickness of aragonite plates was calculated from 100 aragonite plates selected from unique SEM images [15]. AFM images were recorded with a scan rate of 1 Hz in a non-contact mode using silicon tips with a rounding size of 20 nm, force constant of 17 N/m, and a resonance frequency of 139 KHz.

The expressed colors of pearlescent flakes were recorded by a CCD camera (Carl Zeiss, AxioCam HRc) attached on an optical microscope (OM, Carl Zeiss Axio Scope.A1). The reflection spectra of pearlescent flakes were collected by a fiber optic spectrometer (OceanOptics USB4000 portable UV-visible spectrometer) coupled to the OM. Figure 1 shows instrumental setup with CCD camera and fiber optic spectrometer capable of recording OM images and spectroscopic data simultaneously.

### 3. RESULTS AND DISCUSSION

Calcium carbonate flakes of AGM shells, abalone shells, and oyster shells prepared by a consecutive thermal/chemical treatment appeared white powder. When viewing under an OM (10X objective), they showed vivid color (Figure S1) not observed in regularly crushing technique (Figure S2) and precipitated calcium carbonate (Figure S3). The vivid reflected colors also indicated the structural integrity as the flakes did not break down into an individual aragonite plate. The flakes from AGM shells showed the most vivid colors covering the entire visible region. Therefore, it was selected as a model material for our study on color expression of the nacre structure. The pearlescent effect of a virgin AGM shell originated by an interaction between light with nacre is well-known, Figure 2A. To acquire the structural information of the shell, we recorded SEM images across the thickness of the AGM shell. The cross-section SEM images in Figure 2C show a gradual increment of the thickness of aragonite plates as they aged (i.e., the thickness increases toward the outside layers).

After the removal of organic matrix, the treated shells showed stronger reflection with more vivid colors compared to the virgin shells. The shells became brittle and easily broken into small fragments (i.e., the pearlescent flakes). Due to scattering effect, the pearlescent flakes appeared white to the naked eyes (Figure 3A) but expressing vivid colors at normal angle of OM (Figure 3B) \*\* the bulk white powder \*\*. The SEM images suggest that the pearlescent flake is in fact an alternated stack of aragonite layers and air gaps [11]. The removal of organic binder with a consecutive development of air gaps was confirmed by TGA analyses (Figure S4). The 200-to-500-nm-thick aragonite layer is a single ply assembly of 3-5  $\mu\text{m}$  bisector

length pseudo-hexagonal aragonite plates, Figures 2 and S5. The Raman spectra corroborate that the AGM shells are aragonite calcium carbonate (Figure S6) [17-19].

Figure 3B shows OM image of pearlescent flakes while Figure 3C shows the corresponding reflection spectra of selected pearlescent flakes. Although, the flakes were white powder when observed by the naked eyes, the vivid colors appeared under an OM. The strong and narrow reflection spectra corresponded to the expressed colors under OM. The purple-blue, blue, green and red pearlescent flakes show spectra with reflection maxima at 457, 485, 553, and 654 nm, respectively. We hypothesized that the expressed color was directly associated with the structural architecture of the individual flake. The relatively flat surface also contributed to the strong reflection colors (Figure S5). In Figure 3B, the aragonite flake 'f' appears dark while its corresponding reflection spectrum in Figure 3C was rough across the visible region as the flake does not reflect any incident radiation. The corresponding SEM images (Figure S7) suggest that the flake was fragmented from the outer part of the shell where the aragonite plates are irregularly thick with highly rough surface.

The pearlescent flakes with blue, green, and red were selected for further detailed investigation (Figure 4). As indicated by the OM images and the corresponding SEM and AFM images (Figures 4A-4I), the aragonite plates of the flakes expressing blue, green, and red colors with reflection maxima at 441, 523, and 577 nm have thickness of  $256\pm 10$ ,  $310\pm 12$ , and  $353\pm 10$  nm, respectively. The histogram in Figure 4J suggests that the pearlescent flakes expressing single vivid color composed of aragonite layers having narrow thickness distribution. When the thicknesses were employed for spectral simulations, the calculated spectra agreed very well with the experimentally measured spectra (Figure 4K). The results in Figure

4 confirm that the thickness of transparent aragonite layers govern the expressed colors of the pearlescent flakes.

To verify the influence of the structural architecture on the color expression of pearlescent flakes, the modified transfer matrix method for stratified bilayers was employed [11,20]. The pearlescent flake consists of  $N$  aragonite/air gap bilayers. The aragonite layer is represented by layer A while the air gap is represented by layer B. The  $j^{\text{th}}$  bilayers consists of layer A and layer B with a thickness of  $d_A$  and  $d_B$  and reflective indices of  $n_A$  and  $n_B$ . All stratified layers are assumed transparent. (i.e., the aragonite calcium carbonate does not absorb visible light). In the simulation algorithm, the stratified bilayer was bounded by air (i.e., air function as both incident medium and substrate). When an incident radiation of wavelength  $\lambda$  impinges on the stratified bilayer with an angle of incident  $\theta$ , the reflectance is given in terms of the Fresnel reflection coefficients as [11,20]

$$R = (R_{\perp} + R_{\parallel}) / 2; \text{ for non-polarization,} \quad (\text{Eq. 1})$$

$$R_{\perp} = |r_{\perp}|^2; \quad \text{for perpendicular polarization,} \quad (\text{Eq. 2})$$

$$R_{\parallel} = |r_{\parallel}|^2; \quad \text{for parallel polarization,} \quad (\text{Eq. 3})$$

$$r_{\parallel,\perp} = \frac{(M_{11} + M_{12} q_{\text{air}}) q_{\text{air}} - (M_{21} + M_{22} q_{\text{air}})}{(M_{11} + M_{12} q_{\text{air}}) q_{\text{air}} + (M_{21} + M_{22} q_{\text{air}})}. \quad (\text{Eq. 4})$$

Where  $\parallel$  indicates parallel-polarized radiation and  $\perp$  indicates perpendicular-polarized radiation.  $M_{mn}$  is an element of the characteristic matrix  $M(2 \times 2)$  of stratified bilayers. This matrix  $M$  is given in terms of reflective index and experimental condition as

$$M = \prod_{j=1}^N \left\{ \begin{array}{cc} \left[ \begin{array}{cc} \cos(k_{A_j} d_{A_j}) & \frac{-i}{q_{A_j}} \sin(k_{A_j} d_{A_j}) \\ -iq_{A_j} \sin(k_{A_j} d_{A_j}) & \cos(k_{A_j} d_{A_j}) \end{array} \right] & \left[ \begin{array}{cc} \cos(k_{B_j} d_{B_j}) & \frac{-i}{q_{B_j}} \sin(k_{B_j} d_{B_j}) \\ -iq_{B_j} \sin(k_{B_j} d_{B_j}) & \cos(k_{B_j} d_{B_j}) \end{array} \right] \end{array} \right\} \quad (\text{Eq. 5})$$

where  $i = (-1)^{1/2}$ ,  $q_j = k_j / n_j^2$  for parallel-polarized ( $\parallel$ ) radiation, and  $q_j = k_j$  for perpendicular-polarized ( $\perp$ ) radiation.  $k_j$  ( $k_j = [(2\pi / \lambda)^2 n_j^2 - k_{\text{air}}^2]^{1/2}$ ) is the wavevector in each layer while  $k_{\text{air}}$  ( $k_{\text{air}} = (2\pi / \lambda)[n_{\text{air}}^2 \sin^2 \theta]^{1/2}$ ) is the wavevector in air.

To calculate the reflection spectra of pearlescent flakes expressing blue, green, and red colors, the thickness of the aragonite layers were assigned according to the experimental results shown in Figure 4 with a refractive index of 1.6 ( $n_A=1.6$ ). The air gaps ( $n_B=1.0$ ) with 20 nm thick assumed [11]. At an incident angle perpendicular to the stratified layers, the calculated reflection spectrum with aragonite thicknesses of 256, 310, and 353 nm showed reflection peaks centered at 439, 519 and 583 nm, respectively (Figures 4K and S8A). The calculated spectra agreed very well with the experimentally measured spectra (Figure 4K). Since the flake was constructed from transparent aragonite layers and air gaps, the interaction between incident light and structural architecture of the flake (i.e., aragonite thickness, air gap thickness, and number of layer) induced color selective reflection spectrum. The noticeable broader reflection peaks in the experimentally measured spectra in Figure 4K were expected to originate from a non-uniform thickness and surface roughness aragonite plates (Figure S5). The simulated results shown in Figures S8 and S9 confirm that the aragonite layers with thickness of 250-450 nm (i.e., a common thickness range of

naturally occur aragonite calcium carbonate) are capable of selectively reflected visible light across the visible region [11-15]. The pearlescent flakes with thicker aragonite layer selectively reflected colors with longer wavelength (Figure S8B). However, an increment of the thickness of the air gap (i.e., 5-40 nm) insignificantly shifts the reflected colors (Figure S9).

The uniform blue and green colors of aragonite flake with rough surfaces (Figures 5A and 5B) suggest that the number aragonite layers did not alter the color expression. We employed spectral simulation to verify this experimentally observed phenomenon. The thicknesses of aragonite plates were assigned to 256 nm for the blue pearlescent flakes and 310 nm for the green pearlescent flakes. As the number of bilayers was increased from 1 to 120 bilayers, the reflected intensity was increased with a concomitant blue-shift of peak position. The color-selective reflection of the transparent aragonite layers was noticeable at 5-bilayer with ~50% reflectivity of the incident light (Figures 5C and 5D). Interestingly, the total reflection was achieved when the number of the aragonite layer was greater than 30 layers (Figure 5E). As a result, a thick pearlescent flake composes of aragonite plates of narrow thickness distribution expresses its unique color. As shown in Figure 5, aragonite flake with 256 nm thick plates selectively reflect blue color ( $\lambda_{\max}=439$  nm) while that with 310 nm plates selectively reflect green color ( $\lambda_{\max}=519$  nm) across their rough surfaces.

According to the spectra in Figure 4K, a flake with a certain thickness of aragonite layer selectively reflect a particular color. The pearlescent flake shows red-shifted reflecting color as the thickness of aragonite layer increases. In the experimental observation, flakes with multicolor were frequently observed (Figures 2 and 6). To gain an insight understanding of the phenomenon, we performed spectral



simulation on pearlescent flake containing aragonite layers with two different thicknesses (i.e., 256 nm and 310 nm). We calculate spectra of a flake containing 50-bilayer with various combinations on the number of layers from each aragonite. Although the thin 256-nm layer was covered by a thick 310-nm layer, the blue reflection could be observed since the green reflection spectrum is transparent in the blue reflection. The blue reflection became more intense as the number of the 310-nm layer decreased. The results from Figure 6 suggest that the multicolor expression of a pearlescent flake is due to the thickness variation of the aragonite layers within the flake.

#### 4. CONCLUSIONS

The white aragonite calcium carbonate flakes express vivid color when viewing under an optical microscope. The unique structural architecture of this bio-material containing transparent aragonite layers and air gaps enabled a color selective reflection under a bright-field illumination while optically transparent under a dark-field illumination. The results from spectral simulation confirm the governing function of the structural architecture (i.e., aragonite thickness and number of aragonite layer) over the expressed colors. The flakes with thin aragonite layers selectively reflected short wavelength (i.e., blue color) while those with thicker layers reflected longer wavelengths (i.e., red-shifted colors). A thick flake totally reflects the incident radiation without interfering the reflected color while a thin flake partially reflected the color. Unlike the metal oxide-coated mica pearlescent flakes that express single color change, the AGM pearlescent flakes reflect multiple colors as they contain aragonite layers with various thicknesses.

## ACKNOWLEDGMENTS

The authors gratefully acknowledge financial supports from the National Research University Project of Thailand, Office of the Higher Education Commission (WCU-020-FM-57) and the National Research Council of Thailand (NRCT).

## REFERENCES

- (1) Tan TL, Wong D, Lee P. 2004 Iridescence of a shell of mollusk *Haliothis Glabra*. *Optics Express* **12**, 4847-4854. (doi: 10.1364/OPEX.12.00484)
- (2) Adachi E. 2007 Unexpected Variability of Millennium Green: Structural Color of Japanese Jewel Beetle Resulted From Thermosensitive Porous Organic Multilayer. *J. Morphol.* **268**, 826–829. (doi: 10.1002/jmor.10557)
- (3) Ding Y, Sheng Xu, Wang ZL. 2009 Structural colors from *Morpho peleides* butterfly wing scales. *J. Appl. Phys.* **106**, 074702. (doi: 10.1063/1.3239513)
- (4) Shawkey MD, Morehouse NI, Vukusic P. 2009 A protean palette: colour materials and mixing in birds and butterflies. *J. R. Soc. Interface* **6**, S221-S231. (doi: 10.1063/1.3239513)
- (5) Thomas KR, Kolle M, Whitney HM, Glover BJ, Steiner U. 2010 Function of blue iridescence in tropical understorey plants. *J. R. Soc. Interface* **7**, 1699–1707. (doi: 10.1098/rsif.2010.0201)
- (6) Kolle M, Salgard-Cunha PM, Scherer MRJ, Huang F, Vukusic P, Mahajan S, Baumberg JJ, Steiner U. 2010 Mimicking the colourful wing scale structure of the *Papilio blumei* butterfly. *Nat. Nanotechnol.* **5**, 511-515. (doi: 10.1038/nano.2010.101)

- (7) Yoshioka S, Kinoshita S, Iida H, Hariyama T. 2012 Phase-Adjusting Layers in the Multilayer Reflector of a Jewel Beetle. *J. Phys. Soc. Jpn.* **81**, 054801 (doi: 10.1143/JPSJ.81.054801)
- (8) Kinoshita S, Yoshioka S. 2005 Structural Colors in Nature: The Role of Regularity and Irregularity in the Structure. *ChemPhysChem* **6**, 1442–1459. (doi: 10.1002/cphc.200500007)
- (9) Meadows MG, Butler MW, Morehouse NI., Taylor LA, Toomey MB, McGraw KJ, Rutowski RL. 2009 Iridescence: views from many angles. *J. R. Soc. Interface* **6**, S107-S113. (doi: 0.1098/rsif.2009.0013)
- (10) Chung K, Yu S, Heo C, Shim JW, Yang S, Han MG, Lee H, Jin Y, Lee SY, Park N, Shin JH. Flexible, 2012 Angle-Independent, Structural Color Reflectors Inspired by Morpho Butterfly Wings. *Adv. Mater.* **24**, 2375–2379. (doi: 10.1002/adma.201200521)
- (11) Lertvachirapaiboon C, Jirapisitkul T, Pienpinijtham P, Wongravee K, Thammacharoen C, Ekgasit S. 2014 Air-gap-enhanced pearlescent effect in periodic stratified bilayers of *Perna viridis* shell. *J. Mater. Sci.* **49**, 6282-6289. (doi: 10.1007/s10853-014-8353-6)
- (12) Jackson AP, Vincent JFV, Turner RM. 1988 The mechanical design of nacre. *Proc. R. Soc. B* **234**, 415–440. (doi: 10.1098/rspb.1988.0056)
- (13) Leung HM, Sinha SK. 2002 Scratch and indentation tests on seashells. *Tribol. Int.* **42**, 40–49. (doi: 10.1016/j.triboint.2008.05.015)
- (14) Lin A, Meyers MA. 2005 Growth and structure in abalone shell. *Mat. Sci. Eng. A-Struct.* **390**, 27–41. (doi: 10.1016/j.msea.2004.06.072)

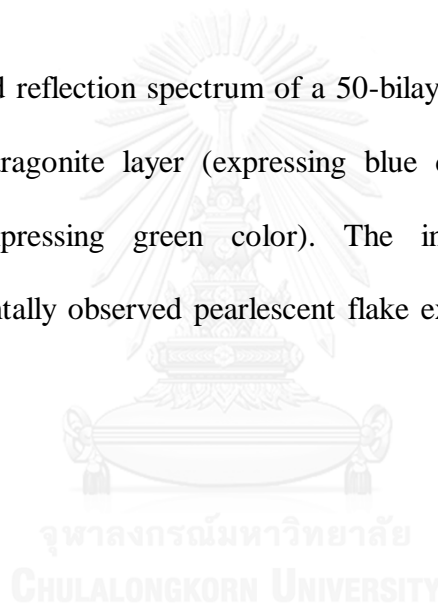
- (15) Lopez MI, Martinez PEM, Meyers MA. 2014 Organic interlamellar layers, mesolayers and mineral nanobridge: contribution to strength in abalone (*Haliotis rufescence*) nacre. *Acta Biomater.* **10**, 2056–2064. (doi: 10.1016/j.actbio.2013.12.016)
- (16) Meyers MA, Chen PY, Lin AYM, Seki Y. 2008 Biological materials: structure and mechanical properties. *Prog. Mater. Sci.* **53**, 1–206. (doi: 10.1016/j.pmatsci.2007.05.002)
- (17) Parker JE, Thompson SP, Lennie AR, Potter J, Tang CC. 2010 A study of the aragonite-calcium transformation using Raman spectroscopy, synchrotron powder diffraction and scanning electron microscopy. *CrysEngComm* **12**, 1590-1599. (doi: 10.1039/B921487A)
- (18) Perdikouri C, Kasioptas A, Geisler T, Schmidt BC, Putnis A. 2011 Experimental study of the aragonite to calcite transition in aqueous solution. *Geochim. Cosmochim. Acta* **75**, 6211-6224. (doi: 10.1016/j.gca.2011.07.045)
- (19) Lin AYM, Chen PY, Meyers MA. 2008 The growth of nacre in the abalone shell. *Acta Biomater.* **4**, 131-138. (doi: 10.1016/j.actbio.2007.05.005)
- (20) Hasen WN. 1968 Electric fields produced by the propagation of plane coherent electromagnetic radiation in a stratified medium. *J. Opt. Soc. Am.* **58**, 380-390. (doi: 10.1364/JOSA.58.000380)

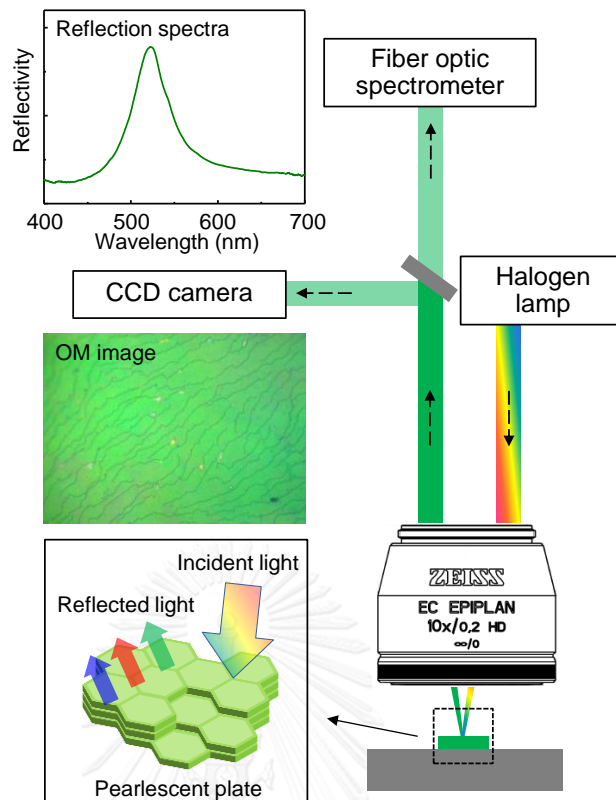
## List of figure captions

- Figure 1. Experimental setup capable of simultaneously acquires a visible spectrum and the corresponding OM image of a pearlescent flake.
- Figure 2. (A) Pearlescent colors of AGM shell. (B) Thickness of AGM shell. (C) A cross-section SEM images of AGM shell. The detailed SEM images across the thickness (C1-C4) show a gradual thickness increment of the aragonite plates from the inner layers towards the outside layers. The scale bars indicate 1  $\mu\text{m}$ .
- Figure 3. (A) SEM images of pearlescent flakes. The flakes are stratified bilayers of aragonite layers and air gaps. The flakes appear white to the naked eyes. (B) OM image of pearlescent flakes under a bright-field illumination (10X objective). The inset shows the corresponding dark-field illumination image. (C) Reflection spectra of selected pearlescent flakes acquired by coupling the reflected light into a fiber optic spectrometer via a 50X objective.
- Figure 4. OM, cross-section SEM and AFM images of pearlescent flakes expressing colors: (A, D, G) blue, (B, E, H) green, and (C, F, I) red. Histogram (J) show thickness distribution of aragonite layers within the colored pearlescent flakes. (K) Comparisons of experimental (solid line) and calculated (dash line) reflection spectra of pearlescent flakes. The experimentally measured thicknesses were employed for the calculations.

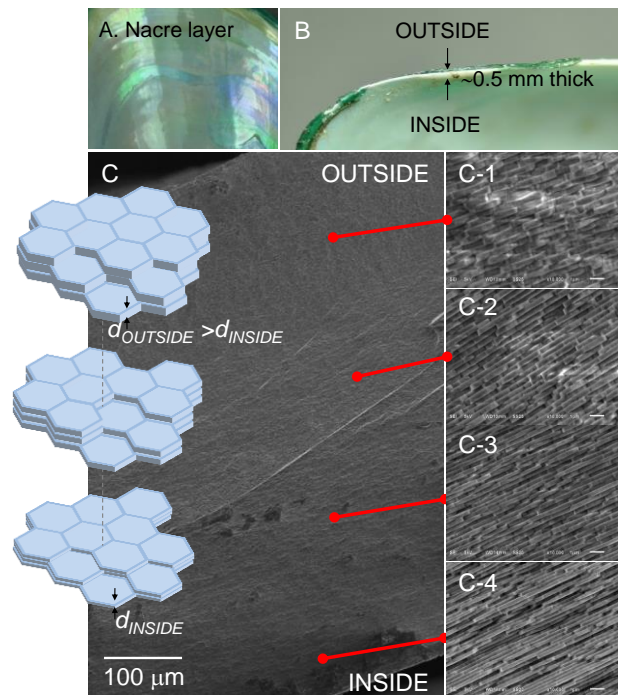
Figure 5. OM images of pearlescent flake selectively reflect (A) blue and (B) green colors. The flakes show thickness variation across the surfaces but expressing uniform colors. Calculated reflection spectra of stratified bilayers of (C) the blue pearlescent flakes ( $d_A=256$  nm) and (D) the green pearlescent flake ( $d_A=310$  nm). The thickness of the air gap was assumed 20 nm. (E) The reflectivity-number of bilayer plot for blue and green flakes. The total reflection (color saturation) was achieved after a 30-bilayer.

Figure 6. Calculated reflection spectrum of a 50-bilayer flake with different ratio of 256-nm aragonite layer (expressing blue color) and 310-nm aragonite layer (expressing green color). The inset OM image shows an experimentally observed pearlescent flake expressing both blue and green colors.





**Figure 1.** Experimental setup capable of simultaneously acquires a visible spectrum and the corresponding OM image of a pearlescent flake.



**Figure 2.** (A) Pearlescent colors of AGM shell. (B) Thickness of AGM shell. (C) A cross-section SEM images of AGM shell. The detailed SEM images across the thickness (C1-C4) show a gradual thickness increment of the aragonite plates from the inner layers towards the outside layers. The scale bars indicate 1 μm.



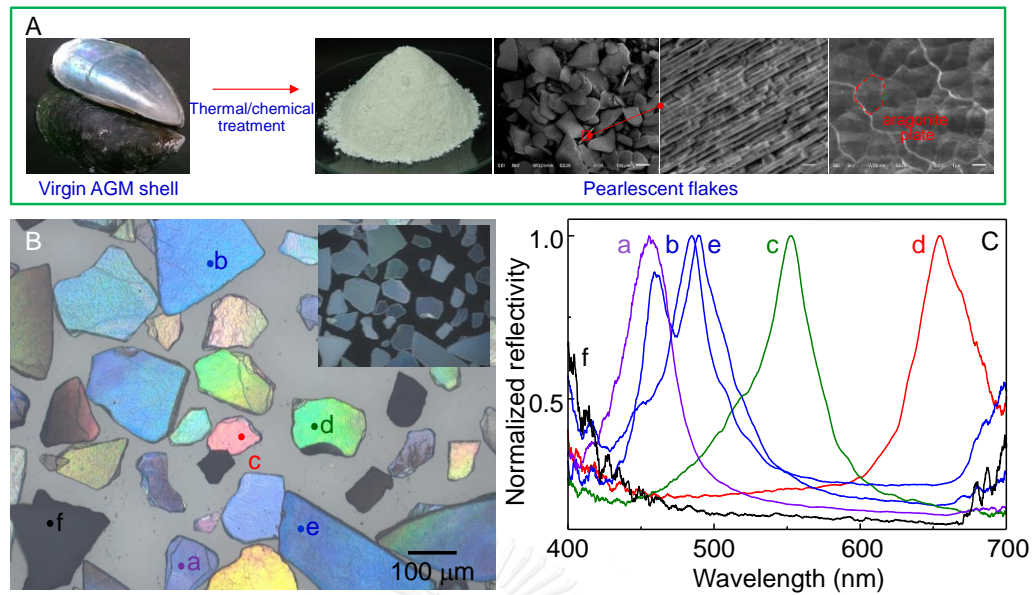


**Figure 3.** (A) SEM images of pearlescent flakes. The flakes are stratified bilayers of aragonite layers and air gaps. The flakes appear white to the naked eyes. (B) OM image of pearlescent flakes under a bright-field illumination (10X objective). The inset shows the corresponding dark-field illumination image. (C) Reflection spectra of selected pearlescent flakes acquired by coupling the reflected light into a fiber optic spectrometer via a 50X objective.

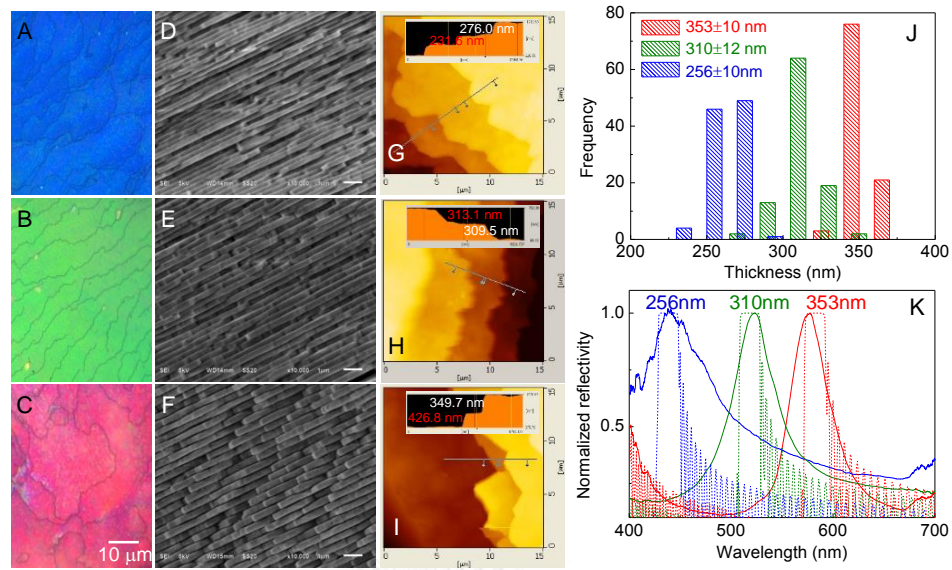


**Figure 4.** OM , cross-section SEM and AFM images of pearlescent flakes expressing colors: (A, D, G) blue, (B, E, H) green, and (C, F, I) red. Histogram (J) show thickness distribution of aragonite layers within the colored pearlescent flakes. (K) Comparisons of experimental (solid line) and calculated (dash line) reflection spectra of pearlescent flakes. The experimentally measured thicknesses were employed for the calculations.

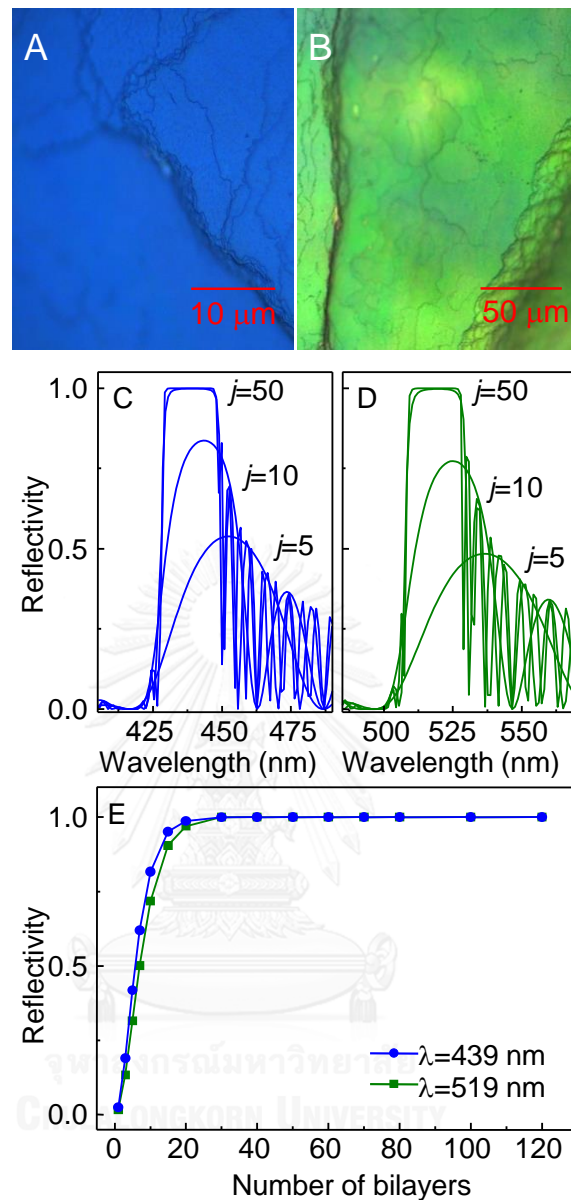


**Figure 5.** OM images of pearlescent flake selectively reflect (A) blue and (B) green colors. The flakes show thickness variation across the surfaces but expressing uniform colors. Calculated reflection spectra of stratified bilayers of (C) the blue pearlescent flakes ( $d_A=256$  nm) and (D) the green pearlescent flake ( $d_A=310$  nm). The thickness of the air gap was assumed 20 nm. (E) The reflectivity-number of bilayer plot for blue and green flakes. The total reflection (color saturation) was achieved after a 30-bilayer.

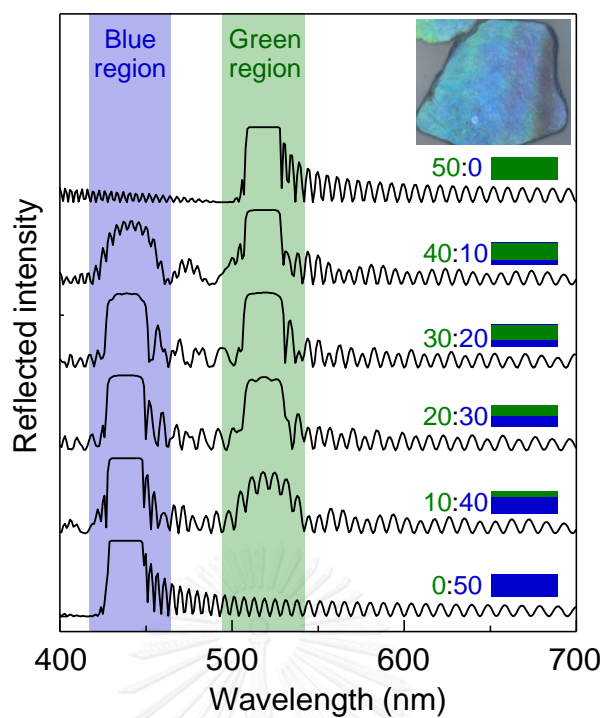


**Figure 6.** Calculated reflection spectrum of a 50-bilayer flake with different ratio of 256-nm aragonite layer (expressing blue color) and 310-nm aragonite layer (expressing green color). The inset OM image shows an experimentally observed pearlescent flake expressing both blue and green colors.

## **Electronic supplementary material**

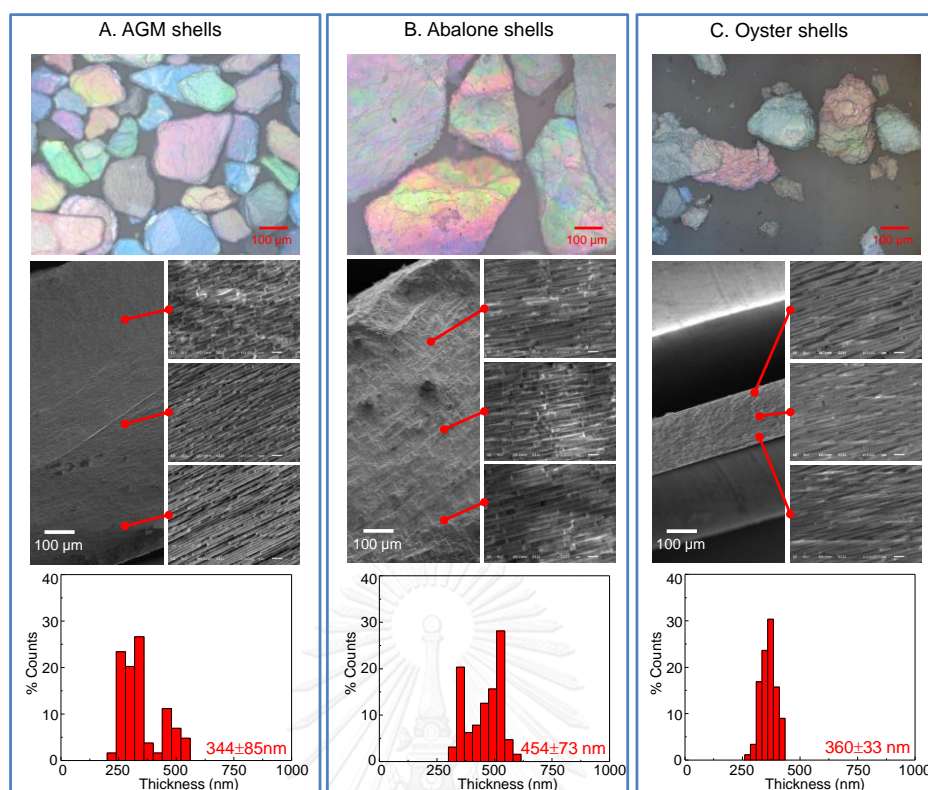
### **Selective colors reflection from stratified aragonite calcium carbonate plates of mollusk shells**

Chutiparn Lertvachirapaiboon, Tewarak Parnklang, Prompong Pienpinijtham, Kanet  
Wongravee, Chuchaat Thammacharoen, and Sanong Ekgasit\*

Sensor Research Unit, Department of Chemistry, Faculty of Science, Chulalongkorn  
University, Bangkok 10330, THAILAND.

E-mail: \*[sanong.e@chula.ac.th](mailto:sanong.e@chula.ac.th)

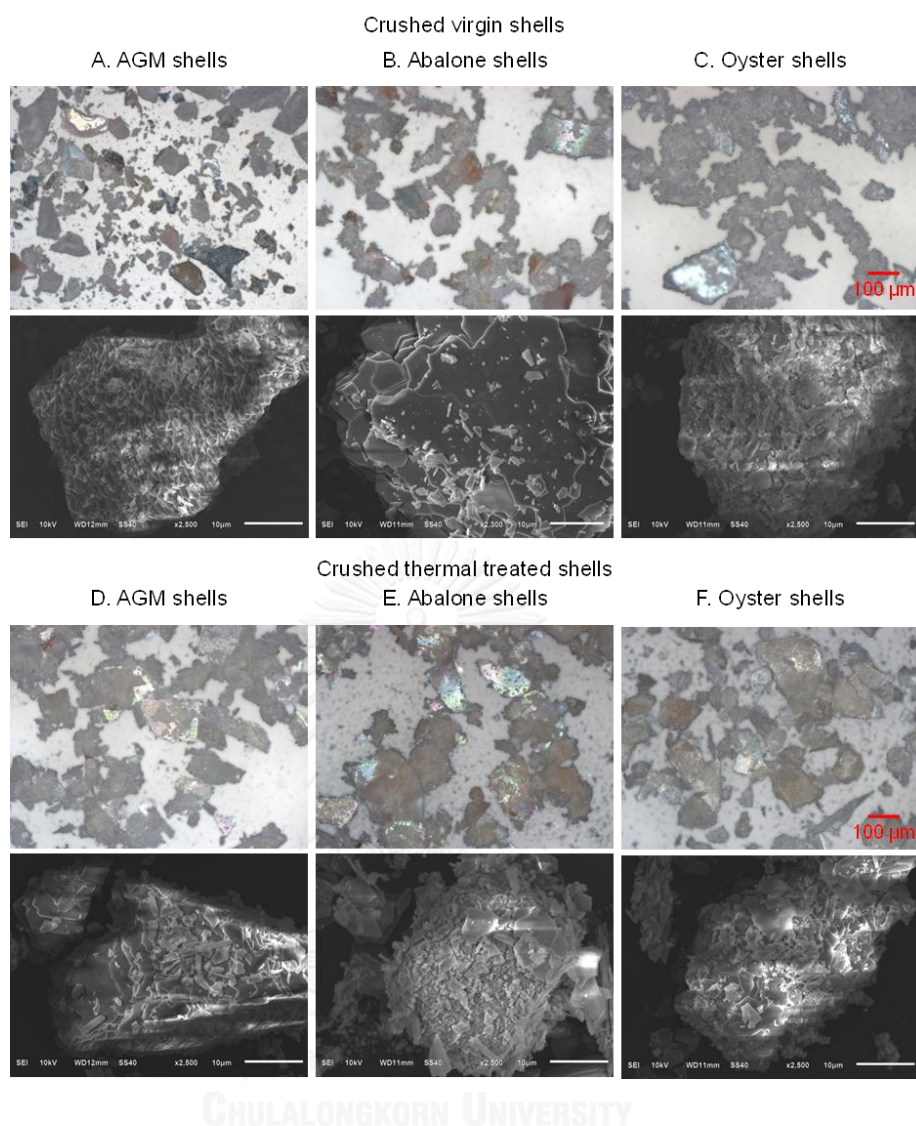




**Figure S1.** Optical microscope images, SEM images, and aragonite thickness distribution of (A) AGM shells, (B) abalone shells, and (C) oyster shells. The aragonite powder from shells appeared white to the naked eyes as normal calcium carbonate powder. Under an optical microscope (10X objective), the aragonite flakes selectively reflected certain frequency of visible light and appeared colorful. The SEM images indicated that all shells composed of aragonite layers bounded by organic binder [1-6]. The thickness distribution of AGM shells, abalone shells, and oyster shells are  $344 \pm 85$ ,  $454 \pm 73$ , and  $360 \pm 33$   $\mu\text{m}$ , respectively. The unique reflective colors seem to be associated with the structural architecture of the shells.

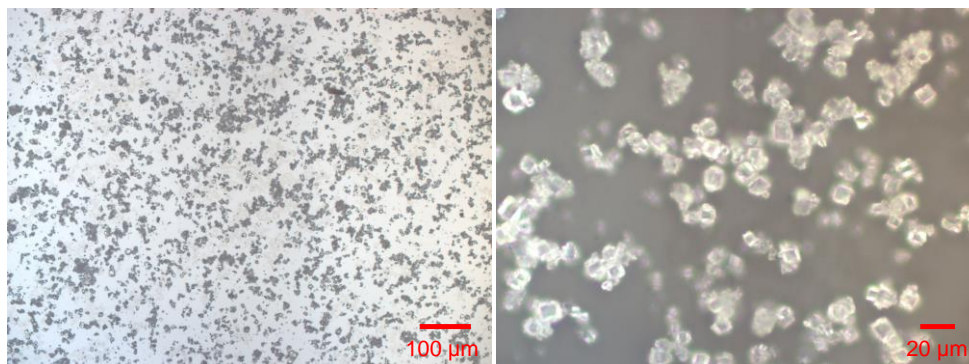
## References

- (1) Jackson AP, Vincent JFV, Turner RM. The mechanical design of nacre. *Proc. R. Soc. B* 1988; 234: 415–440.
- (2) Leung HM, Sinha SK. Scratch and indentation tests on seashells. *Tribol. Int.* 2002; 42: 40–49.
- (3) Lin A, Meyers MA. Growth and structure in abalone shell. *Mat. Sci. Eng. A-Struct.* 2005; 390: 27–41.
- (4) Meyers MA, Chen PY, Lin AYM, Seki Y. Biological materials: structure and mechanical properties. *Prog. Mater. Sci.* 2008; 53: 1–206.
- (5) Lopez MI, Martinez PEM, Meyers MA. Organic interlamellar layers, mesolayers and mineral nanobridge: contribution to strength in abalone (*Haliotis rufescence*) nacre. *Acta Biomater.* 2014; 10: 2056–2064.
- (6) Lertvachirapaiboon C, Jirapisitkul T, Pienpinijtham P, Wongravee K, Thammacharoen C, Ekgasit S. Air-gap-enhanced pearlescent effect in periodic stratified bilayers of *Perna viridis* shell. *J. Mater. Sci.* 2014; 49: 6282–6289.

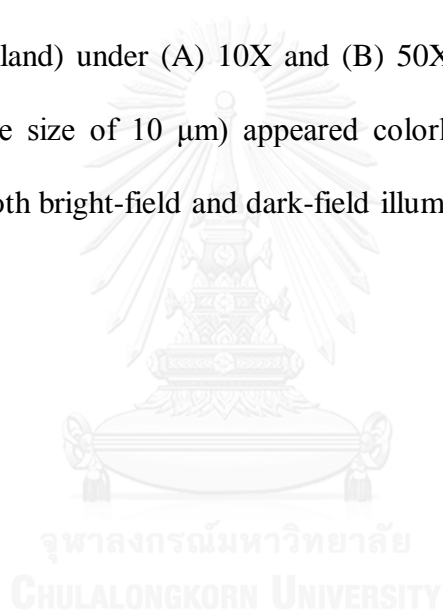


**Figure S2.** Optical microscope (10X objective) and SEM images of crushed virgin and thermal treated shells.





**Figure S3.** Optical microscope images of precipitated calcium carbonate (PCC) powder (Merck, Thailand) under (A) 10X and (B) 50X objectives. The cubic calcite PCC (average particle size of 10  $\mu\text{m}$ ) appeared colorless under optical microscope when viewing with both bright-field and dark-field illuminations.



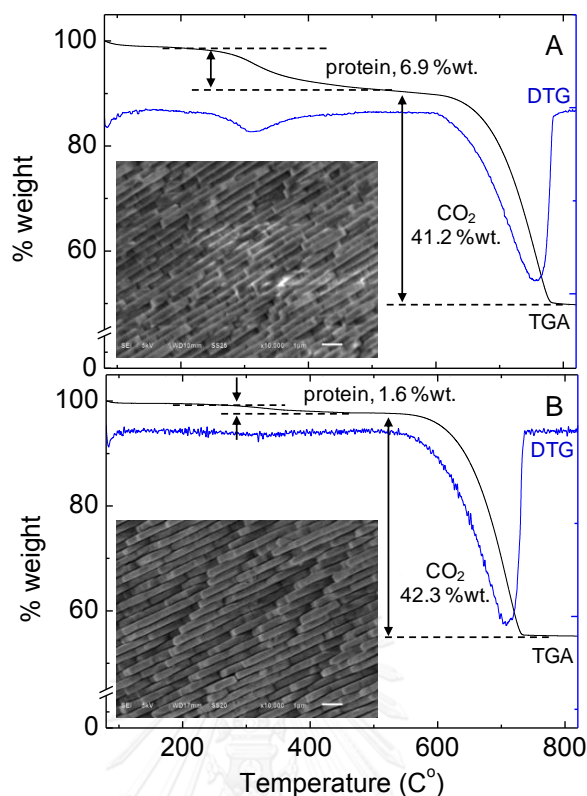


**Figure S4.** TG and DTG curves of (A) AGM shell and (B) pearlescent flakes and their corresponding cross-section SEM images. The thermal analyses results indicated a removal of organic binding layers between aragonite layers. The remaining organic binder (1.6 % wt.) is expected to be those within the aragonite plates [1]. The SEM images confirm the removal of the organic binder layers. Air gaps could be noticed in Figure S4B. The significant reduction of the electron charge up in SEM image in Figure S4B compare to that in Figure S4A corroborate the removal of the organic binding layer [2].

## References

- (7) Levi-Kalisman Y, Falini G, Addadi L, Weiner S. Structure of the nacreous organic matrix of a bivalve mollusk shell examined in the hydrated state using cryo-TEM. *J. Struct. Biol.* 2001; 135: 8–17.
- (8) Lin A, Meyers MA. Growth and structure in abalone shell. *Mat. Sci. Eng. A-Struct.* 2005; 390: 27–41.

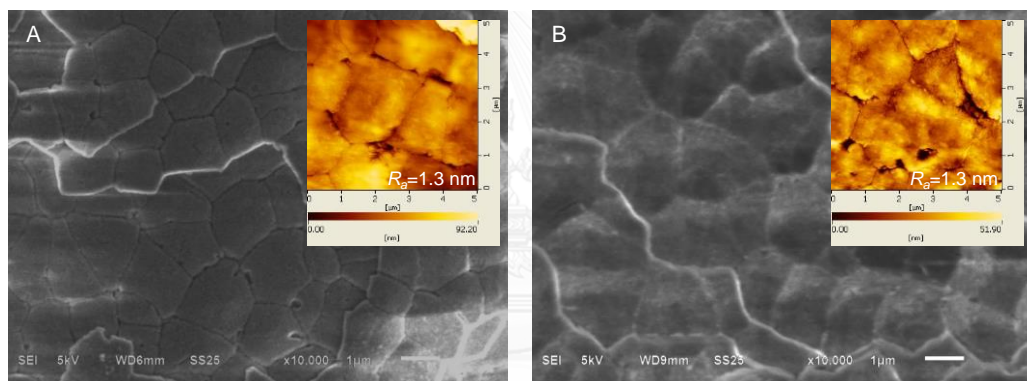
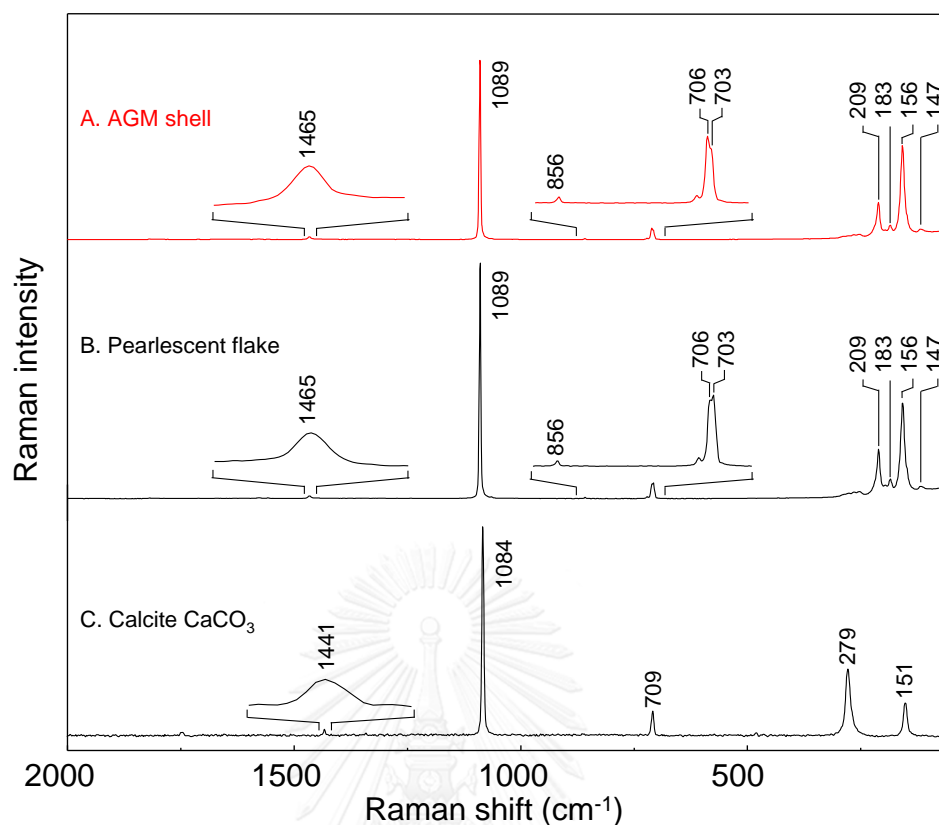


**Figure S5.** Top view SEM images of (A) AGM shell and (B) pearlescent plate and the corresponding AFM images. The AFM images suggest that the aragonite calcium carbonate layer has a relatively smooth surface with average roughness ( $R_a$ ) 1.3 nm.



Vibrational modes	Raman shift (cm <sup>-1</sup> )	
	Aragonite	Calcite
In-plane bending, $\nu_4$	703, 706 (m)	709 (m)
Out-of-plane bending, $\nu_2$	856 (w)	
Symmetric stretching, $\nu_1$	1089 (s)	1084 (s)
Asymmetric stretching, $\nu_3$	1465 (w)	1441 (w)
External lattice vibration	147 (m)	151 (s)
	156 (s)	279 (s)
	183 (w)	
	194 (w)	
	209 (s)	

**Figure S6.** Raman spectra of (A) AGM shell, (B) pearlescent flake, and (C) commercial calcite calcium carbonate. The Raman spectra confirm that A and B are aragonite  $\text{CaCO}_3$  while C is a calcite  $\text{CaCO}_3$  [1-3].

## References

- (1) Parker JE, Thompson SP, Lennie AR, Potter J, Tang CC. A study of the aragonite-calcium transformation using Raman spectroscopy, synchrotron powder diffraction and scanning electron microscopy. *CrysEngComm* 2010; 12: 1590-1599.
- (2) Perdikouri C, Kasioptas A, Geisler T, Schmidt BC, Putnis A. Experimental study of the aragonite to calcite transition in aqueous solution. *Geochim. Cosmochim. Acta* 2011; 75: 6211-6224.
- (3) Lin AYM, Chen PY, Meyers MA. The growth of nacre in the abalone shell. *Acta Biomater.* 2008; 4: 131-138.

## Summary of results shown in Figures S4-S6

The decrease of organic content in AGM shell after the treatment was confirmed by TGA technique. The TG curves in Figure S4 shows two major weight losses. The first weight loss at 200-300 °C was due to the organic matrix decomposition. The TG curve indicated the organic content in the virgin AGM shell was 6.9 % while that of the treated shell was 1.6 %. A 5.3 % reduction was due the degradation and dissolution by the treatment process. The cross-section SEM image of pearlescent flake shows stratified aragonite structure assembly with observable air gaps indicating the decreasing of organic matrix in the shell structure (Figure S4B). The second thermal decomposition with ~42% weight loss at 600-800 °C was due to the liberation of carbon dioxide as calcium carbonate was thermally decomposed to calcium oxide. The aragonite plate showed pseudo-hexagonal aragonite tiles with 3-5 micrometer bisector length and the average roughness ( $R_a$ ) of 1.3 nm, Figure S5. The

Raman spectra of virgin AGM shell and pearlescent flake (Figure S6) show unique external lattice vibration at 147, 156, 183, and 209  $\text{cm}^{-1}$ , and doublet at 703 and 706  $\text{cm}^{-1}$  of carbonate specie of the aragonite crystal [1-3]. These results suggested that the treatment process did not alter the original structure and crystallographic form of the AGM structural assembly. The structure stability was due to the presence of mineral bridges connecting between aragonite layers [4-5].

## References

- (1) Parker JE, Thompson SP, Lennie AR, Potter J, Tang CC. A study of the aragonite-calcium transformation using Raman spectroscopy, synchrotron powder diffraction and scanning electron microscopy. *CrysEngComm* 2010; 12: 1590-1599.
- (2) Perdikouri C, Kasioptas A, Geisler T, Schmidt BC, Putnis A. Experimental study of the aragonite to calcite transition in aqueous solution. *Geochim. Cosmochim. Acta* 2011; 75: 6211-6224.
- (3) Lin AYM, Chen PY, Meyers MA. The growth of nacre in the abalone shell. *Acta Biomater.* 2008; 4, 131-138.
- (4) Lin A, Meyers MA. Growth and structure in abalone shell. *Mat. Sci. Eng. A-Struct.* 2005; 390: 27-41.
- (5) Rousseau M, Lopez E, Stempflé P, Brendlé M, Franke L, Guette A, Naslain R, Bourrat X. Multiscale structure of sheet nacre. *Biomaterials* 2005; 26: 6254-6262.

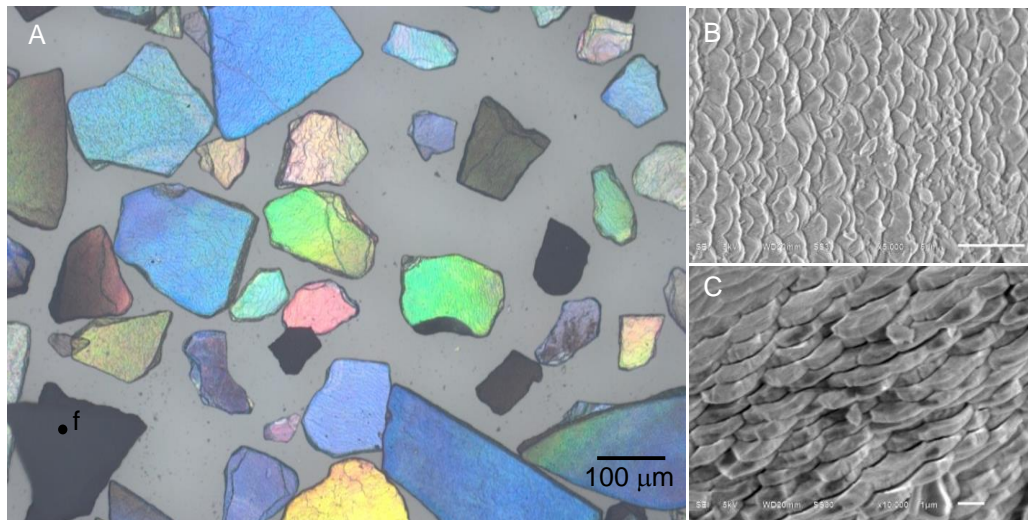


**Figure S7.** OM images of pearlescent flakes with vivid color (the same as shown in Figure 3B). The flake ‘f’ does not express any color due to its structure architecture. The SEM images in Figure S7B and S7C suggest that flake ‘f’ is a fragment of aged aragonite layers at the outer surface of AGM shell. The aragonite plates are irregularly thick with rough surfaces. It does not systematically interact with an incident white light. As a result, the flake ‘f’ does not show a selective reflection capability as the flakes with uniform aragonite layers.

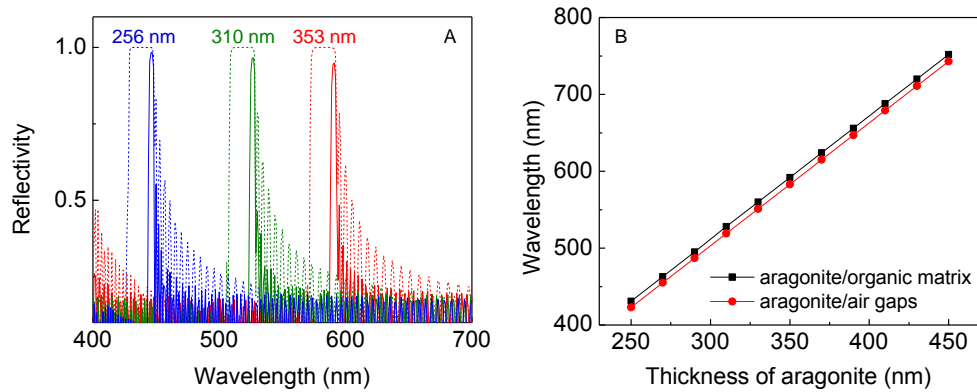


**Figure S8.** (A) Calculated reflection spectrum of aragonite/organic matrix (solid lines) and aragonite/air gaps (dash lines) stratified bilayers. The thicknesses of aragonite ( $d_A$ ) were assigned to 256 (blue line), 310 (green line), and 353 (red line) nm. The following parameters were employed:  $n_A=1.6$ ,  $n_B=1.5$  for organic matrix (solid lines) and 1.0 for air gaps (dash lines),  $d_B=20$  nm,  $N=50$  bilayers,  $\theta=0^\circ$  and  $\lambda=400-700$  nm. (B) The reflectivity plots as a function of thicknesses of aragonite layer.



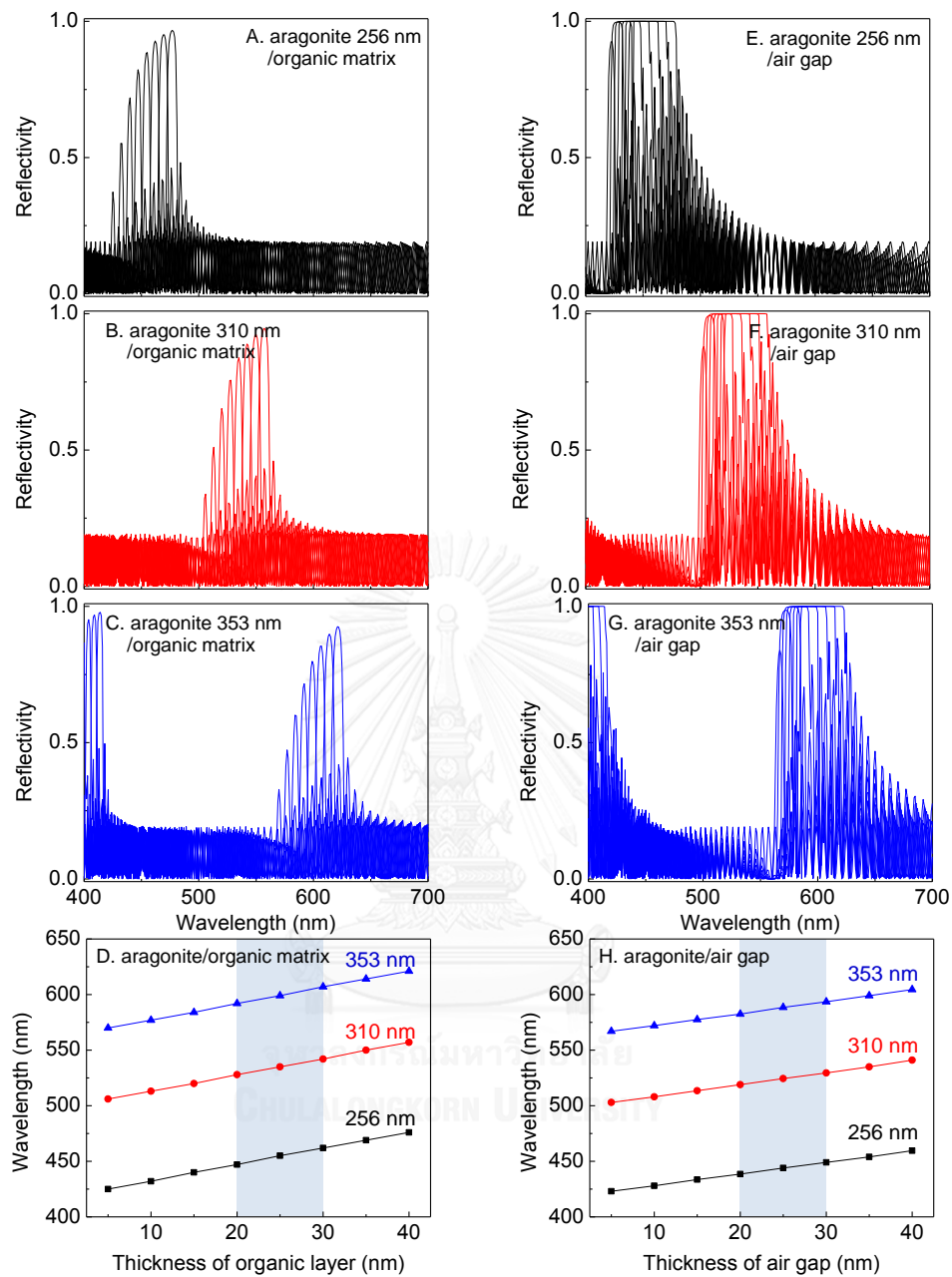


**Figure S9.** Calculated reflection spectrum of aragonite/organic matrix and aragonite/air gaps stratified bilayers; the thicknesses of aragonite ( $d_A$ ) were assigned to 256 (blue line), 310 (green line), and 353 (red line) nm. The following parameters were employed:  $n_A=1.6$ ,  $n_B=1.5$  for organic matrix (solid line) and 1.0 for air gaps (dash line),  $d_B=20$  nm,  $N=50$  bilayers,  $\theta=0^\circ$  and  $\lambda=400-700$  nm. (B) The reflectivity plots as a function of thicknesses of aragonite layer.

**VITA**

Name: Mr. Chutiparn Lertvachirapaiboon

Date of Birth: December 28, 1984

Birth place: Bangkok, Thailand

E-mail address: l\_chutiparn@hotmail.com

Education:

2009-2014

Ph.D. in Engineering, Niigata University, Japan

Ph.D. in Chemistry, Chulalongkorn University, Thailand

2007-2009

Master of Science in Chemistry

Chulalongkorn University, Thailand

2004-2007

Bachelor of Science in Chemistry

King Mongkut's University of Technology Thonburi,

Thailand

